Durham E-Theses

Synthesis and kinetic evaluation of triazolium salt organocatalysts: towards the d1-deuteration of aldehydes

ZHU, JIAYUN

How to cite:

ZHU, JIAYUN (2016) *Synthesis and kinetic evaluation of triazolium salt organocatalysts: towards the d1-deuteration of aldehydes*, Durham theses, Durham University. Available at Durham E-Theses Online: http://etheses.dur.ac.uk/11771/

Use policy

The full-text may be used and/or reproduced, and given to third parties in any format or medium, without prior permission or charge, for personal research or study, educational, or not-for-profit purposes provided that:

- a full bibliographic reference is made to the original source
- a link is made to the metadata record in Durham E-Theses
- the full-text is not changed in any way

The full-text must not be sold in any format or medium without the formal permission of the copyright holders.

Please consult the full Durham E-Theses policy for further details.

Academic Support Office, Durham University, University Office, Old Elvet, Durham DH1 3HP
e-mail: e-theses.admin@dur.ac.uk Tel: +44 0191 334 6107
http://etheses.dur.ac.uk

Synthesis and kinetic evaluation of triazolium salt organocatalysts: towards the d^1-deuteration of aldehydes

Jiayun Zhu

A thesis submitted in partial fulfillment of the requirements for the degree of Master of Research

Department of Chemistry
Durham University

Sep 2016

Abstract

Triazolyl precursors to *N*-heterocyclic carbenes (NHCs) have been recognized as versatile organo-catalysts for synthetic modifications. Recently, a kinetic evaluation for benzoin condensation in the presence of NHC suggested a possible pathway towards the d^1-deteration of aldehydes.

Overall, seven *N*-aryl substituted triazolium salts have been prepared, and six mechanistic studies of the triazol-3-ylidene-catalyzed benzoin condensation has been performed. *In situ* ^{1}H NMR spectroscopic studies of the reaction in triethylamine-buffered methanol-d_4 solution at 25 °C suggest the 3-hydroxyaryl adduct to be the only intermediate which can be observed. The formation of Breslow intermediate could be proved by the trace of adduct deuteration.

Equilibrium constants, K_1, M^{-1}, for hydroxyaryl adduct formation were determined from the reaction of triazolium catalyst with aldehyde, clearly suggest the *ortho*-substituents on the *N*-aryl group of both catalysts and aldehydes *increase* K_1. Our results suggest the dramatically *decrease* (1.2-fold) in K_1 for the reaction of benzaldehyde in the order of increasing steric hindrance of aryl-substituents of catalysts (*N*-mesityl to *N*-triisopropyl). By contrast, the reaction of 2-methoxybenzaldehyde do shows the increases of K_1 in the order *N*-phenyl (118) < *N*-mesityl (524) < *N*-triisopropyl (1738), which is caused by the larger variables in the decomposition rate constant of adduct, k_{-1} (s^{-1}), than formation, k_1 ($M^{-1}s^{-1}$). In order of the increased steric hindrance, k_1 shows the values of *N*-phenyl (3.44×10^{-2}) > *N*-mesityl (2.45×10^{-2}) > *N*-isorpopyl (1.91×10^{-2}), and k_{-1} of *N*-phenyl (2.92×10^{-4}) > *N*-mesityl (4.67×10^{-5}) > *N*-isorpopyl (1.10×10^{-5}).

The trace of H/D-exchange of aldehyde at d^1 position was evaluated under same condition. The further reaction of Breslow intermediate to benzoin, deuterated adduct and deuterated aldehyde was only observed for the reaction of benzaldehyde with

N-mesityl and triisopropyl catalysts. 48 hours reaction suggest the slightly higher deuterium incorporation into adduct/aldehyde for *N*-mesityl than triisopropyl. For the reaction 2-methoxybenzaldehyde with *N*-mesityl and triisopropyl catalysts, the sluggish onwards reaction of adducts prevent the quantitative assessment, although we expect larger variations of reaction parameters. The highly reactive *N*-pentafluorophenyl triazolium catalyst breaks the threshold of benzoin product formation for 2-methoxybenzaldehyde, however, also results in the fast consumption of aldehyde to adduct. The rapid formation of deuterated adduct and deuterated benzoin product suggest the formation of d^1-deuterated aldehyde while with extremely fast decay.

Finally, X-ray crystallography suggested the formation of a novel NHC adduct of *N*-pentafluorophenyl triazolium salts.

Acknowledgement

Above all, I would sincerely thank my supervisor, AnnMarie O'Donoghue, for her expert knowledge and guidance over my MSc. Her invaluable support and encouragement enabled me to complete my work successfully.

Thank you to David Tucker, Peter Quinn, Lami Nnamounu, Oliver Maguire, David Wong-Pascua, Kevin Maduka, Bryony Hockin, and Natalie Farmer for their kind helps on my project. Thanks to all the academic and technical staff who helped me to obtain all of the NMR, Mass spectrometry and X-ray crystallography data. Working in Durham University, Chemistry department has been consistently entertaining, and I am so honored to be a member in CG115.

Finally, I would like to thank my mum and dad for their love, encouragement and support.

Contents

Abbreviation

aq.	aqueous	**Hz**	hertz
Ar	aryl	**IR**	Infrared
Bu	butyl	***J***	coupling constant
Boc	butoxycarbonyl	***k***	rate constant
ºC	degree centigrade	***K***	equilibrium constant
cm^{-1}	wavenumbers	**K_a**	acidity constant
^{13}C	carbon nuclear magnetic	**kcal**	kilocalorie (s)
NMR	resonance	**λ**	wavelength
δ	chemical shift	**L**	litre (s)
D_2O	deuterium oxide	**ln**	natural logarithm
D_2	deuterium gas	**Me**	methyl
DBAD	di-*tert*-butyl azodicarboxylate	**MeO**	methoxy
DBU	1,8-diazabicycloundec-7-ene	**MeOD**	methanol-d_4
DCM	dichloromethane	**M**	molar (moles/litre)
DMSO	dimethylsulfoxide	**mmol**	millimole
EA	elemental analysis	**mol**	mole
ee	enantiomeric excess	**m/z**	mass to charge ratio
ESI-MS	Electrospray Ionisation Mass Spectrometry	**NaOH**	sodium hydroxide
		NMR	nuclear magnetic resonance
equiv.	equivalent	**NHC**	nitrogen heterocyclic carbene
Et	ethyl	**Ph**	phenyl
g	gram (s)	**pH**	acidity of aqueous solution
HCl	hydrogen chloride	**ppm**	parts per million
^1H	proton nuclear magnetic	**R**	alkyl group
NMR	resonance	**s**	second (s)
h	hour (s)	***t-, tert-***	tertiary

Chapter 1. Introduction

1.1. Properties and Applications of Deuterium Sources

Deuterium, known as the stable isotope of hydrogen, contains one more neutron than a proton, leading to different properties and applications. The natural abundance of deuterium relative to hydrogen in carbon-containing organic compounds is lower than 0.02%. Generally, deuterium has a natural abundance of 0.0156% in the ocean, which predominantly exists as HOD, and usually needs initial enrichment to deuterium oxide for sufficient purity. Due to the high speed isotopic exchange, heavy water, or deuterium oxide is not found in nature[1-3]. The Girdler-Sulfide process, followed by distillation, electrolysis and other purification methods, is the most efficient way to obtain deuterated water for scientific utilization in industry, which can attain purity of up to 99.9994%[4]. Although the bond lengths and bond angles between heavy and light water are similar, D_2O is 10% heavier than H_2O, which results in the different vibrational energy between an O-H and O-D bond, and a change of physical-chemical properties[1, 5].

Moreover, the detectability of the deuterium label in molecules by NMR, IR spectroscopy, and mass spectrometry, and the absence of radioactivity lead to a wide applications of deuterium oxide. For example, deuterated compounds can be used as NMR solvents[6]. Moreover, there is increasing demand for deuterium-containing molecules for a variety of applications, including the analysis of chemical properties of human red blood cells[7], the generation of deuterated drugs, metabolic profiling and testing the water absorption ability of poly (vinyl alcohol) hydrogels[8].

1.2. H/D-Exchange Method

Hydrogen-deuterium exchange of protons attached to heteroatoms is facile and process occurs rapidly in deuterated alcohol or deuterium oxide. By contrast, H/D-exchange at carbon is substantially slower thus requiring harsher conditions[9].

Generally, two methodologies are followed to access isotopically labeled compounds. First, isotopically labeled precursors which are commercially available may be used in synthetic preparations. However, this method is restricted due to the high cost and limited range of available precursors[10]. The second and more common approach is to label compounds by the direct H/D-exchange. Although H/D-exchange has been studied for some time, it was not until the mid-1990s that this research area experienced resurgence. This was largely due to the development of C-H bond activation catalysts and the growing demand of isotopically labeled reagents to facilitate the evaluation of catalytic mechanism[10, 11].

To date, two main strategies are followed for H/D-exchange: transition metal-catalyzed H/D-exchange, and pH-dependent H/D-exchange. Metal complex catalysts usually require mild conditions, and have wide application ranges, generating products with good regio- and stereo-selectivity[12]. The complicated preparation and poor control of by-products, however, are difficulties associated with this process. Meanwhile, pH-dependent H/D-exchange can achieve relatively pure product, but the reliance on relatively high kinetic acidities largely limits its development[13-18]. In the following sections, these two H/D-exchange methods will be overviewed with several specific examples.

1.2.1. Transition metal complex catalyzed H/D-exchange

The first study of metal catalyzed H/D-exchange was in the late 1960s[19-22], after which, a plethora of methods of deuteration for both aromatic and aliphatic compounds with efficient deuterium incorporation and high regioselectivities have been developed[10, 12]. Typically, H/D-exchange reactions with a transition metal catalyzed system can be classified by three different pathways: 1) Lewis acid-based pathways, 2) C-H bond activation, and 3) β-insertion/elimination (Scheme 1.1)[12].

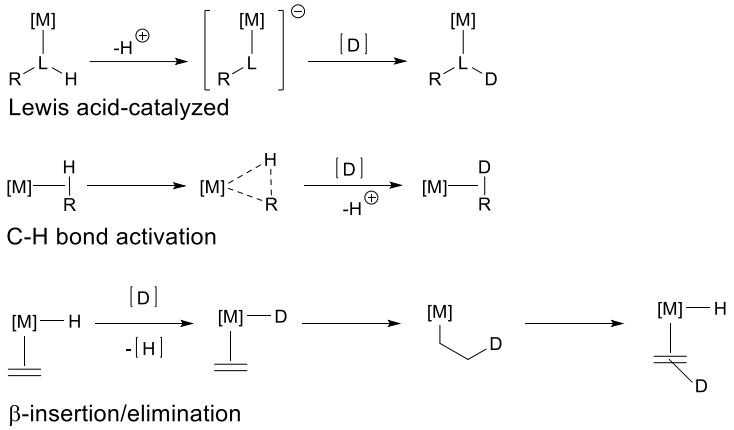

Scheme 1.1. Three general pathways for the metal-catalyzed H/D-exchange

The Lewis acid-catalyzed pathway must involve a strong electron withdrawing metal, typically, Hg, Ag, Co, Cr, and Pt complexes, and are mainly applicable to nitrogenated compounds, like azoles and purines[23-30]. The electronic properties of metal center have a large impact on the catalytic efficiencies under this pathway. For instance, the catalytic efficiencies follow the order: Cr(III) > Co(III) > Pt(II). This phenomenon results from the different electronic properties among the metal centers, which has different impacts upon ligands [23-30]. Especially, Cr(III) presents predominantly a σ-withdrawing electrostatic effect, while the Co(III) and Pt(II) have a combination of σ-withdrawing and π-back-donating effects[12].

The direct C-H bond activation mediated by transition metals is one of the most widely applied synthetic tools in the field of deuteration[31-33]. However, as this activation method is sensitive to reaction conditions, in many cases, the mechanisms are still not clear. There are three types of mechanisms by which the metal complexes activate the C-H bonds: oxidative addition, σ-bond metathesis and electrophilic activation[34-36]. Oxidative addition is the most common mechanism for C-H activation, which usually applies to late transition metals, such as Re, Fe, Ir. The σ-bond metathesis is generally observed for transition metal complexes with d^0 configurations, with alkyl or hydride ligands. The electrophilic activation is formally a substitution process, as there is no net change of oxidation states and coordination geometries for the metal centre. The late- and post-transition metals in strong polar media, like water or acid, have a strong tendency to obey this type of mechanism.

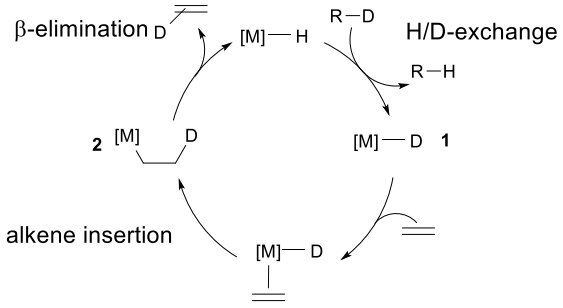

Scheme 1.2. General mechanism of β-insertion/elimination pathway

To successfully deuterate olefin species, especially with aromatic substituents, a β-insertion/elimination pathway has been developed[37-40]. As shown in Scheme 1.2, the deuterium source first exchanges with the hydrido complex to form a metal-deuteride **1**. After the coordination of alkene, the double bond inserts to the metal-deuterium bond to form the metal-alkyl intermediate **2**. Finally, the alkyl ligand undergoes the β-elimination process to generate the deuterated alkene.

Furthermore, due to the different solubilities of metal complexes, the metal catalyzed H/D-exchange reactions outlined above can also be divided into homogeneous

reactions and heterogeneous reactions.

1.2.1.1. Homogenous metal-catalyzed H/D-exchange

Compared with heterogeneous catalysis, the homogeneous systems are more broadly applicable[41, 42]. The stereoelectronic properties of the metals can be modified, which allows adjustment of catalytic activity and selectivity. These soluble catalysts require comparably mild conditions with better tolerance of many functional groups. Side reactions, like dehalogenation, deuterium addition, and even protecting group cleavage, can be avoided[10]. Moreover, as the reaction is maintained in a homogeneous phase, monitoring experiments is relatively easy[12].

A range of transition metal complexes may be applied for deuteration purposes in homogeneous solution. Cationic iridium complexes are particularly suitable for C-H activation, including the *ortho*-deuteration of acetanilides **3** and aryl-ketones **4** (Scheme 1.3)[43, 44].

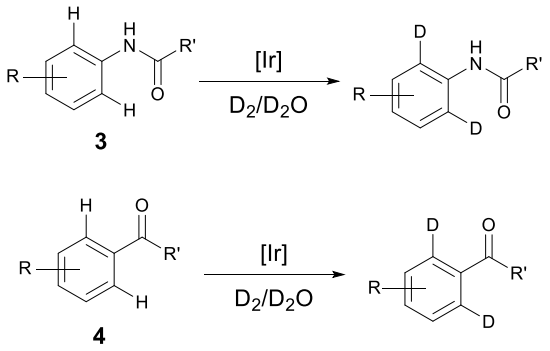

Scheme 1.3. Cationic iridium catalyzed *ortho*-deuteration of acetanilides and aryl-ketones

Apart from cationic iridium, platinum complexes are also widely used, however, restricted to tetrachloridoplatinate (II) salts, and mainly for the deuteration of arenes[45].

Soluble rhodium and ruthenium complexes have been applied frequently in H/D-exchange, while other metals, like manganese, rhenium, chromium and mercury have found limited applications[21, 46-49].

Recently, several ligand-directed *ortho*-selective H/D-exchange reactions of aromatic compounds using palladium complexes have been published[50-52]. As a representative example, Jung et al. found that the palladium-NHC **5** reacts more favourably with aromatic amides, ketones, and amino acids in a trifluoroacetic acid environment with the assistance of silver trifluoroacetate, than common palladium catalysts[53]. As Scheme 1.4 shows, for aromatic ketone **6**, normal palladium catalysts result in deuterium incorporation lower than 10%, while the Pd-NHC can lead to 86% incorporation selectively.

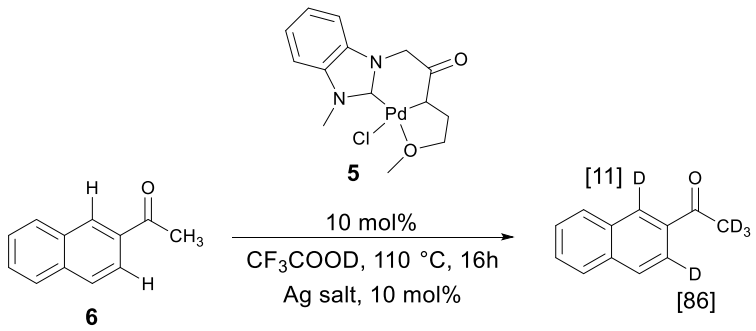

Scheme 1.4. Highly selective deuteration catalyzed by Palladium-NHC 5

1.2.1.2. Heterogeneous metal-catalyzed H/D-exchange

Compared with homogeneous catalysis, the most significant advantage of heterogeneous systems is the simple separation of the catalysts. A simple filtration can yield the pure product if there are no side reactions[54]. However, as harsh conditions are required, unavoidable reactions generally also occur, such as epimerization and racemization, increasing difficulties with the purification [55].

Palladium, platinum, rhodium, nickel, and cobalt catalysts, with D_2, D_2O and deuterated protic solvents as deuterium sources, are reported with high H/D-exchange efficiencies[56-58]. While iridium and ruthenium catalysts are widely applied within homogeneous catalytic systems, these have not been applied in heterogeneous systems[59].

1.2.2. pH-Dependent H/D-exchange

Although metal complex catalysts have many advantages, there are still some drawbacks, including the complicated preparation procedures, the possibility of catalyst poisoning, and the formation of unwanted by-products[53, 60].

The oldest deuteration method, pH-dependent H/D-exchange, is still widely applied to date[61]. Typically, acid- and base-catalyzed enolizations constitute the foundation of these reactions, which leads to the particular regioselectivity. Furthermore, extra reaction steps are often necessary to quench H/D-exchange as these reactions are usually reversible.

1.2.2.1. Uncatalyzed H/D-exchange by deuterium oxide

Due to autoprotolysis, deuterium oxide may be used both as an acid or a base, which can be used to deuterate acidic C-H positions. As an example, the hydrogen atoms at α-position of 2-indanone can be exchanged to deuterium by heating with deuterium oxide (Scheme 1.5)[62].

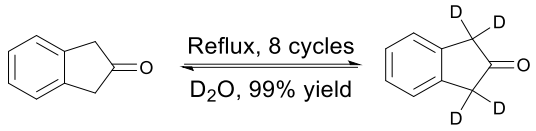

Scheme 1.5. Synthesis of [1,1,3,3-D4]-2-indanone under D2O

However, most H/D-exchange reactions in the absence of catalysts commonly require harsh conditions, such as supercritical media. Supercritical fluids, like supercritical deuterium oxide (D_2O_{SC}), are widely used as solvents in the deuteration of thermally stable compounds[63]. The utilization and analysis of deuteration in D_2O_{SC} was first reported in 1946, when Weldon and Wilson attempted to prepare sodium benzoate from sodium deuteroxide[64]. The higher concentrations of D^+ and OD^- within supercritical deuterium oxide (D_2O_{SC}) than ambient water increase the solubilities of organic compounds[65]. At the critical point of water (374 °C, 221 bar), organic compounds are even completely miscible. The hydrocarbon K_a value is increased from about 10^{-43} under ambient conditions to 10^{-19} at 400 °C, which allows the exchange of these normally unreactive hydrogen atoms[66, 67].

Therefore, with the increased ionic character, deuterium exchange among various arenes and heteroarenes are accessible under supercritical deuterium oxide conditions. Catallo and Junk demonstrated several H/D-exchange reactions of arenes at 380-430 °C. For instance, D_{10}-phenanthrene can be prepared with 82% yield and over 98% deuterium incorporation[68] (**Scheme 1.6**). Furthermore, this method avoids the necessity for repeating cycles to achieve the high deuterium incorporation. However, the high temperature leads to the decomposition of many compounds with poor thermostabilities, like benzothiazole and phenylacetic acid[68].

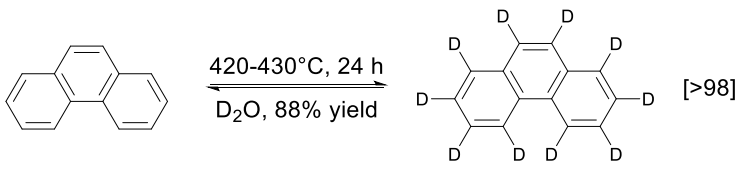

Scheme 1.6. Deuteration of phenanthrene under supercritical conditions

Although the two examples above result in deuteration at all positions, other examples show greater regioselectivity. Weistiuk and Ju in 1989 claimed that both a benzo-annelated heterocycle **7** and 2-hydroxypyridine **8** can undergo H/D-exchange (Scheme 1.7), under different conditions[69, 70]. The deuteration of 2-methylbenzimidazole and 2-hydroxypyridine are used as examples to show that the deuteration on inactivated aromatic rings (e.g. Scheme 1.6) generally needs harsher reaction conditions than the side chain among the benzo-substituted heterocycles (Scheme 1.7). Both examples demonstrate the high regioselectivity of neutral deuterium exchange.

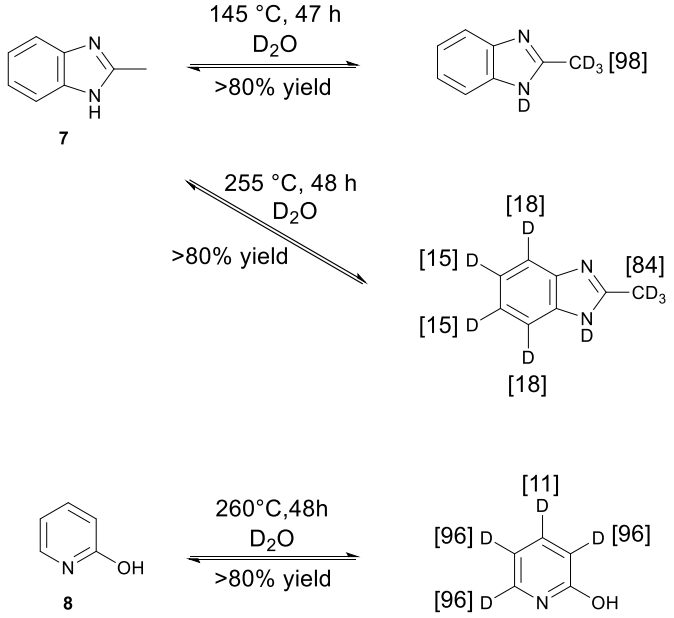

Scheme 1.7. H/D-exchange of 2-methylbenzimidazole and 2-hydroxypyridine

Another example of an uncatalyzed deuteration reaction is shown in Scheme 1.8, which involves the deuteration of the cyclopentadienyl (Cp) ligands of calcium complex **9**. Under the environment of d_6-DMSO, not only the hydrogen atoms on the Cp ring can be exchanged, however, also those of the cyclic alkenyl substituent, which is π-conjugated with the Cp ring[71]. Furthermore, the deuteration of the Cp ligands is still retained upon replacement of calcium by other transition metals.

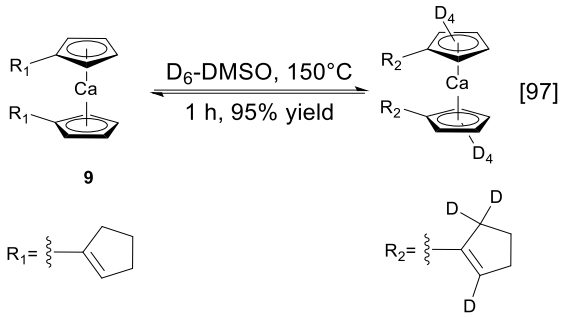

Scheme 1.8. H/D-exchange of calcocenes

Microwave promoted deuteration shows better performance than conventional heating conditions, with increased efficiencies, and shorter reaction times, reduced from several days to a few minutes[72]. Another potential H/D-exchange method is to photochemically excite the aromatic rings, thus decreasing C-H pK_a, and assisting the deuterium exchange with good selectivity (Scheme 1.9)[73].

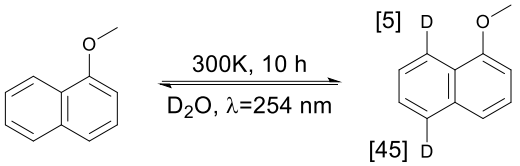

Scheme 1.9. Photochemical assisted H/D-exchange of 1-methoxynaphthalene

1.2.2.2. Acid-catalyzed H/D-exchange methods

Since the 1960s, classical Lewis acid catalysts have been applied to H/D-exchange reactions. The commonly used catalysts include boron trifluoride, alkylaluminium dihalides (*e.g.* $EtAlCl_2$) transition metal salts (*e.g.* $MoCl_5$) perfluorocarboxylic acids, and concentrated or hot dilute mineral acids[10, 11].

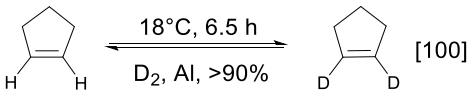

Scheme 1.10. Aluminium catalyzed deuteration of cyclopentene

Under harsh conditions, silica-aluminium based catalysts have been studied since 1948 to obtain deuterated olefin species. It was not until 1965 that the properties of pure aluminium catalysts were studied[74]. Hightower and Hall found that catalysis of deuteration was accessible by pure aluminium for benzene, cyclic alkenes, and even cyclic alkane substrates, and Scheme 1.10 shows the deuteration of cyclopentene as an example[75-77]. Although aluminium catalysts show good regioselectivities under mild temperatures, they are limited to non-polar, small organic molecules, and can be deactivated easily with many poisons, like water and carbon dioxide.

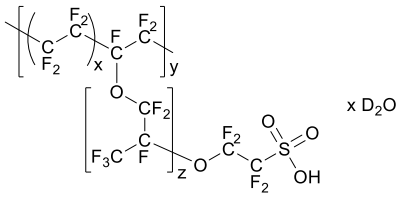

Figure 1.1. Structure of Nafion

To overcome the limitation that simple Lewis acid catalysts are restricted to nonpolar arenes, polymer-supported acidic catalysts, like flavonoids, and the sulfonated fluoropolymer Nafion (Figure 1.1) were introduced for the deuteration of aromatic and heteroaromatic compounds[10, 11]. To study the metabolism of homocanillic alcohol, homovanillic acid, and vanillin, Tuch and Hayball employed the more regioselective polymer support Nafion for the deuteration process (Scheme 1.11)[78]. Furthermore, Nafion was also applied to the tritiation of antimalarial agent chloroquine **10**[79].

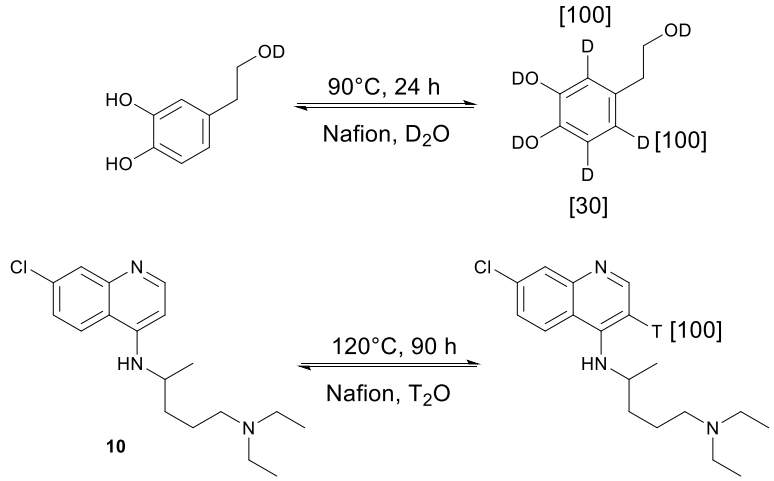

Scheme 1.11. Nafion catalyzed deuteration and tritiation reactions

Apart from polymer-supported catalysts, Wähälä et al. introduced a method of applying Lewis and Brønsted acid mixtures for the H/D-exchange of polyphenolic compounds[80]. By utilizing D_3PO_4, BF_3, and D_2O, they successfully exchanged the hydrogen atoms with deuterium on the activated positions in arenes, with good yield and low temperature conditions. The less accessible positions can also be deuterated if an autoclave process was employed[81]. In an extreme case, even at room temperature, H/D-exchange of the unactivated meta-position within an enterolactone is accessible (Scheme 1.12)[82]. However, no deuteration of the α-hydrogen of the lactone was observed.

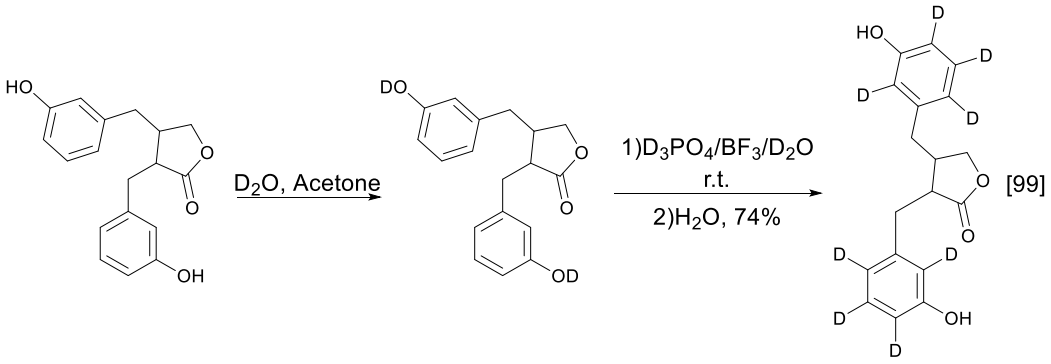

Scheme 1.12. H/D-exchange of an enterolactone with mixed Lewis and Brønsted acid

For deuteration reactions using only Brønsted acids as catalysts, Heinkele claimed that a catalytic amount of deuterosulfuric acid can significantly increase the reaction speed, and obtain higher extents of deuteration for several H/D-exchange reactions, like dextromethorphan, and imidazole species (Scheme 1.13)[83].

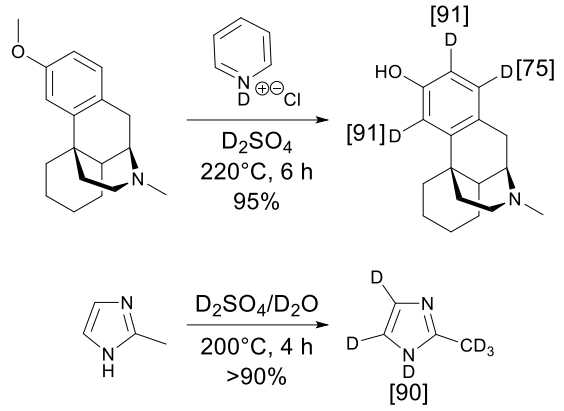

Scheme 1.13. Catalytic amount of D_2SO_4 accelerates the deuteration process

Typically, within most of the acid-catalyzed deuteration reactions, modest, substituent-dependent regioselectivity can be observed. Scheme 1.14. shows the results of an H/D-exchange investigation of a ferrocene complex in trifluoroacetic anhydride (TFAA) solution. If the cyclopentadienyl (Cp) rings are linked with alkyl substituents, the aromatic deuteration will be favored on the Cp ring due to its greater electrophilicity. In the presence of ketone substituents, however, only deuteration of the α-methyl group occurs *via* enolization[84].

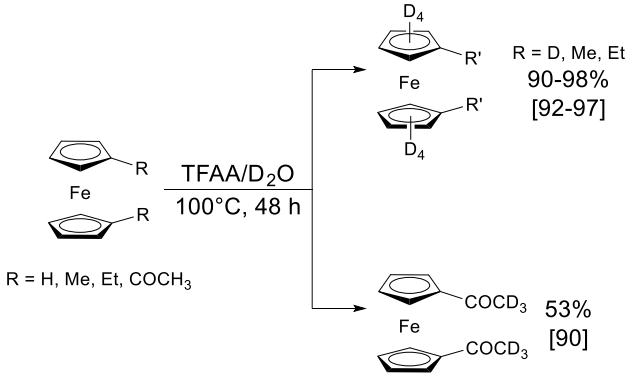

Scheme 1.14. Regioselectivity of ferrocenes

1.2.2.3. Base-Catalyzed H/D-exchange Methods

Overall, base-catalyzed deuteration procedures involve removal of acidic hydrogens by base with subsequent replacement by deuterium. This process can be performed even when the equilibrium significantly favors the protonated species[11]. Compounds containing carbonyl groups, which have the possibility to undergo keto-enol tautomerisation, are expected to generate deuterium compounds with high yield and selectivity. Similarly, γ-hydrogen atoms of α-β-unsaturated ketones undergo H/D exchange easily by this method, and testosterone **11** provides a good example (Scheme 1.15)[10, 85]. Typically, different concentrations of deuterated alkali metal hydroxide solution in D_2O are used as catalyst and deuterium source. A methanol-d_4 solution may be used instead of deuterium oxide if an anhydrous environment is required.

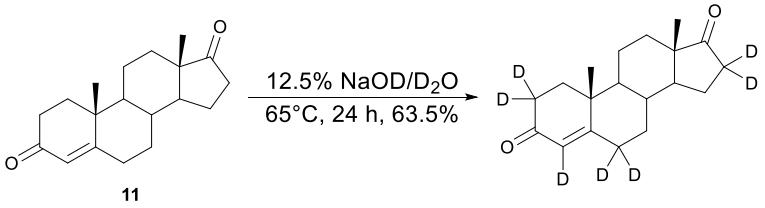

Scheme 1.15. Base catalyzed deuteration of testosterone

Scheigetz et al. claimed to successfully achieve the deuteration of aryl methyl sulfones and ketones by using three types of base catalysts: potassium hydroxide, triethylamine, and 1,8-diazabicycloundec-7-ene (DBU)[86, 87]. The deuteration rate and efficiency depended on the solvent, substrate, and catalyst. As shown in Scheme 1.16, the deuteration of 1-biphenyl-4-ylpropane-1,2-dione **12** can proceed easily, with high yield and incorporation, whereas the use of DBU as base results in decomposition. For sulfone **13**, different catalysts lead to various incorporation percentages.

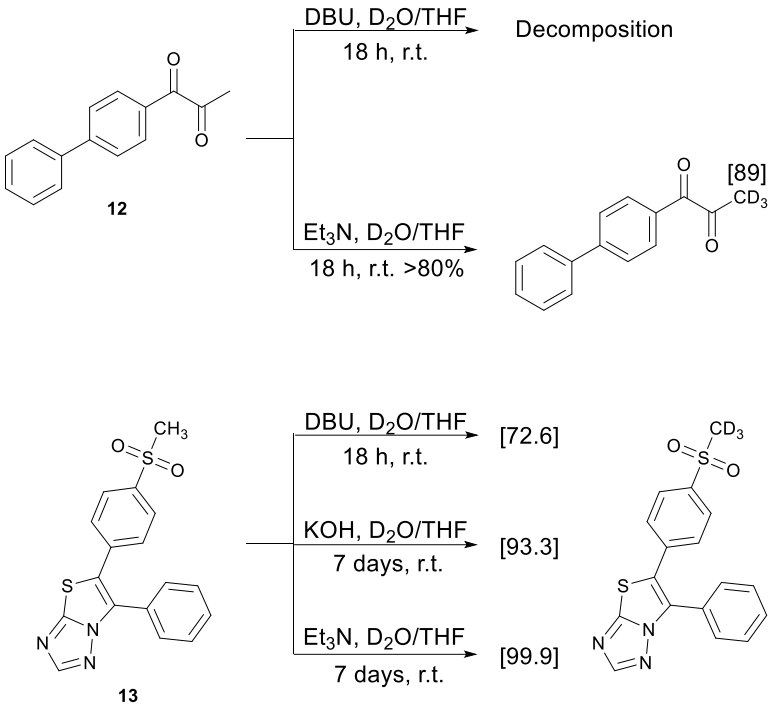

Scheme 1.16. Impact of different catalysts on deuteration process

In 1994, it was found that different pH values could change the regioselectivity of H/D-exchange in D_2O_{sc}, *e.g.* for diphenylamine **14** (Scheme 1.17)[88].

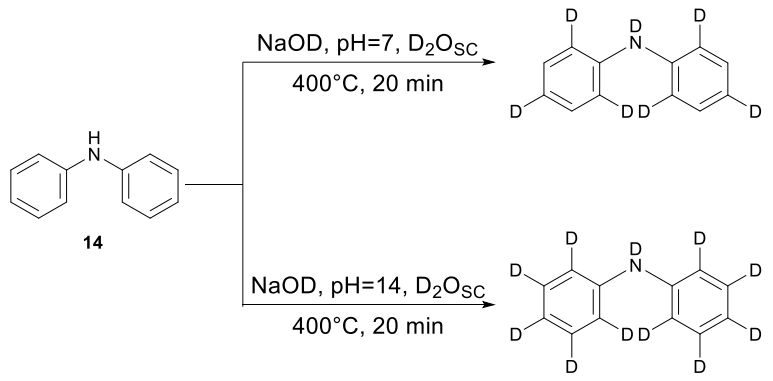

Scheme 1.17. Different regioselectivity caused by a change in pH

For some base catalyzed H/D-exchange reactions, use of microwave conditions can accelerate the reaction, while the application of molecular sieves plays a decisive role[89]. For the preparation of a deuterated Wittig salt, Matsubara et al. reported that the use of a microwave reduced the reaction time from two hours to thirty minutes. In

the case of acetophenone **15**, however, these conditions did not give deuteration unless molecular sieves were also present (Scheme 1.18).

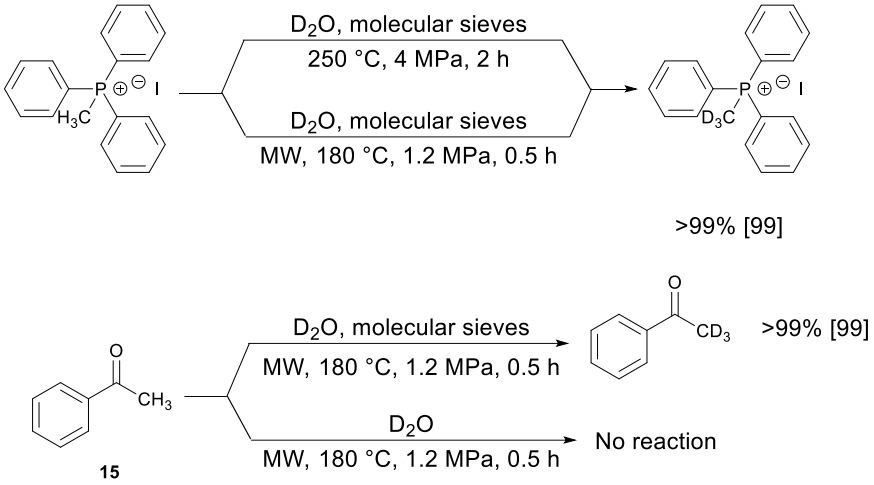

Scheme 1.18. Effect of microwave and molecular sieves

Base-catalyzed deuteration can be applied enantioselectively to synthesize pure α-deuterated amino acids[10]. As illustrated in Scheme 1.19 for glycine, initially, the amino terminal is first protected as iminodisulfide, and carboxyl terminus as methyl ester, respectively. Then with the assistance of a chiral auxiliary, like Oppolzer sultam **16**, or alternatively phase transfer catalysts, the desired side chains are stereo- and enantioselectively inserted after the deuteration (Scheme 1.19).

The protected amino acid **17** is first deuterated in a MeOD/D_2O mixture with a catalytic amount of sodium carbonate, then, attached to an auxiliary, Oppolzer sultam **16**. A butyl lithium assisted alkylation process followed by the deprotection and cleavage of the sultam provide the amino acid with high purity (Scheme 1.19)[90].

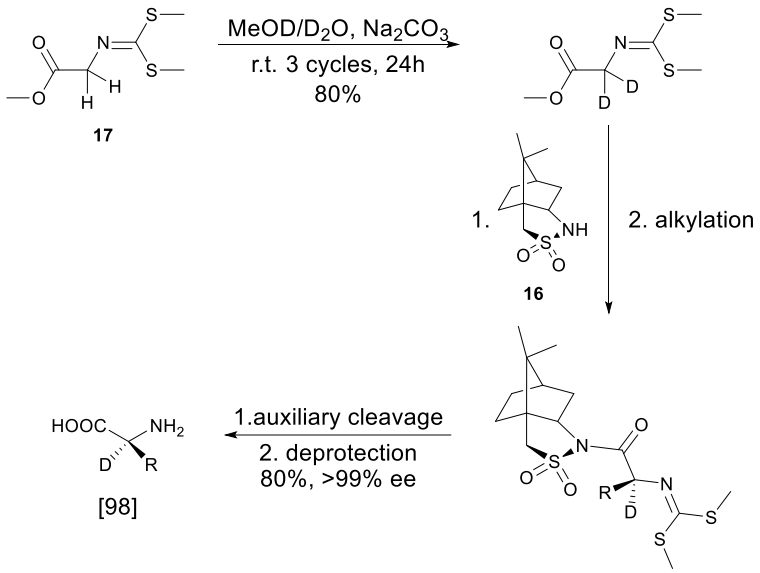

Scheme 1.19. Synthesis of enantioselective deuterated amino acid by using Oppholzer sultam 16

An additional synthetic route to the enantioselective deuteration of amino acids was suggested by Gani et al. in 1992, which was also regioselective[91]. This method should be separated into two parts, the deuteration (Scheme 1.20), and the alkylation (Scheme 1.21) followed by ring cleavage. As Scheme 1.20 shows, due to the steric hindrance effect of the bulky isopropyl group, the C3-position of the dihydropyrazine **18** remains unchanged, while the C-6 position is deuterated with high yield and purity.

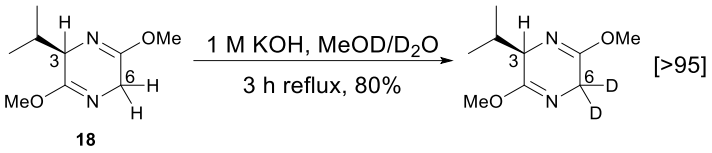

Scheme 1.20. Regioselective deuteration of dihydropyrazine 1.18.

The alkylation on the C-6 position is highly diastereoselective, and can be applied to the synthesis of a series of amino acids, like serine, allyl-glycine, and aspargic acid. Furthermore, the by-product of the ring cleavage, valine **19**, is also enantiopure (Scheme 1.21).

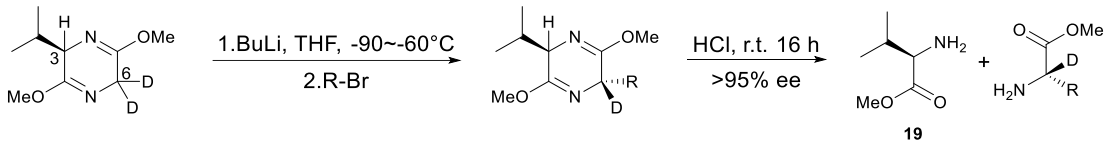

Scheme 1.21. Alkylation and ring cleavage process of enatioselective deuterated amino acids

To simplify the enantioselective synthesis access to deuterated amino acids, Lygo and Humphreys suggested the utilization of a chiral phase-transfer catalyst (PTC, **20**)[92].With the aid of PTC, they successfully combined the H/D-exchange process and the alkylation processes for activated glycine derivatives **21** within a single step (Scheme 1.22). The imine **22** was subsequently converted to the *tert*-butyl protected amino acid in good yield and purity.

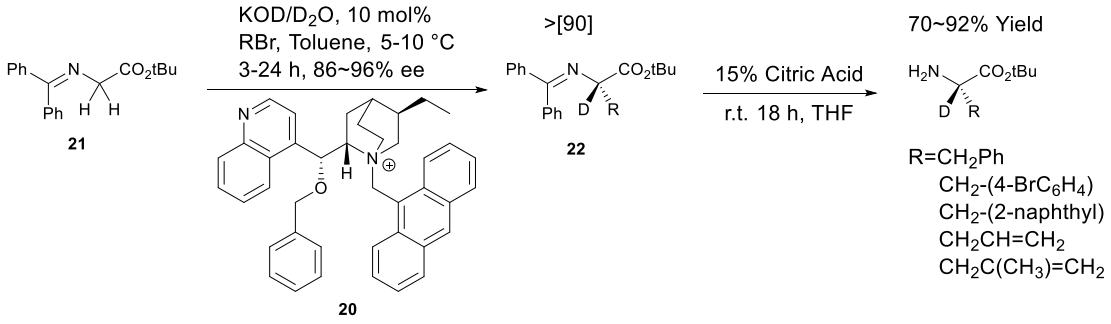

Scheme 1.22. Enantioselective synthesis of various deuterated amino acids with chiral phase transfer catalyst 20

Apart from deuteration based on keto-enol tautomerism, organometallic compounds can also be utilized for H/D-exchange reactions. Within the deuteration process, Grignard reagents and alkyl lithium compounds are two common organometallic species for deprotonation, and followed by addition of D_2O, MeOD, and AcOD as deuterium sources[93-96].

Furthermore, metal salts can also be used as deuteration catalysts, for instance, Larrosa et al. published a selective deuteration method among aromatic compounds (Scheme 1.23). *Via* an aryl-silver (I) intermediate, *ortho*-substituted aromatic

compounds can be deuterated simply through decarboxylation by using a catalytic amount of Ag_2CO_3[97].

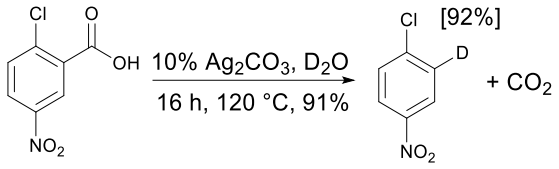

Scheme 1.23. Silver salt catalyzed deuteration of aromatic ring

1.2.2.4. Kinetic isotope effect on H/D-exchange

Generally, large excesses of deuterium sources are used to limit reverse reactions between the deprotonated compounds and protons within the H/D-exchange processes[98]. Based on their experimental result, Huang et al. utilized density functional theory (DFT) to explain the first chiral guanidine **23** catalyzed asymmetric H/D-exchange reaction of α-fluorinated aromatic ketones (Scheme 1.24)[99]. However, the primary kinetic isotope effect allows for the success of this process since the deuterated products have a higher energy barrier towards dedeuteration compared to the original proton counterparts for keto-enol tautomerisation[100].

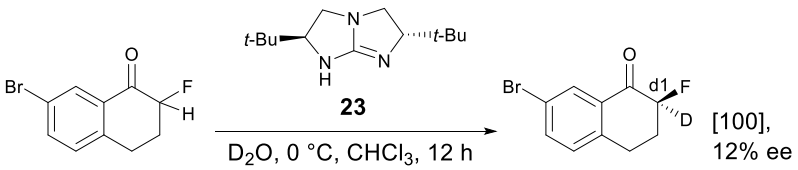

Scheme 1.24. Guanidine-catalyzed asymmetric deuteration reaction

The DFT result indicated that both of the *R*- and *S*- d1-deuterated products' activation energies are 1.3 kcal/mol lower than their corresponding protonated species, which leads to the high deuterium incorporation. Moreover, since the catalyst guanidine **23**

is chiral, the *S*- product is kinetically favored by 0.6 kcal/mol over the *R*- product, leading to the enantioselectivity of this process[99].

1.2.2.5. Intramolecular catalysis of H/D-exchange of carbonyl-bound protons

H/D-exchange of protons, which are bonded directly to carbonyl groups, is quite rare[101]. However, the aldehyde proton of malonganenone B **24** is reported to undergo H/D-exchange without any catalyst according to its NMR and mass spectra (Scheme 1.25)[102, 103].

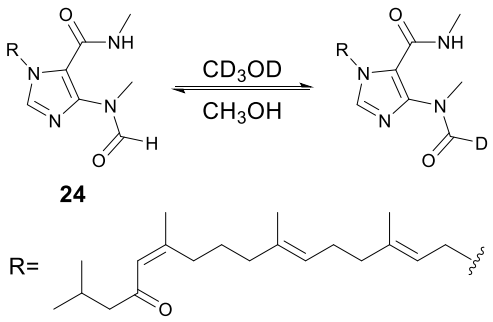

Scheme 1.25. Deuteration of malonganenone B 24

Following on from the formamide case in Scheme 1.25[104], Keyzers et al. reported the mechanism of deuterium exchange of **24** *via* a N-heterocyclic carbene (NHC) intermediate **25** , which is fully reversible. The attack of the N-methyl amide towards the carbonyl group forms an N-C-N ring, and the neighboring nitrogen atoms assist the elimination of water, which generates a NHC precursor **26**. The equilibrium between carbene **25** and its precursor **26** allows the participation of deuterium (Scheme 1.26)[101].

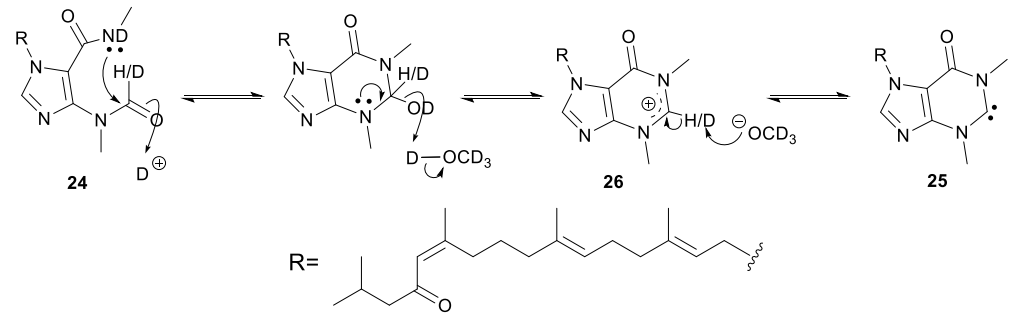

Scheme 1.26. Fully reversible mechanism for H/D-exchange of malonganenone B 24

1.3. Preparation of d^1-deuterated aldehyde

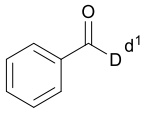

27D

Figure 1.2. d^1-Deuterated benzaldehyde 27D

Compared with other deuterated compounds, access to d^1-aldehydes is difficult and expensive due to the extremely low acidity of the aldehydic hydrogens. Most of the accessible methods are based on complicated organic synthetic processes and not simple H/D-exchange. For instance, in 1939, Pd-$BaSO_4$ was used as a catalyst to reduce *para*-phenylbenzoyl chloride into d^1-benzaldehyde **27D**[105]. The hydrolysis of bisiminium cations, the reduction of *N-tert*-butylbenzamides through lithium aluminium deuteride, and the azeotropic distillation of phenylglyoxylic acid followed by decarboxylation are three possible synthetic pathways towards d^1-benzaldehyde **27D** without the use of metal catalysts[106-108].

1.4. Umpolung Reactions

The benzoin condensation was first achieved with cyanide ions as catalyst by Lapworth in 1903[109-112], and the d^1-deuteration of benzaldehyde was a subsequent

development. The first synthetic route towards the d^1-benzaldehyde **27D** by using potassium cyanide as catalyst was published in 1972, which is still utilized to date (Scheme 1.27)[110-112]. These processes rely on the concept of "umpolung", meaning polarity inversion, a definition which was first introduced by Seebach and Enders in 1975[113].

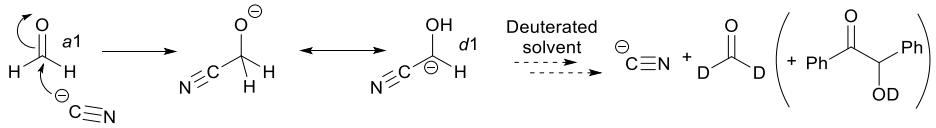

Scheme 1.27. Umpolung process involving cyanide group

For a number of decades, cyanide was utilized as the main source of umpolung reactivity for the reaction of aldehydes[114, 115]. As Scheme 1.27 shows, the negatively charged cyanide attacks the carbonyl group of aldehyde, and donates electron density to the C-O double bond, thereby facilitating the development of a partial negative charge on carbon[116]. Another umpolung reaction involves a dithiane for inversion of polarity[117] (Scheme 1.28). With the assistance of *n*-butyl lithium, a bisthio masked aldehyde can be transformed into a nucleophilic source, which can be applied as d^1 keto synthons[113, 118], although this route has not been applied for the deuteration of aldehydes.

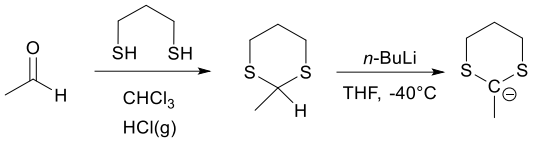

Scheme 1.28. Umpolung reaction between dithiane and aldehyde

To date, compared with the traditional cyanide catalyst, N-heterocyclic carbenes (NHCs) are considered to be more economical and environmentally friendly. Towards umpolung reactions, NHCs can be seen as mimics of traditional catalysts with comparable or even better donating properties[119-121].

1.5. NHC-catalyzed benzoin condensation

In 1943, Ukai delivered the first example of NHC-catalyzed benzoin condensation, when the naturally occuring thiazolium salt, vitamin B_1 **28** was used to catalyze the self-condensation of benzaldehyde[122, 123]. Later on, Mizuhara suggested the catalytic activity was derived from the thiazolium centre[124], and the groundbreaking mechanistic study was published by Breslow in 1958[125]. Although the active form of catalyst represented in ylidic form **29** by Breslow, thiazolyl NHC **30** is now known to also contribute. These early studies underpin a huge volume of more recent research focusing on organocatalysis of the benzoin and related reactions by NHCs and derivatives[126-129].

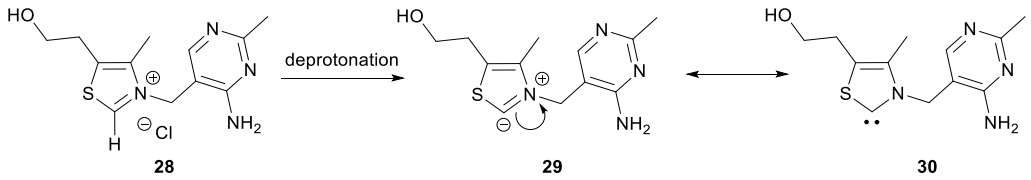

Scheme 1.29. First synthetic pathway of thiazolium carbene 30 from the vitamin B_1 precursor 28

In particular, triazolium-derived NHCs have proven to have particular efficacy as catalysis of the benzoin and related reactions[130]. Recent work from the O'Donoghue and Smith groups has explored the mechanism of the triazolium-catalyzed benzoin reaction (Scheme 1.30)[131, 132]. The triazolyl NHC **31'** first reacts with the aldehyde **32** to form the Breslow intermediate **33**, followed by the reaction with another molecule of aldehyde to form the benzoin product **34**[132]. During their mechanistic studies, evidence of d^1-deuterated aldehyde formation was observed, although levels of incorporation were low. In principle, the reversal of the deprotonation of the tetrahedral intermediate **35** in deuterated protic solvents results in deuteration due to the large excess of deuterium[98], which can lead to the corresponding d^1-aldehyde **32D**[131]. Theoretically, a similar catalytic cycle may be envisaged for aliphatic

aldehydes.

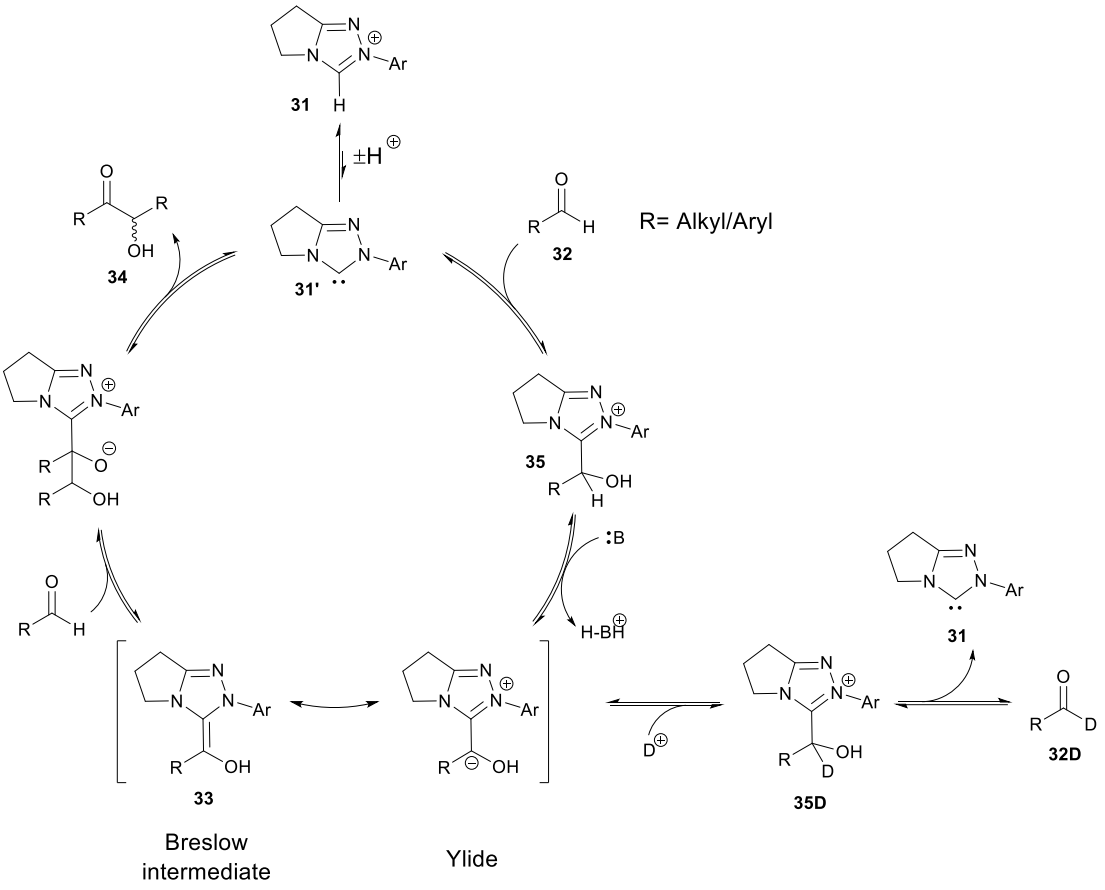

Scheme 1.30. Benzoin condensation based d[1] deuterated aldehyde 32D synthesis

1.6. NHCs and Organocatalysis of the Benzoin Condensation

The longer term aim of my project is to explore whether manipulation of the NHC-catalysed benzoin pathway (e.g. Scheme 1.28), or the related acetoin pathway, can lead to an efficient organocatalytic route for the preparation of d[1]-deuterated aldehydes[130-132]. To achieve this goal, a more quantitative understanding of structure and substituent effects on these pathways is required.

1.6.1. Structural Properties of NHCs

Carbenes have long been recognized as a type of unstable intermediate with short life-times because of their unsaturated coordination and incomplete electron octet[133]. There have been debates on their isolabilities for one hundred years since the evidence of their existence was first estabilished by Buchner and Curtius in 1885[134]. In 1988, Bertrand reported the first isolable free carbene **36**, and three years later, the synthesis of the first commercially available carbene **37** by Arduengo initiated the broader usage of carbenes in organic synthesis and catalysis[135, 136].

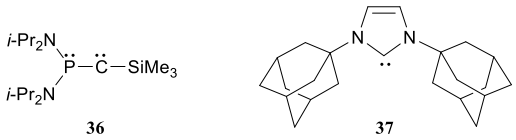

36 **37**

Figure 1.3. First stable phosphinosilyl carbene 36 and first crystallized stable imidazolyl carbene 37

N-Heterocyclic carbenes are defined as formally neutral compounds containing a divalent carbon atom, which connects directly to at least one nitrogen center in a heterocyclic system[133, 137-139]. The conformations at the carbene functional centre results from the combination of *sp* and sp^2 hybridization[137]. The electronic spins of the two valence electrons (singlet or triplet) determine the properties of the carbene (Figure 1.4) [140, 141].

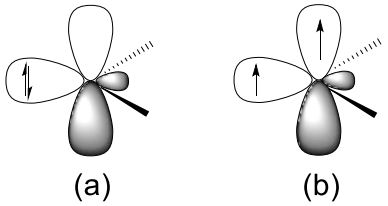

Figure 1.4. Singlet (a) & triplet (b) configurations of sp^2 hybridized carbenes

N-Heterocyclic species are relatively important due to their isolable properties and relative longevities [135, 136, 141, 142]. Initially, it was thought that both the inductive and mesomeric effects are indispensible for carbene stabilization (Figure 1.5) [143].

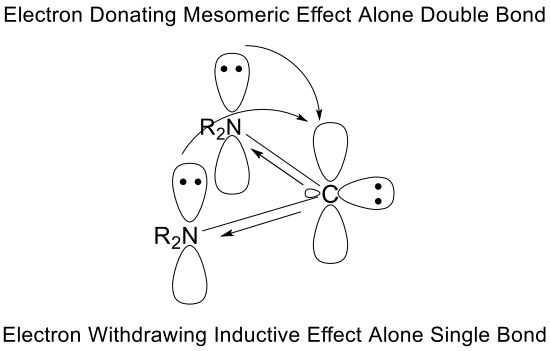

Figure 1.5. Electron donating and inductive effects stabilize the singlet carbene.

Since the isolation of the first crystalline imidazolyl carbene **37**[136], a broad range of NHCs with different architectures have been synthesized. In 1993, Kratz and Kuhn reported a synthetic pathway to imidazole-2-ylidene **39** from the parent imidazole-2-thione **38**[144]. Later on, Enders obtained the crystal structure of triazolyl carbene **40** by vacuum pyrolysis in 1995, which was the first stable triazolyl carbene species[145].

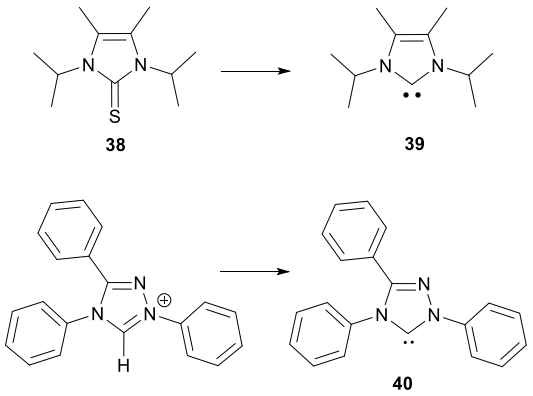

Scheme 1.31. Tipical imidazolyl and triazolyl carbene synthetic pathways

The aromatic stabilization was thought to be key until the isolation of Arduengo's carbene **41** in 1995, which lacks the double bond between *C*4 and *C*5 positions[146].

Moreover, in 1996, the synthesis of the bis-diisopropylamino carbene **42** by Alder further proved that aromaticity is not essential for stability (Figure 1.6) [147-149].

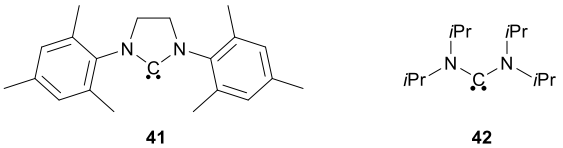

Figure 1.6. Non-aromatic carbenes isolated by Alder and Arduengo

1.6.2. Substituent Effects on the NHC-Catalyzed Benzoin Condensation

As introduced in Section 1.5, the NHC-catalyzed benzoin condensation mainly includes three steps (formation of adduct, Breslow intermediate, and benzoin), for which the rate constants can be calculated by kinetic studies (Scheme 1.30)[132]. Compared with thiazolium salts **43**, the extra aryl substituent of triazolium **44** allows for an increase in the electronic and steric variability of the active NHC scaffold[150], and we focus predominantly on a bicyclic triazolium derived catalyst **45**. The role of the N-aryl substituent has been shown synthetically to be key to the catalytic efficiency of various NHC-processes and, in addition, a small change in substituent can sometimes completely change the reaction outcome. Research in the O'Donoghue and Smith groups has focused on a quantitative evaluation of the effect of the N-aryl substituent on the benzoin and related Stetter reactions[132].

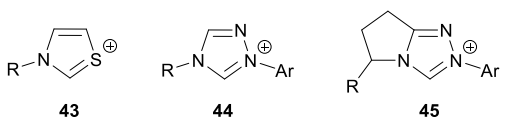

Figure 1.7. Typical architecture of thiazolyl and triazolyl carbene

As all NHC processes rely on an initial deprotonation of precatalyst triazolium ion to yield the carbene *in situ*, initially the effect of *N*-aryl substituent on kinetic acidities

and pK_a were explored. In general, an increase in the electron-withdrawing electronic effect of *N*-aryl substituent increased kinetic acidity and decreased pK_a although the effect was relatively small. The pK_a values of twenty triazolium salts with different architectures have been investigated, showing a change of no more than 2 units across the full range of catalysts[98, 151].

In these studies, it proved possible to directly isolate and characterize the first hydroxyaryl intermediate of the benzoin and Stetter reactions resulting from the reaction of precatalyst with aldehyde in the presence of base[132, 151]. In contrast to a previous literature hypothesis, it was shown that the hydroxyaryl adducts form reversibly in solution irrespective of the substitution pattern on catalyst[152, 153]. The equilibrium constant, K_{exp} (M^{-1}), for formation of a range of hydroxyaryl adducts have been determined allowing an assessment of substituent effects on this step. Table 1.1 summarizes a selection of relevant equilibrium constants for adduct formation.

Table 1.1. Representative equilibrium constants for hydroxyaryl adduct formation under different experimental conditions[131, 132, 151]

Entry	catalyst	aldehyde	K_{exp}, M^{-1} [c]
	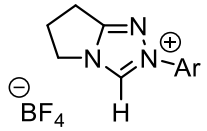	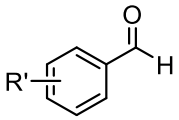	
1a	Ar= Ph	R'= H	**11.4**
1b		R'= 2-OMe	**118**
1c		R'= 4-OMe	**1.92**
1d		R'= 4-F	**6.88**
1e		R'= 2-Me	**14.7**
1f		R'= 4-Me	**6.02**
2a	Ar = Ph	R'= H	**3**
2b		R'= 2-OMe	**56**
2c	Ar = Mesityl	R'= H	**31**
2d		R'= 2-OMe	**143**
2e		R'= 2-Br	**332**
2f		R'= 4-Br	**15**
2g		R'= 2-F	**150**
2h		R'= 2,6-F_2	**785**
2e	Ar = 2,4,6-$Cl_3C_6H_2$	R'= H	**39**
2f		R'= 2-OMe	**601**
2g	Ar = C_6F_5	R'= 2-OMe	**521**
3a	Ar= Ph	R'= 2- (*E*)-$OCH_2CH{=}CHCO_2Et$	**27**
3b	Ar= 4-$OMeC_6H_4$		**31**
3c	Ar= 4-FC_6H_4		**28**
3d	Ar= 2,4,6-$Cl_3C_6H_2$		**336**
3e	Ar = 2,6-$(OMe)_2C_6H_3$		**1283**
3f	Ar = Mesityl		**140**

Starting conditions: Entry 1, aldehyde (0.04 M), NHC precatalyst (0.04 M) in CD_3OD and Et_3N:$Et_3N{\cdot}HCl$ (2:1, 0.18 M) buffer at 25 °C. Entry 2, aldehyde (0.01 M), NHC precatalyst (0.002 M) in CD_2Cl_2 and Et_3N (0.002 M) at 25 °C. Entry 3, aldehyde (0.04 M), NHC precatalyst (0.008 M) in CD_2Cl_2 and Et_3N (0.008 M) at 25 °C.

First, the effect of *para*-substituent of aldehyde on K_{exp} could be assessed. Comparing with entries **1a** and **1c** for the *N*-phenyl catalyst shows the largest observed effect of a *para*-substituent: a 4-methoxy substituent decreases K_{exp} by 5.9-fold. *Para*-methyl and fluoro substituents also decrease K_{exp}, however, only by 1.9 and 1.6-fold, respectively (Entries **1a** versus **1d** and **1f**). Similarly for the *N*-mesityl catalyst, a 4-bromo substituent decreases K_{exp} but by only 2-fold (Entries **2c** versus **2f**). Overall, all *para*-aldehydic substituents resulted in a decrease in K_{exp} irrespective of whether the substituent was electron donating or withdrawing, however, these changes were relatively small. Similarly, the effect of a *para*-substituent of catalyst on K_{exp} was very small. Comparing entries **3a**, **3b** and **3c** show almost identical K_{exp} values for reaction of the same aldehyde with *para*-H, *para*-OMe and *para*-F-phenyl catalysts[130, 132, 151].

By contrast, the effect of *ortho*- (2-) substituents on catalyst or aldehyde consistently show large increases in K_{exp} with this effect being larger for 2-heteroatom compared with 2-alkyl substituents. One potential explanation is that an intramolecular hydrogen bond between the developing adduct OH and the 2-substituent on catalyst or aldehyde could favour adduct formation (shown in Figure 1.8 for a 2-substituent on aldehyde)[151].

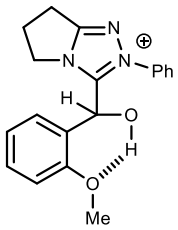

Figure 1.8: Proposed intramolecular hydrogen bond

Existing X-ray crystal structural data for triazolium catalysts support non-coplanarity between the *N*-aryl moiety and triazolyl ring in the presence of 2-substituents. This catalyst conformation may allow easier steric accommodation of the hydroxyaryl moiety, thereby increasing the K_{exp} values[131].

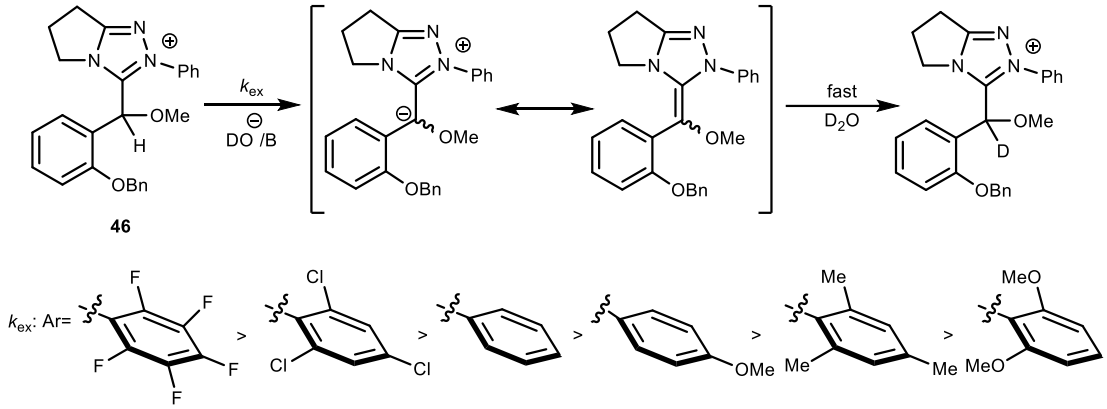

Scheme 1.32. Relative acidities of 3-(methoxybenzyl)azolium salt[131]

To study the acidity of C(α)-H on adducts **35**, in order to determine rate constants for Breslow intermediate formation, the deuterium exchange study of methylated adduct **46** was also undertaken (Scheme 1.32). O-Methylation of the hydroxyaryl adducts was initially performed in order to block decomposition back to aldehyde. It was found that the more electron-deficient adducts provide larger rate constants for Breslow intermediate formation, irrespective of whether the electron withdrawing substituent was on catalyst or aldehyde. This constitutes a normal electronic substituent effect on carbon acidity and there is no evidence of steric acceleration as had been proposed in the literature[131].

1.7. Project aims

As mentioned previously in Section 1.5, some deuterium incorporation back into reactant aldehyde was observed during kinetic analysis of benzoin condensation catalyzed by triazolium salts. Although this was not investigated in detail, it was noted that the use of *N*-aryl mesityl substituent slightly increased the extent of deuterium corporation into deuterated aldehyde in competition with benzoin[151]. We can hypothesize that sterically bulky *ortho*-alkyl substituents on catalyst can potentially suppress the onward reaction of Breslow intermediate to give benzoin product whilst still allowing the reverse deuteration towards aldehyde. The aim of my project is to probe whether the use of bulkier *ortho*-alkyl substituted aryl group on the triazolyl

catalyst can further promote the reverse deuteration to d^1 deuterated aldehyde in competition with benzoin formation. In a broader context, the selectivity of Breslow intermediate towards reaction with a range of different synthetically relevant acceptors is not fully understood. In fact, to date, there is no direct quantification of the nucleophilicity of the Breslow intermediate towards synthetically relevant substrates. Our broader research interests are focused on a quantitative understanding, and the competition between, re-deuteration versus benzoin condensation in this process.

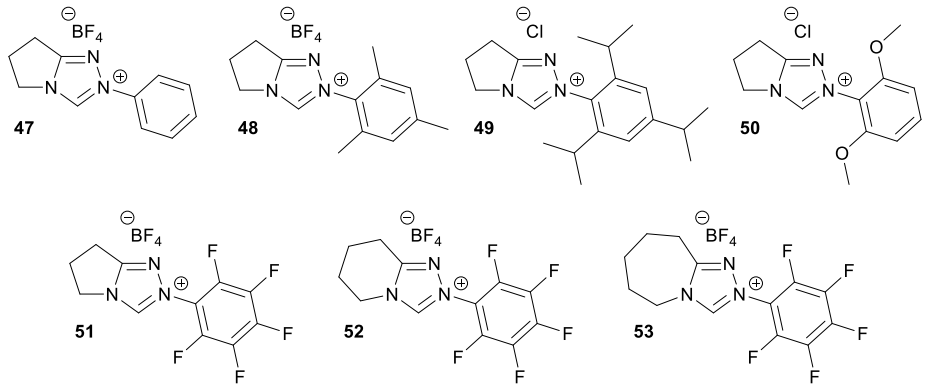

Figure 1.9. Structure of seven *N*-aryl substituted bicyclic triazolyl candidates 47-53 for preparation

Initially, my project aims to prepare synthesize several triazolyl precatalyst with various aryl substituents, especially the bulky *ortho*-di- or tri-isopropyl substituted phenyl triazolium salt (Figure 1.9). Moreover, my aim was also to probe these catalysts quantitatively in the benzoin condensation. In particular, we hoped to establish the reaction preference of the Breslow intermediate between benzoin and deuterated adduct through kinetic studies. Therefore, we aim to work towards an efficient organocatalytic synthetic route towards d^1 deuterated aldehydes.

Chapter 2. Syntheses of Triazolium salts

2.1. General Procedure

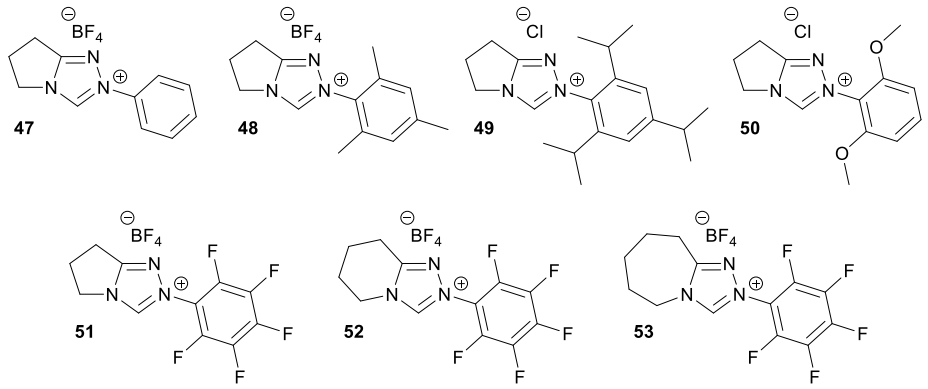

Figure 2.1 Structure of seven *N*-aryl substituted bicyclic triazolium salts 47-53

Seven *N*-aryl substituted bicyclic triazolium salts **47-53** were synthesized through the general procedure illustrated in Figure 2.1. The synthetic details for preparation of **47**, **48** and **50-53** were based on a range of published literature procedures[154-161]. There was no reported synthetic pathway directly towards **49**. The following sections provide detailed information of the syntheses of **47-53**.

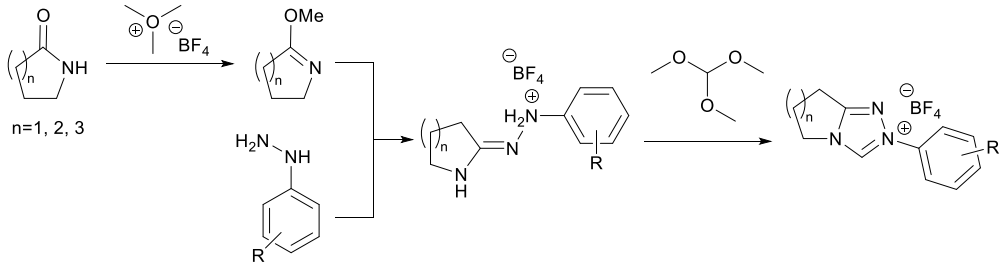

Scheme 2.1. General procedure for triazolium salt formation

2.2. 2-Phenyl-6,7-dihydro-*5H*-pyrrolo[2,1-c][1,2,4]triazol-2-ium tetrafluoroborate 47

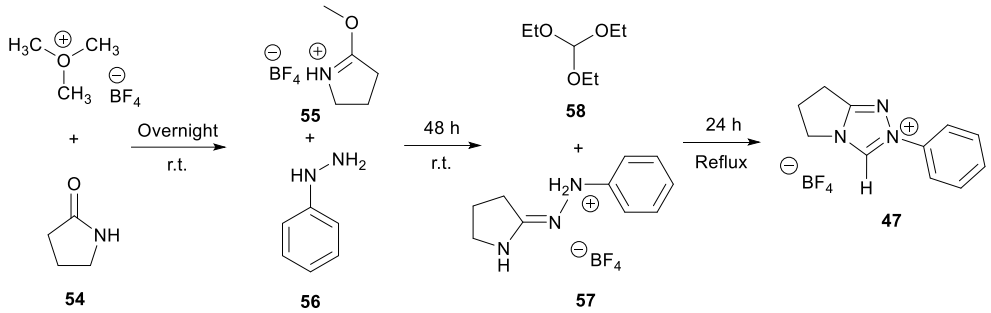

Scheme 2.2. Synthetic procedure towards 2-phenyl-6,7-dihydro-5*H*-pyrrolo [2,1-c][1,2,4] triazol-2-ium tetrafluoroborate 47

The synthesis of phenyl triazolium salt **47** followed the procedure illustrated in Richard Massey's thesis[151], based on a publication by Rovis[161], and outlined in Scheme 2.2. Methylation of 2-pyrrolidinone **54** provided imino ether **55**, followed by the addition of commercially available phenyl hydrazine **56** resulting in amidrazone **57**. Finally, the cyclization of amidrazone **57** under reflux in chlorobenzene and triethylorthoformate **58** yielded the product **47** in 52% yield.

2.3. 2-Mesityl-6,7-dihydro-5*H*-pyrrolo[2,1-c][1,2,4]triazol-2-ium tetrafluoroborate 48

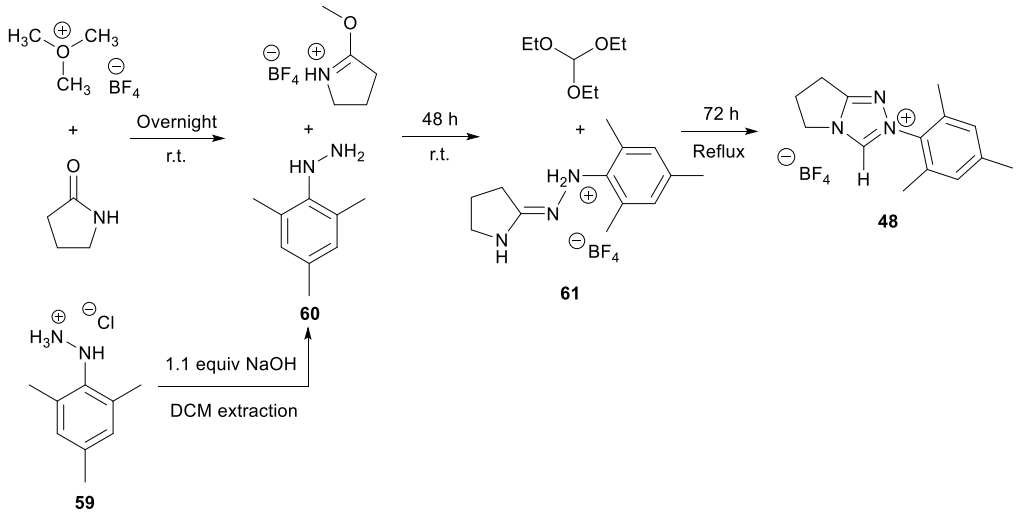

Scheme 2.3. Synthetic procedure towards 2-mesityl-6,7-dihydro-5*H*-pyrrolo[2,1-c] [1,2,4]triazol-2-ium tetrafluoroborate 48

In the case of the synthesis of the *N*-mesityl triazolium salt **48**[151], the mesityl hydrazine hydrochloride **59** was commercially available rather than the neutral hydrazine **60**. To generate the free hydrazine, neutralization was achieved by the addition of sodium hydroxide solution followed by dichloromethane extraction. Since there was a possibility for hydrolysis of the hydrazine under these conditions, an NMR based study was undertaken to assess the stability of 2,4,6-trimethyl phenyl hydrazine **60**.

2,4,6-Trimethyl phenyl hydrazine hydrochloride (**59**, ~5 mM) was mixed with 1.1 equivalents sodium hydroxide solution (1M), and deuterated dichloromethane (CD_2Cl_2) was utilized to extract the mesityl hydrazine. NMR spectroscopy was used to trace both the aqueous and organic phases at regular intervals.

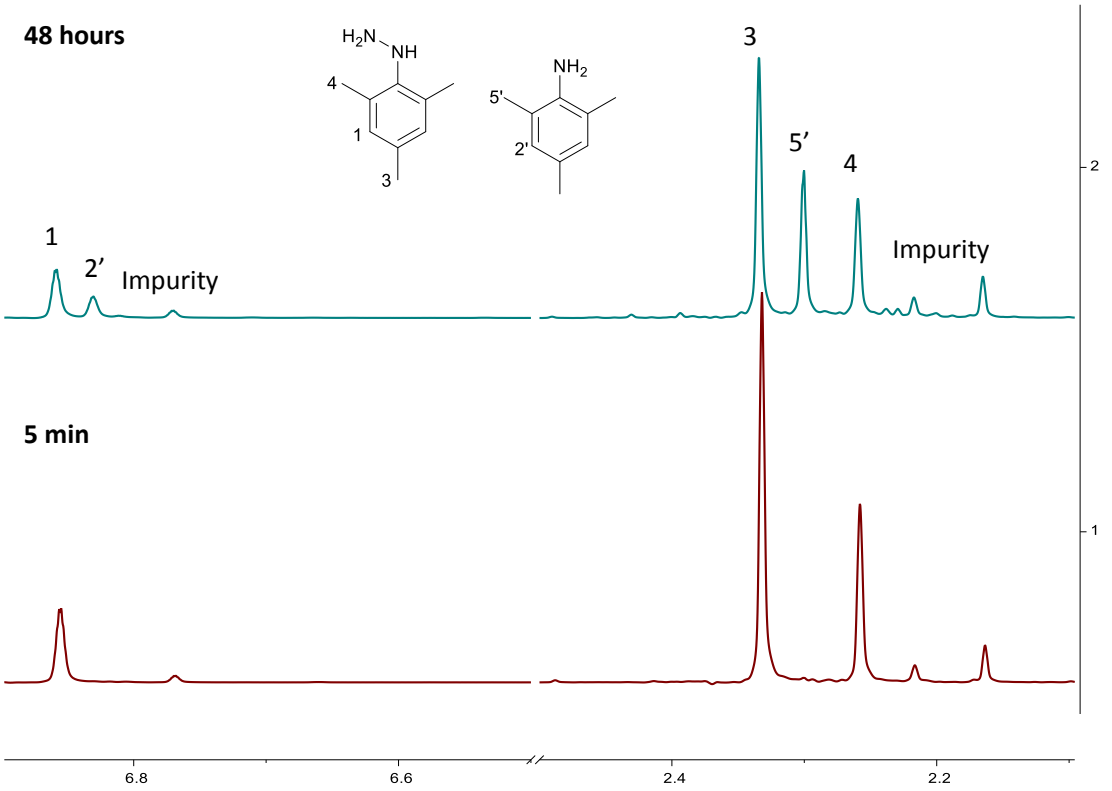

Figure 2.2. Representative NMR spectra of CD_2Cl_2 layer containing 2,4,6-trimethyl phenyl hydrazine 60 with extraction after 5 min and 48 hours, respectively, subsequent to mixing with sodium hydroxide solution.

The partitioning of the mesityl hydrazine largely favoured the organic phase, as no hydrazine signals could be found in the aqueous phase by NMR spectroscopy. According to Figure 2.2, no significant decomposition can be observed within the first few hours. After 48 hours, approximately one-third of the hydrazine had reacted. ^1H NMR spectral details are most consistent with the formation of mesityl aniline (2 singlet ArH, 2 broad NH, 9 singlet CH_3).

Compared with the phenyl triazolium salt **47**, the cyclization process of the amidrazone **61** to triazolium salt **48** required an extra 48 hours of reflux according to Rovis et al (72 hours in total). It could be assumed that the increased electron density and steric hindrance provided by the extra *ortho*-methyl groups near the reaction center may hinder the cyclization.

The crude product was obtained as a sticky red solid, with some white crystal formed on the sides of round-bottomed flask. The crude product was further triturated with ethyl acetate to give the product **48** as a brown coloured solid in 92% yield. Initially it was speculated whether further crystallization could be achieved towards mesityl product, thus slow evaporation of the mesityl triazolium salt's solution in chloroform was undertaken in an NMR tube to give yellow/white crystals. The crystal structure was obtained by single X-ray crystallography, which suggested a monoclinic package, with the mesityl group orthogonal to the triazolium (Figure 2.3).

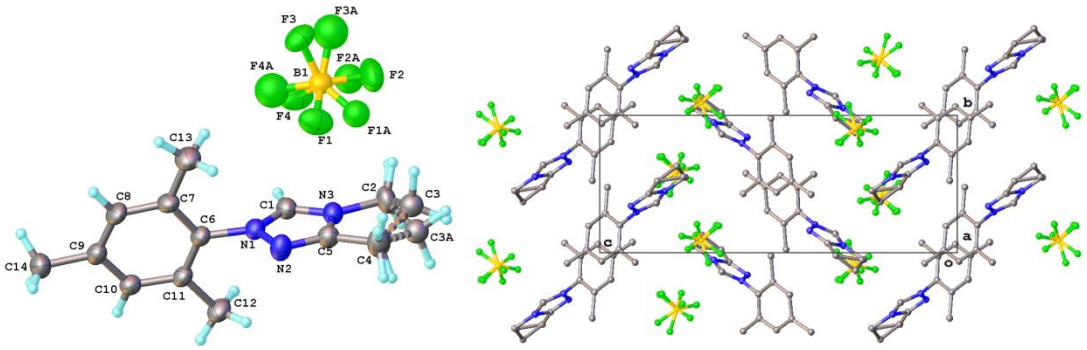

Figure 2.3. Crystal structure of 2-mesityl-6,7-dihydro-5*H*-pyrrolo[2,1-c][1,2,4] triazol-2-ium tetrafluoroborate 48

2.4. 2-Pentafluorophenyl-6,7-dihydro-*5H*-pyrrolo[2,1-c][1,2,4]triazol-2-ium tetrafluoroborate 51

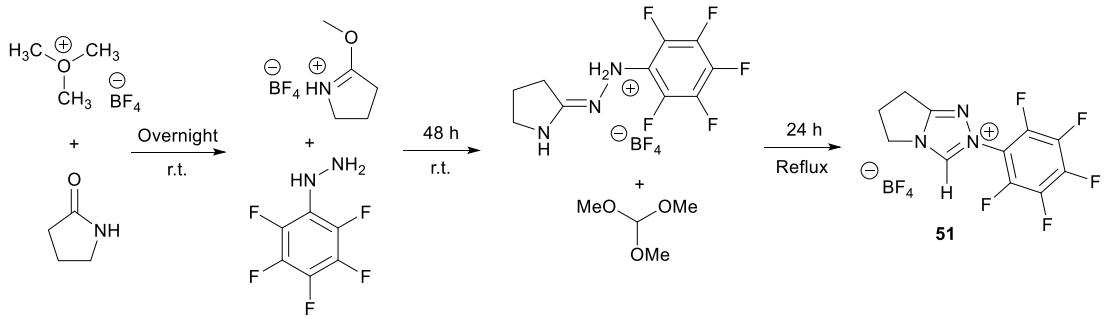

Scheme 2.4. Synthetic procedure towards 2-pentafluorophenyl-6,7-dihydro-*5H*-pyrrolo[2,1-c][1,2,4]triazol-2-ium tetrafluoroborate 51

The synthetic procedure towards pentafluorophenyl triazolium salt **51** was identical to

that used for the phenyl triazolium salt **47**, apart from the final purification[151]. The pentafluorophenyl group largely decreased the product's solubility both in polar and non-polar solvents, leading to the agglomeration of some needle like crystals, however, some impurities were visible inside the crystal package. Trituration from ethyl acetate and diethyl ether for several times provided the product as a pale yellow powder with 67% yield. Slow evaporation of recrystallization solvent in methanol over 15 days at room temperature provided some crystals, however, too small for crystallography. Therefore, a slower evaporation method should be undertaken to access suitable crystals.

2.5. 2-Perfluorophenyl-5,6,7,8-tetrahydro-[1,2,4]triazolo[4,3-a]pyridin-2-ium tetrafluoroborate 52

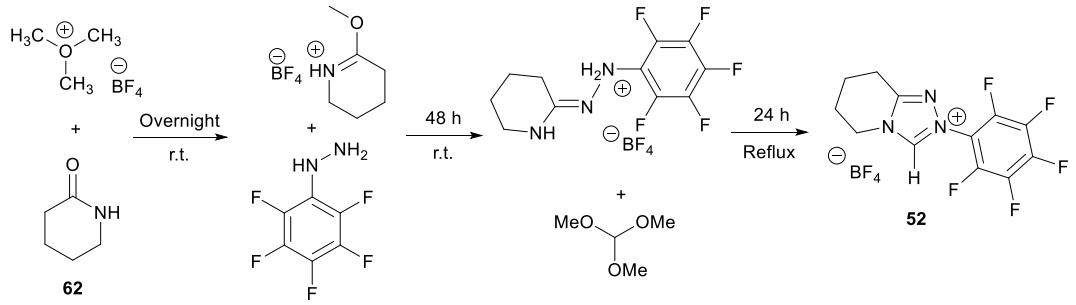

Scheme 2.5. Synthetic procedure towards 2-Perfluorophenyl-5,6,7,8-tetrahydro-[1,2,4]triazolo[4,3-a]pyridin-2-ium tetrafluoroborate 52

The synthetic procedure used to access the 2-perfluorophenyl -5,6,7,8-tetrahydro-[1,2,4]triazolo[4,3-a]pyridin-2-ium tetrafluoroborate **52** was closely similar to that used for 5-membered pyrrolidinone derivative **51**, instead using 2-piperidone **62** to introduce a six-membered fused ring[156, 161]. The solubility of the product in organic solvents was increased likely due to the larger aliphatic ring size, which resulted in an easier trituration process. The triazolium salt was obtained as a white needle like solid in 56% yield.

2.6. 2-Perfluorophenyl-6,7,8,9-tetrahydro-*5H*-[1,2,4]triazolo[4,3-a] azepin-2-ium Tetrafluoroborate 53

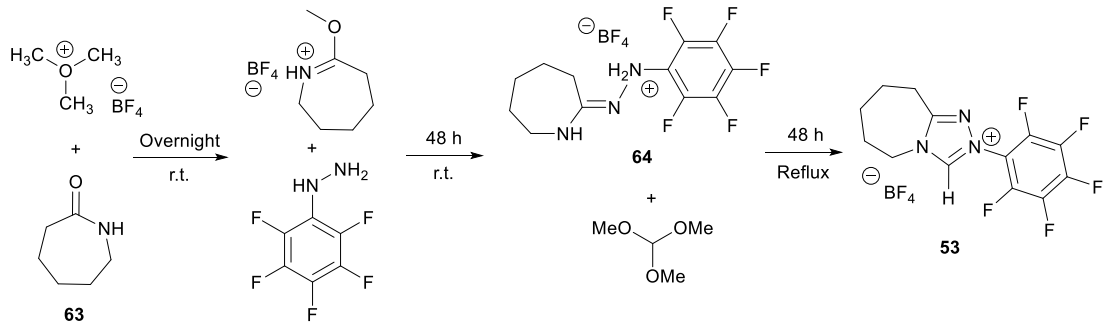

Scheme 2.6. Synthetic procedure towards 2-perfluorophenyl-6,7,8,9-tetrahydro-*5H*-[1,2,4]triazolo[4,3-a]azepin-2-ium tetrafluoroborate 53

Apart from the usage of *ε*-caprolactam **63** to introduce the seven-membered fused ring, and the final purification process, the synthetic procedure of the title compound was similar to those used to access the five- and six-membered ring analogues **51** and **52**[156].

During the procedure for formation of amidrazone **64**, a solid precipitate was observed. Mass spectrometry suggested the solid might be the corresponding amidrazone, and TLC suggested several new compounds formed possibly including **64**. However, none of the subsequent purification methods (trituration, recrystallization, slow evaporation) were successful in further identification and isolation of pure amidrazone.

The solubility of the triazolyl product **53** was further increased in organic solvents compared with pentafluoro triazolium salts **51** and **52**. The accompanying impurities, however, also appeared to be more soluble and, therefore, the purification of the title compound **53** proved extremely difficult. The crude product was obtained as a viscous dark brown oil after the removal of solvent. Repeated multi-phase recrystallization (×5) from dichloromethane: diethyl ether generated a brown oil of much-improved

purity. Further repeated multi-phase recrystallization (×10) from chloroform: diethyl ether provided the crucial product as a beige solid. Washing with toluene several times removed further the remaining insoluble impurities as a brown oil, leaving the title compound **53** as colorless needle-like crystals. In total two litres of solvent were used in the purification process. Through slow evaporation of the filtrate from the multi-phase recrystallization, more triazolium salt **53** was obtained, and the total yield was increased from 18% to 27%.

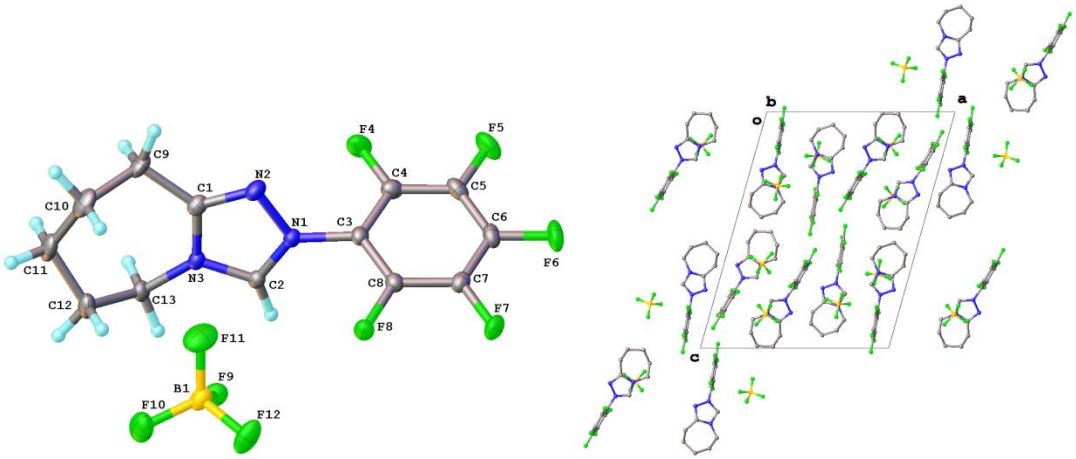

Figure 2.4. Crystal structure of 2-perfluorophenyl-6,7,8,9-tetrahydro-*5H*-[1,2,4] triazolo[4,3-a]azepin-2-ium tetrafluoroborate 53

This slow evaporation of methanol solvent yielded transparent, needle like crystals suitable for X-ray crystallography. Figure 2.4. shows the crystal structure of **53** highlighting the monoclinic crystal packaging of the title compound, with the pentafluorophenyl group orthogonal to the triazolium ring.

In parallel experiments, another slow evaporation was undertaken of a methanol solution of mainly pentafluorophenyl triazolium salt **53** (judged from an initial test NMR spectrum prior to dissolution). However, single X-ray crystallography in this case showed the presence of dimethoxy acetal adduct **65** rather than the triazolium salt **53**, and the triclinic crystal packaging is illustrated by Figure 2.5.

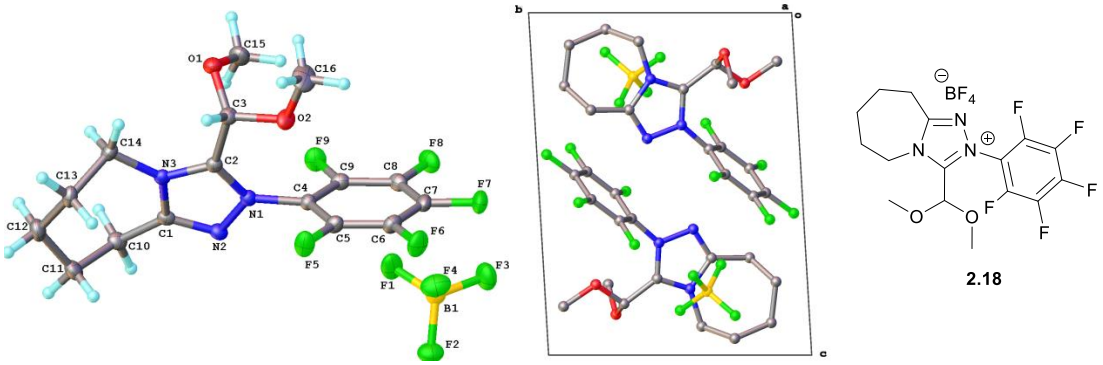

Figure 2.5. Crystal structure of dimethoxy acetal adduct of 2-perfluorophenyl-6,7,8,9-tetrahydro-*5H*-[1,2,4]triazolo[4,3-a]azepin-2-ium tetrafluoroborate 65

To access an NMR spectrum of the adduct **65**, all the solid obtained from slow methanol evaporation was dissolved in DMSO-d_6. As Figure 2.6 suggests, triazolium salt **53** still remained as the *C6'* peak at 10.57 ppm was clearly visible, however, at a decreased relative concentration. The 6.16 and 3.39 ppm peaks may correspond to the methinyl proton at the *C6* position and the six methoxyl protons (*C7*), respectively.

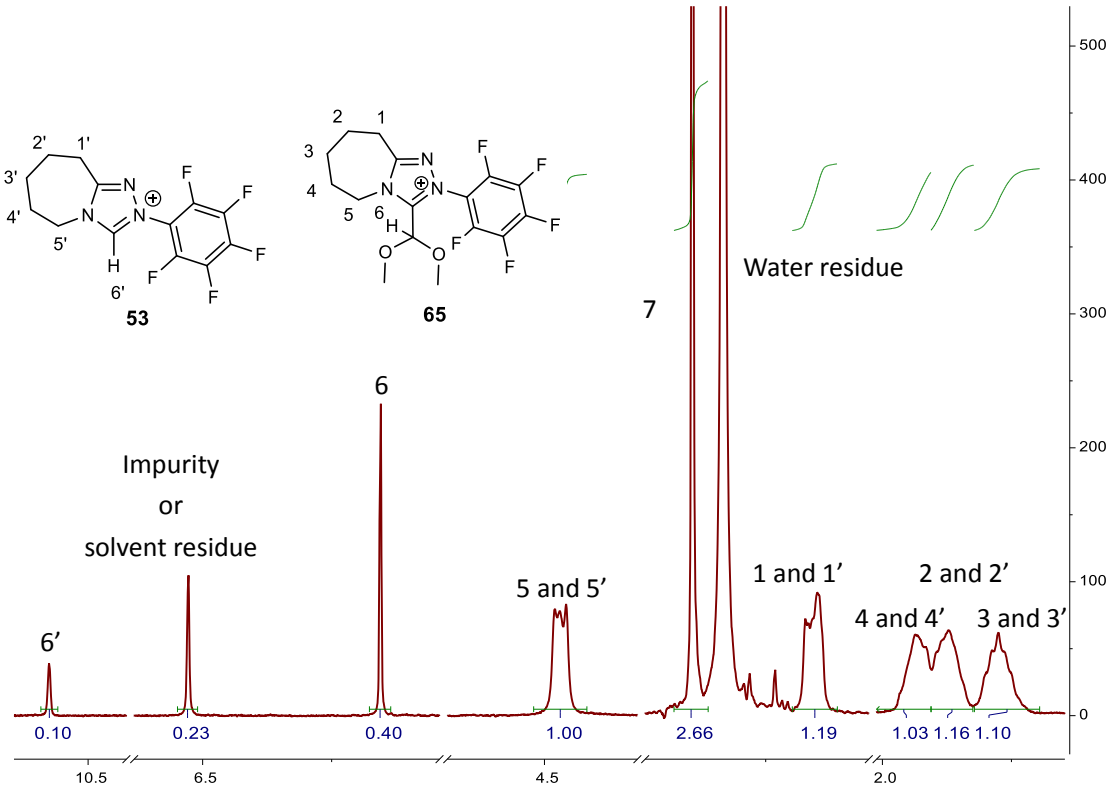

Figure 2.6. NMR spectrum in DMSO-d_6 of the dimethoxy acetal adduct 65 along with the triazolium salt 53.

Furthermore, the integrations of peaks due to protons on the 7-membered fused ring corrected to the area of one hydrogen are similar to the sum of the adduct and triazolium salt (from the *C6* and *C6'* peaks), which suggested the overlap between these two molecules. However, there are still a number of unidentified peaks. Thus further purification would be necessary to access clearer spectroscopic evidence for dimethoxy acetal adduct **65**.

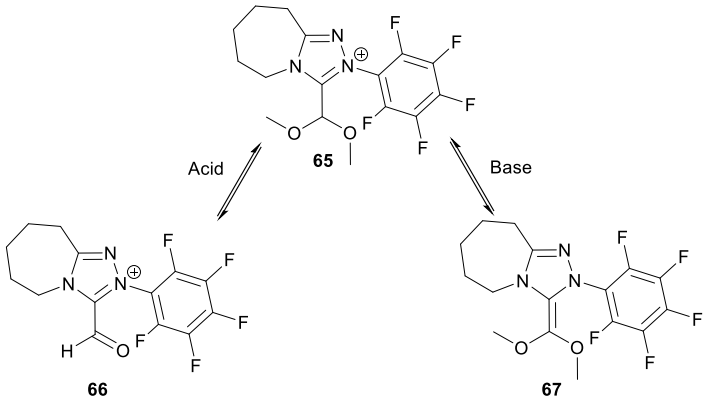

Scheme 2.7. Application of the 2-perfluorophenyl-6,7,8,9-tetrahydro-*5H*-[1,2,4] triazolo[4,3-a]azepin-2-ium tetrafluoroborate dimethoxy acetal adduct 65

This adduct **65** can be seen as a useful precursor to potentially useful NHC derivatives: in acidic conditions, NHC-formaldehyde **66** could result, while basic conditions may provide access to Breslow intermediate **67** (Scheme 2.7). Fortuitously, this dimethoxy acetal adduct **65** has not been reported previously, and neither has NHC-formaldehyde **66** and potential Breslow intermediate **67** to our knowledge. Furthermore, there are no reports of simple structural variants of the above molecules on Reaxys and Chem Spider.

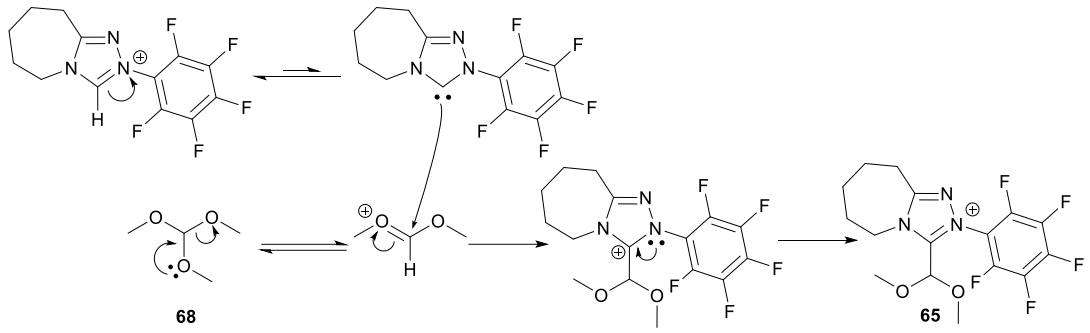

Scheme 2.8. Possible mechanism of the dimethoxy acetal adduct's formation

One possible mechanism of dimethoxy acetal adduct formation is illustrated in Scheme 2.8. The small amount of carbene present at equilibrium may attack the oxacarbenium ion generated from trimethylorthoformate **68** present in excess (50 equivalents). Finally resulting in the adduct **65**. To obtain some proof for this mechanism, pure pentafluorophenyl triazolium salt **53** was dissolved in excess trimethyl orthoformate, and refluxed for 24 hours. Figure 2.7 includes the mass spectral analysis of the reaction outcome, which provides the evidence of adduct formation: at 1.78 minute (retention time), a peak of correct molecular weight (m/z 378) can be observed, however, other impurities are clearly present. The subsequent purification proved to be difficult, and a further, more-detailed synthetic evaluation of the adduct's formation including mechanistic studies will be performed during the initial stage of my PhD programme.

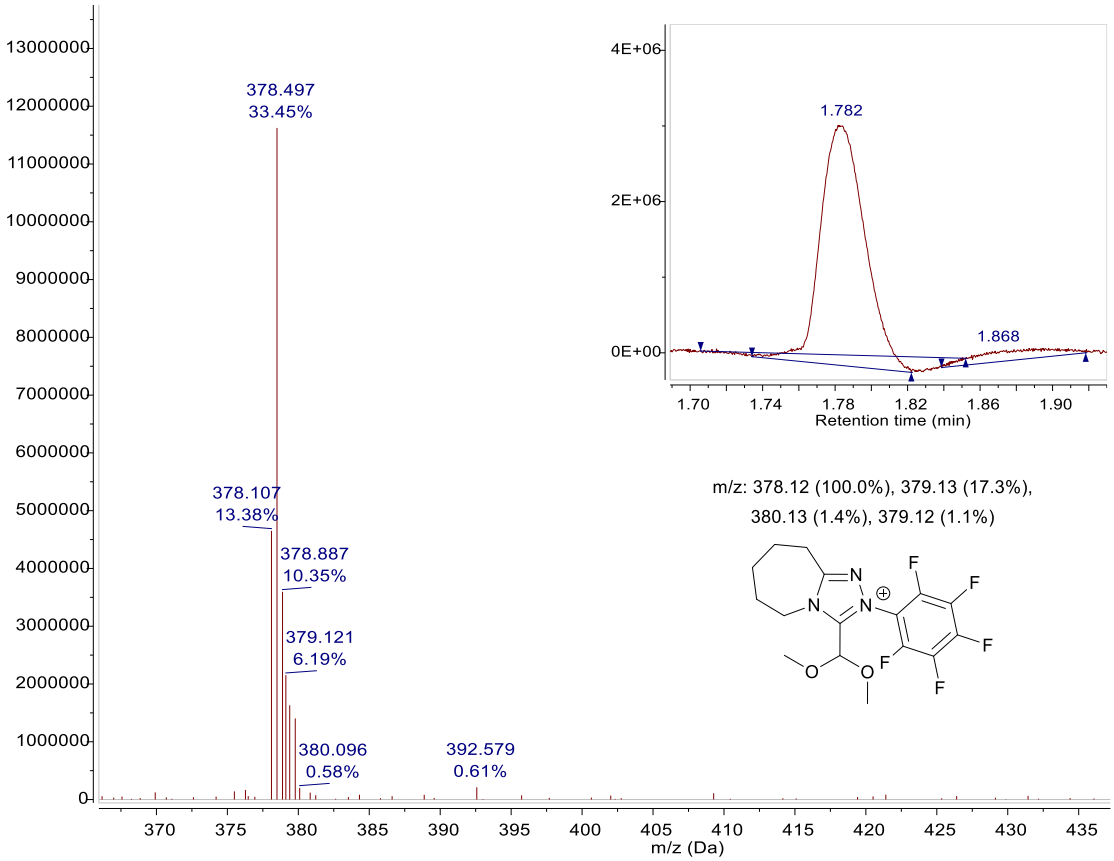

Figure 2.7. Mass spectrum of solution containing the dimethoxy acetal adduct 53

2.7. 2-(2,6-Dimethoxyphenyl)-6,7-dihydro-*5H*-pyrrolo[2,1-c][1,2,4]triazol-2-ium chloride 50

2.7.1. Synthesis of di-*tert*-butyl 1-(2,6-dimethoxyphenyl)hydrazine-1,2-dicarboxylate 69

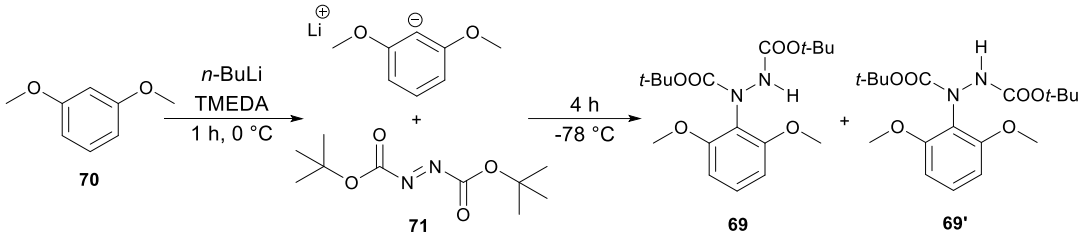

Scheme 2.9. Synthetic procedure towards the two conformational isomers of di-*tert*-butyl 1-(2,6-dimethoxyphenyl) hydrazine-1,2-dicarboxylate 69 and 69'

Unlike the previous aryl hydrazines utilized synthetically, the dimethoxyphenyl hydrazine and corresponding hydrochloride salt are not commercially available. A DBAD-protected precursor to the dimethoxyphenyl hydrazine could be accessed by the procedure generated by Scheme 2.9[154, 155]. Deprotonation of dimethoxybenzene **70** by *n*-butyl lithium, followed by the addition of di-*tert*-butyl diazo-1,2-dicarboxylate **71** (DBAD) to the lithiated component, generated the crude DBAD-protected hydrazine as a yellow oil. Further purification by column chromatography yielded the pure product as a white/yellow sticky solid, where it existed as a 2.5:1 mixture of carbamate conformational isomers **69** and **69'** in solution. Owing to the two *ortho*-methoxyl groups to the reaction center, the lithiation of 1,3-dimethoxybenzene **70** was relatively straightforward, with only small amount of unidentified by-products observed.

The synthesis of the DBAD-protected hydrazine **69**, **69'** was repeated several times with different equivalents of reagents and different aging of the *n*-BuLi solution (Section 4.3.6.1, Table 4.2, page 95). The optimal yield of the Boc-protected hydrazine **69** and **69'** of 78% was obtained by using 1.5 equivalents, freshly opened lithiation reagent.

2.7.2. Kinetic investigation of ortho-lithiation of 2,6-dimethoxyl benzene 70

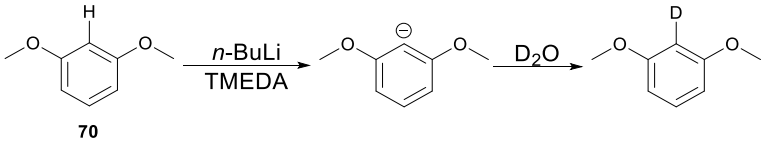

70

Scheme 2.10. Quantification of lithiation of 1,3-dimethoxybenzene 70

A kinetic investigation by NMR spectroscopy was undertaken to estimate the best lithiation conditions. After mixing *n*-butyl lithium (opened for 4 months, 1 equiv) with tetramethylethylene diamine (TMEDA, 1 equiv) and 1,3-dimethoxybenzene **70** (1

equiv) at 0 °C under argon, a small portion of the mixture was taken out by syringe of various time intervals, and quenched immediately with deuterium oxide. The time intervals were mainly limited by the washing of the syringes to prevent blocking by lithium salts. The extent of deuterium exchange of the aryl hydrogen in the 2-position was accessed by NMR.

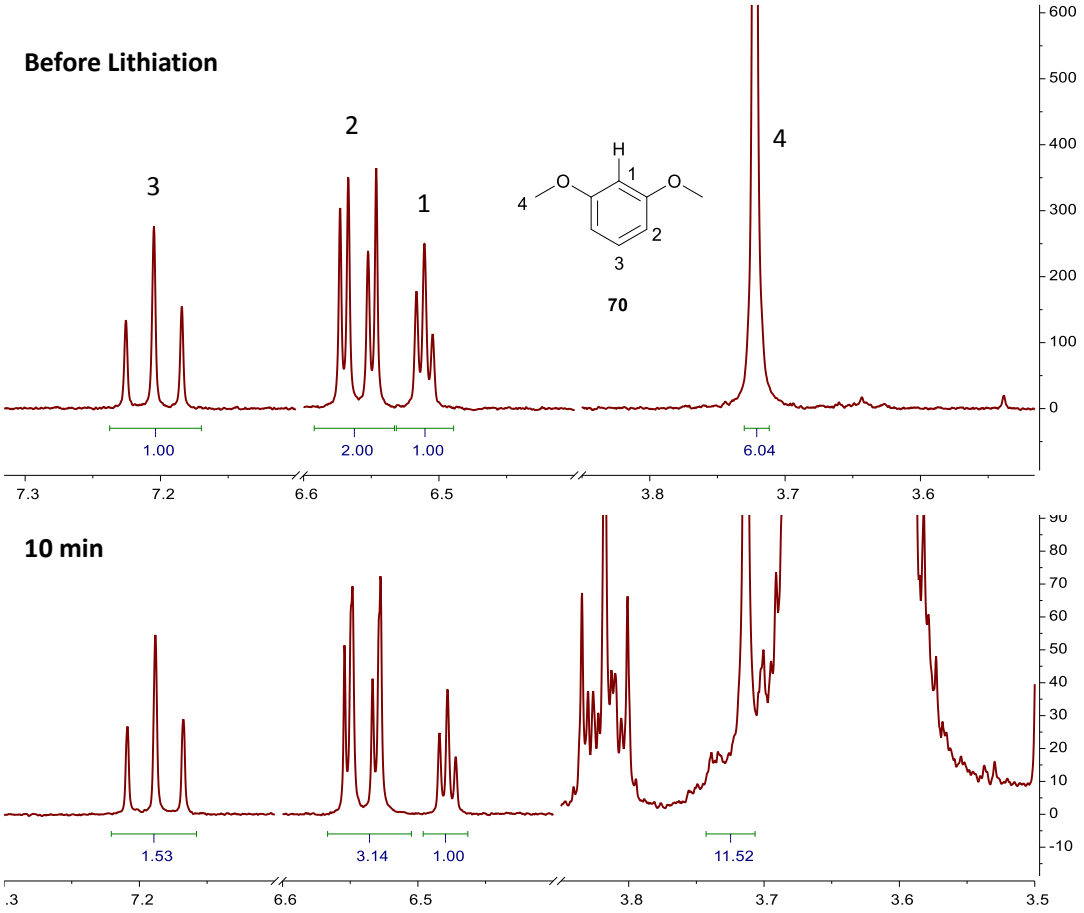

Figure 2.8. NMR spectra of *1)* 1,3-dimethoxybenzene 70 and *2)* reaction with BuLi for 10 minutes followed by quenching with D_2O

According to the NMR spectra (*e.g.* Figure 2.8), after lithiation and quenching with deuterium oxide, the integration of *H1* of 1,3-dimethoxybenzene was decreased compared with *H2*, *H3*, and *H4*. The unreacted 1,3-dimethoxybenzene was assigned by the triplet at 6.51 ppm (*H1)*. Using Figure 2.8, the percentage of the deuteration was ascertained by Equation 2.1 and 2.2, within which, *f*(s) represents the ratio of unreacted benzene substrate, %D suggested the deuteration degree. Figure 2.9

illustrates the trends in the % deuteration over time.

$$f(s) = A_{H1} / \left[\frac{1}{2}\left(A_{H_2}/2 + A_{H_3}\right)\right] \times 100\% \qquad \textbf{Equation 2.1.}$$

$$\%D = [1 - f(s)] \times 100 \qquad \textbf{Equation 2.2.}$$

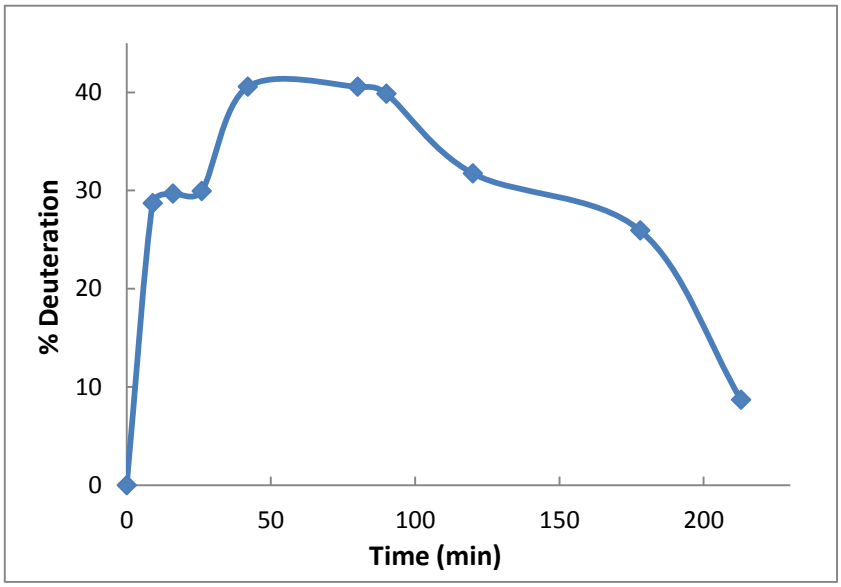

Figure 2.9. % Deuteration of 1,3-dimethoxybenzene 2.23

As the crude kinetic study suggested, the deuteration ratio reached the maximum after the addition of *n*-BuLi for 42 minutes, however, dropped substantially at later times. Furthermore, NMR spectrometry suggested the appearance of impurities after 90 minutes which could include decomposition products from the onwards reaction of the carbanion. Therefore, the best addition time for the DBAD reagent **71** should be 42-90 minutes after the start of lithiation.

However, although the optimal time identified is likely reliable, the test deuteration experiments underestimated the degree of lithiation as ultimately a 78% yield of DBAD-protected hydrazine could be obtained. The yield disparity was likely due to the age of the BuLi solution as concluded in Section 4.3.6.1 (page 95). Therefore, 1.5 equivalents of freshly opened lithiation reagent is suggested to be ideal.

2.7.3. Synthesis of 2-(2,6-Dimethoxyphenyl)-6,7-dihydro-5*H*-pyrrolo[2,1-c] [1,2,4]triazol-2-ium chloride 50

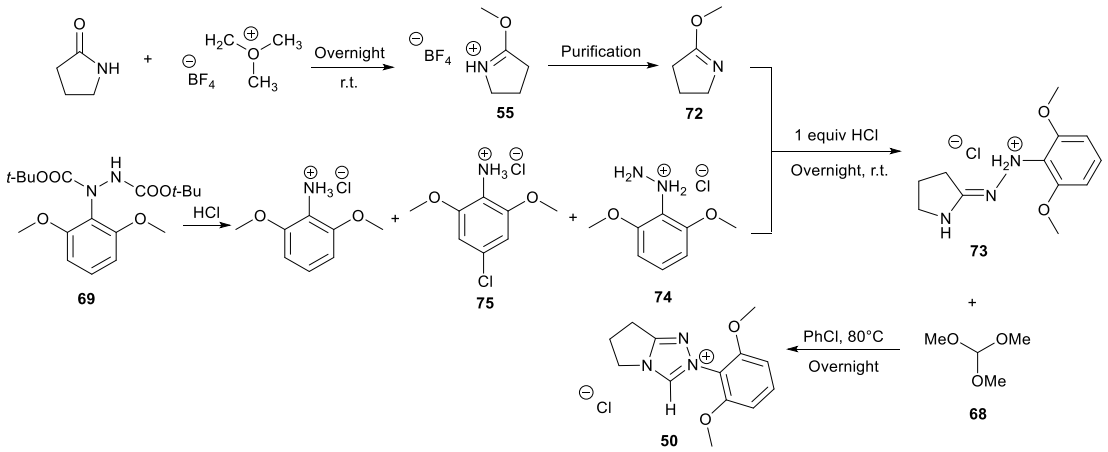

Scheme 2.11. Synthetic procedure towards 2-(2,6-dimethoxyphenyl)-6,7-dihydro -*5H*-pyrrolo[2,1-c][1,2,4]triazol-2-ium chloride 50

The synthetic procedure towards triazolium salt **50** was quite different to the previous triazolium salts **47**, **48**, **51-53**. According to literature[154, 155], the Boc-protected dimethoxyphenyl hydrazine **69** should be deprotected, followed by the addition of purified imino ether **72** to generate amidrazone **73** in acidic condition. The cyclization of amidrazone **73** with trimethyl orthoformate **68** involved an overnight heating at 80 °C and generated the crude triazolium salt as a brown sticky oil. Column chromatography yielded the dimethoxyl phenyl triazolium salt **50** as a dark brown oil with 16% yield.

According to Glorius[154, 155], the deprotection step towards the hydrazine hydrochloric salt **74** should also yield ~15% of 2,6-dimethoxy-4-chloroaniline **75**. Mass spectrometry also supported this observation, however, the mechanism of formation of chloro-aniline **75** is unknown, and there was no evidence supporting that chlorine was only added to the *para*- position.

Different from the synthesis of phenyl and mesityl triazolium salts **47** and **48**, and according to previous literature[154, 155, 159], all the amidrazone syntheses involving the direct usage of the hydrochloride salt of aryl-hydrazines require relatively pure imino ether. Therefore, the isolation and purification of imino ether was undertaken. However, there is no explanation towards the requirement of pure imino ether, and a further attempt may be needed to check if the amidrazone's formation will be affected by the addition of hydrazine hydrochloric salt directly into the imino ether solution. Furthermore, there is a disagreement about the necessity of HCl addition for amidrazone formation. According to Berkessel's procedure[159], it is possible to obtain a high yield of amidrazone only with a catalytic amount of hydrochloric acid, whereas Glorius suggests the use of one equivalent of HCl.

According to the Glorius procedure[154, 155], the final cyclization towards the triazolium salt **50** utilized triethyl orthoformate, 4 Å molecular sieves and one equivalent of hydrochloric acid. Our experiments utilized trimethylorthoformate, and were performed in the absence of molecular sieves and HCl. Fortunately, the yield surprisingly increased compared with the literature under these modified conditions (from 10 to 16%).

According to Glorius, the dimethoxyl phenyl triazolium salt **50** was obtained as a solid, and a crystal structure was reported[155]. A multi-phase recrystallization was undertaken to try to purify the crude product without column chromatography since the product proved relatively polar. Therefore, dichloromethane: diethyl ether recrystallization solvent mixtures followed by chloroform: diethyl ether systems were used. Several non-polar, soluble impurities (chlorobenzene and something unknown) were removed, and after multiple recrystallizations, a solid mixture was obtained, which converted to a sticky oil quickly after filtration. However, impurities still remained after recrystallization thus column purification proved necessary.

An attempt to synthesize the dimethoxylphenyl triazolium salt with a tetrafluoroborate counter ion was also undertaken. During the formation of amidrazone **73**, with small modifications to the previous synthesis, an excess of tetrafluoroboric acid-diethyl ether complex was added instead of HCl, which generated a large amount of white gas. In the final cyclization progress, a catalytical amount of tetrafluoroboric acid-diethyl ether complex was also added. Both NMR and mass spectrometry of the crude product both suggested the successful formation of triazolium cation, but further purification still needs to be attempted.

2.8. Synthesis of 2-[2,4,6-tri(2-propyl)phenyl]-6,7-dihydro-5*H*-pyrrolo[2,1-c][1,2,4]triazol-2-ium chloride 49

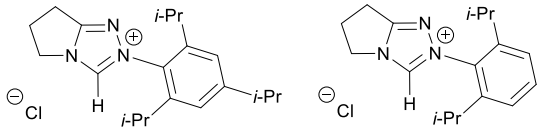

Figure 2.10. Structure of 2-[2,4,6-tri(2-propyl)phenyl]-6,7-dihydro-5*H*-pyrrolo[2,1-c][1,2,4]triazol-2-ium chloride 49 and diisopropylphenyl triazolyl precatalyst 76

There are no reported synthetic routes to tri-isopropyltriazolium salt **49** although di-isopropyltriazolium salt **76** has been prepared previously[159]. The precursor hydrazines and hydrazinium chlorides are not commercially available in either case. Three synthetic pathways were attempted to access the relevant hydrazine or hydrazinium chloride.

2.8.1. Attempted hydrazine synthesis from di-ortho-isopropylaniline 77

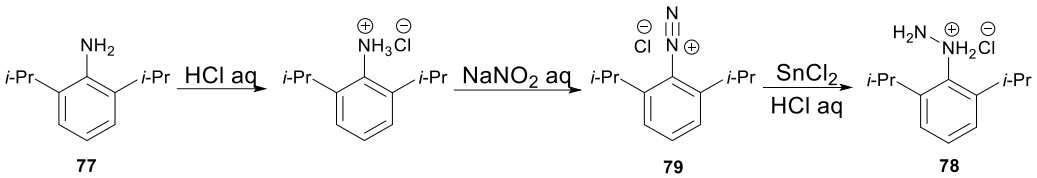

Scheme 2.12. Synthetic procedure towards *ortho*-diisopropylphenyl hydrazine hydrochloride 78 *via* di-*ortho*-isopropylaniline 77

Based on published synthetic procedures towards *ortho*-isopropyl phenyl, and di-*ortho*-methyl/chloro phenyl hydrazines[162-165], the commercially available 2,6-diisopropyl aniline **77** was first reacted in an acidified solution of sodium nitrite to give the diazonium salt, and tin(II) chloride was utilized in an attempted reduction to form the 2,6-di-isopropyl phenyl hydrazine hydrochloric salt **78**. However, this procedure was unsuccessful.

The two isopropyl groups largely decreased the solubility of the anilinium salt, and the addition of the hydrochloric acid required a thorough stirring and a very slow addition speed to avoid aggregation into a precipitate. The subsequent formation of the diazonium salt **79** always resulted in a thick layer of dark red solid, and subsequent aggregation after the addition of tin (ii) chloride, which prevented the successful reduction. Longer reaction times were attempted for the reduction of diazonium salt **79** to the 2,6-diisopropyl hydrazine hydrochloric salt **78**, however, only a trace amount of product could be detected by mass spectrometry.

2.8.2. Preparation of di-*tert*-butyl 1-(2,4,6-triisopropylphenyl) hydrazine-1,2-dicarboxylate (DBAD-protected hydrazine) *via* *Ortho*-lithiation

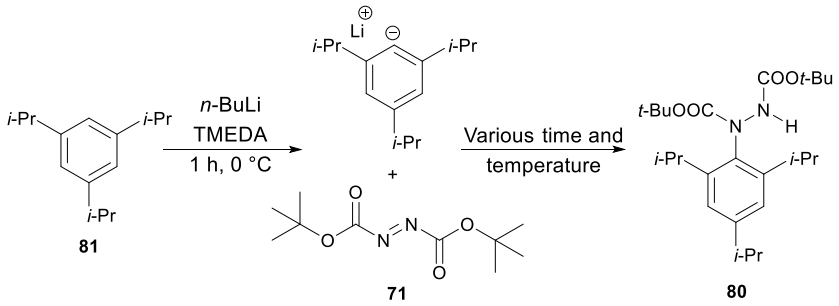

Scheme 2.13. Synthetic procedure towards Boc-protected triisopropyl phenyl hydrazine 80 *via* lithiation

Using the successful synthetic procedure of di-*tert*-butyl 1-(2,6-dimethoxyphenyl) hydrazine-1,2-dicarboxylate **69**[154, 155, 166], a similar methodology was attempted towards the preparation of di-*tert*-butyl 1-(2,4,6-triisopropylphenyl) hydrazine-1,2-dicarboxylate **80** using 1,3,5-triisopropyl benzene **81** as starting material.

By using the same method introduced in Section 2.7.2 (Page 45), a crude kinetic study was undertaken to quantify the possible deprotonation degree of the triisopropyl benzene, which suggested that no more than 20% of 1,3,5-triisopropyl benzene **81** could be deprotonated.

Three attempts were performed at this synthetic procedure with small variation of conditions summarized in Section 4.3.8.2 (Table 4.4, page 104). The reaction temperature and time were changed to see if the threshold provided by steric hindrance could be overcome. Some product formation was possible according to TLC, and column chromatography was undertaken to try to separate and analyze the components, however, no products were isolated.

2.8.3. Grignard reagent-based procedure towards di-*tert*-butyl 1-(2,4,6-triisopropylphenyl)hydrazine-1,2-dicarboxylate 80

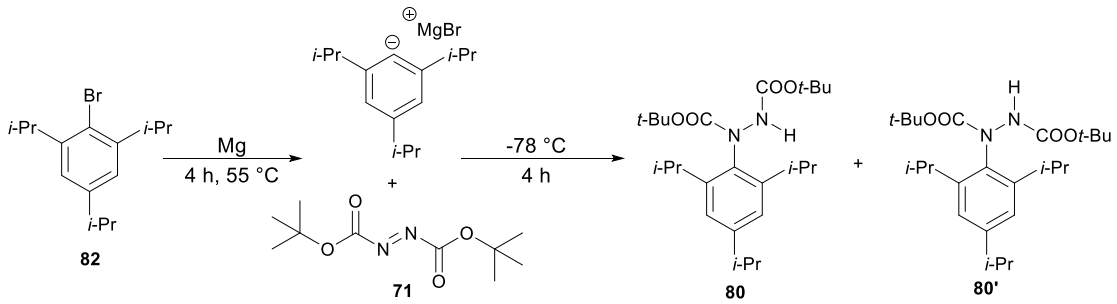

Scheme 2.14. Synthetic procedure towards Boc-protected triisopropyl phenyl hydrazine 80 and 80' *via* Grignard reagent generation

Based on a recently published procedure, 2-bromo-1,3,5-triisopropyl benzene **82** was utilized as the starting material to form a Grignard reagent[159, 167, 168]. As the Grignard reagent should be added into the DBAD solution *via* cannula, an excess amount of the magnesium turnings were used. Following addition of di-*tert*-butyl diazo-1,2-dicarboxylate (DBAD, **71**) to pre-formed Grignard reagent, the crude product **80** was obtained as a viscous yellow oil. Initially an excess of DBAD starting material was employed, however, this proved unnecessary (see Section 2.8.4).

An initial attempt was made at purification of **80** using column chromatography. Irrespective of the change in the eluant gradients, TLC suggested the product always came out as a mixture of three different spots. Two of the spots were assigned as the carbamate rotamers **80** and **80'**, while the component of the other spot was unknown. Both NMR and mass spectrometry did not provide any convincing evidence of product formation suggesting possible decomposition on the column. Therefore, the purification was abandoned, and the crude product was used directly in the following step.

2.8.4. 2,4,6-Triisopropylphenyl hydrazine hydrochloride 83

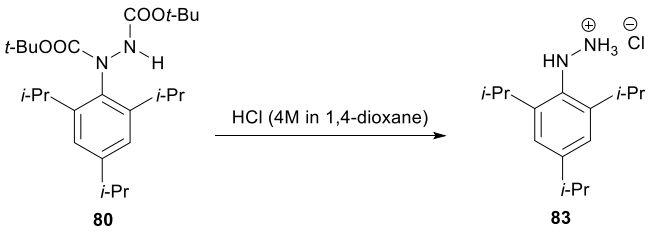

80 **83**

Scheme 2.15. Synthetic procedure towards 2,4,6-triisopropyl phenyl hydrazine hydrochloride 83

Based on procedure towards 2,6-bis(2-propyl)phenyl hydrazine hydrochloride **78**[159], deprotection of di-*tert*-butyl 1-(2,4,6-triisopropylphenyl)hydrazine-1,2-dicarboxylate **80** to give 2,6-bis(2-propyl)phenyl hydrazine hydrochloride **83**, was achieved by stirring at room temperature for 4 hours in HCl added to anhydrous methanol. After the removal of solvent, followed by diethyl ether and cold ethyl acetate washing, the title compound **83** was obtained as a pure white solid with 58% yield.

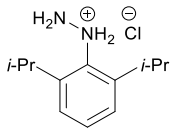

78

Figure 2.11. Structure of 2,6-bis(2-propyl)phenyl hydrazine hydrochloride 78

In contrast to the deprotection of di-*tert*-butyl 1-(2,6-dimethoxyphenyl) hydrazine-1,2-dicarboxylate **69** in Section 2.7.3, which generated 15% of inseparable *para*-chloro aniline **75**, the triisopropyl phenyl hydrazine hydrochloric salt **83** was obtained with good purity. This indicated the potential ability of *para*-substituents upon the blocking of chloro-aniline's formation. Furthermore, according to Klaubert's paper, the direct deprotection of the bis(*tert*-butoxycarbonyl) aryl-hydrazine species without column purification generally provides better yields[160].

2.8.5. Synthesis of 2-[2,4,6-tri(2-propyl)phenyl]-6,7-dihydro-5*H*-pyrrolo [2,1-c][1,2,4] triazol-2-ium chloride 49

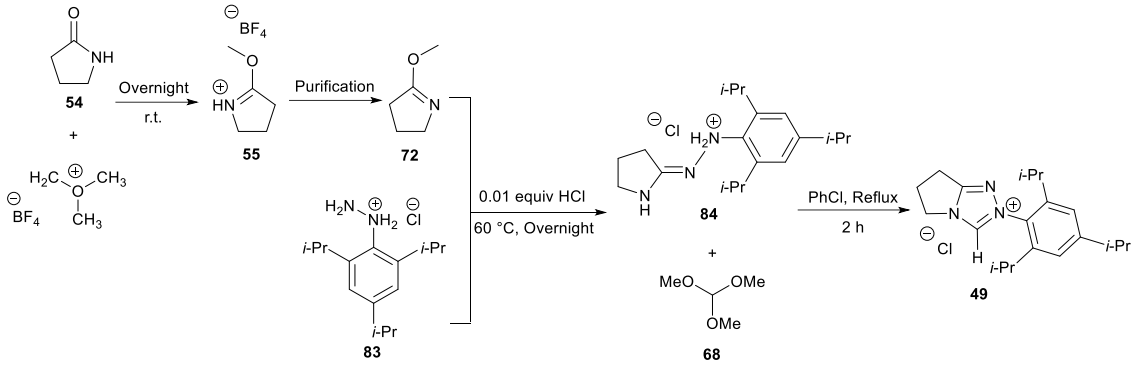

Scheme 2.16. Synthetic procedure towards 2-[2,4,6-tri(2-propyl)phenyl]-6,7-dihydro-5*H*-pyrrolo[2,1-c][1,2,4]triazol-2-ium chloride 49

Scheme 2.16 illustrated the pathway which successfully generated the title product **49**, while other attempted manipulations of each step will be discussed in the following paragraphs.

Based on the synthetic procedure used for the preparation of mesityl triazolium salt **49** in Section 2.3, the first methodology involves the methylation of 2-pyrrolidinone **54**, and without any purification, the neutralized triisopropyl hydrazine was added directly into the crude solution of imino ether **55**. However, only trace amount of amidrazone **84** was formed, and the subsequent cyclization failed. The failure of amidrazone formation might be due to the following 2 reasons: the steric hindrance provided by *ortho*-isopropyl group; and the fast decomposition speed of the neutralized triisopropyl phenyl hydrazine.

Before being mixed with imino ether **55**, the kinetic study introduced in Section 2.3 was also performed to quantify the decomposition speed of neutralized triisopropyl hydrazine. After being exposed to atmosphere for 10 hours, half of the hydrazine was consumed into aniline, which shows a much quicker decomposition speed than for the analogous mesityl hydrazine **60**.

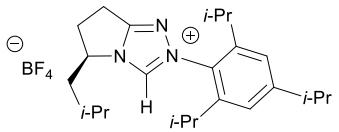

85

Figure 2.12. Structure of the (*R*)-5-isobutyl-2-(2,4,6-triisopropyl-phenyl) -6,7-dihydro-5*H*-pyrrolo[2,1-c][1,2,4]triazol-2-ium tetrafluoroborate 85

Interestingly, a recent paper claimed a successful synthesis of a similar triisopropyl phenyl triazolium salt **85** by using this procedure[169]. Therefore, further investigations might be undertaken towards this synthetic pathway.

Secondly, using the procedure successfully employed for the preparation of dimethoxyl phenyl triazolium salt **50**, the amidrazone **84** was attempted using purified imino ether **72**, followed by the addition of triisopropyl phenyl hydrazine hydrochloride **83**, and one equivalent of HCl (4M in 1,4-dioxane). However, after being stirred over 48 hours, only a trace amount of amidrazone **84** was formed, and the subsequent cyclization also did not work.

Fortunately, Berkessel's procedure towards 2-[2,6-di(2-propyl) phenyl]-6,7-dihydro-5H-pyrrolo[2,1-c][1,2,4] triazol-2-ium chloride **76** was successfully employed for the synthesis of the target triazolium salt **49**[159]. Aryl hydrazine hydrochloride **83** was mixed with purified imino ether **72**, with a catalytic amount of HCl (4M in 1,4-dioxane, <1%), and overnight heating at 60 °C under argon successfully yielding amidrazone. There was one attempt without any HCl addition, which only generated very small amount of amidrazone **84**, while with impurities and remaining aryl hydrazine hydrochloride **83**. Furthermore, compared with the procedure in Section 2.7.3, the heating at 60 °C was also vital to overcome the threshold provided by the *ortho*-diisopropyl group.

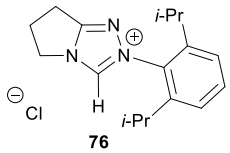

76

Figure 2.13. Structure of Berkessel's 2-[2,6-di(2-propyl) phenyl]-6,7-dihydro-5*H*-pyrrolo [2,1-c] [1,2,4] triazol-2-ium chloride 76

Unlike other synthetic procedures, the cyclization process to **49** was achieved by just a two hours reflux. To establish what would happen if refluxed for a longer time, one of the attempted final cyclizations was refluxed for 24 hours, which generated a dark brown solution. After the removal of solvent, a sticky brown oil was obtained. Part of the brown oil dissolved in hexane, and ethyl acetate could dissolve every component, while the triazolium salt **49** has a relatively lower solubility in ethyl acetate. Luckily, the hexane soluble component was recrystallized through slow evaporation, and single X-ray crystallography suggested it to be a formamide with monoclinic package. The mechanism for the formation of formamide by-product **86** is still unknown.

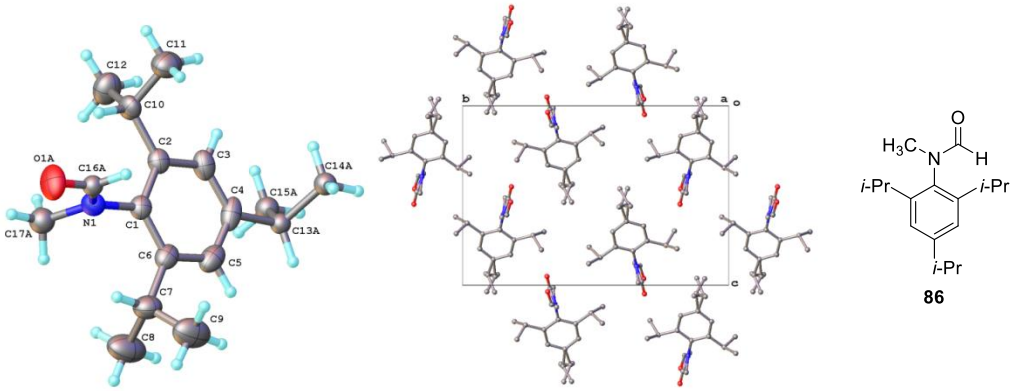

86

Figure 2.14. Crystal structure of the formamide species 86 obtained from hexane washing phase

2.9. Attempt towards the synthesis of 2-(2,6-dimethoxyphenyl)-5,6,7,8-tetrahydro-[1,2,4]triazolo[4,3-a]pyridin-2-ium tetrafluoroborate 87

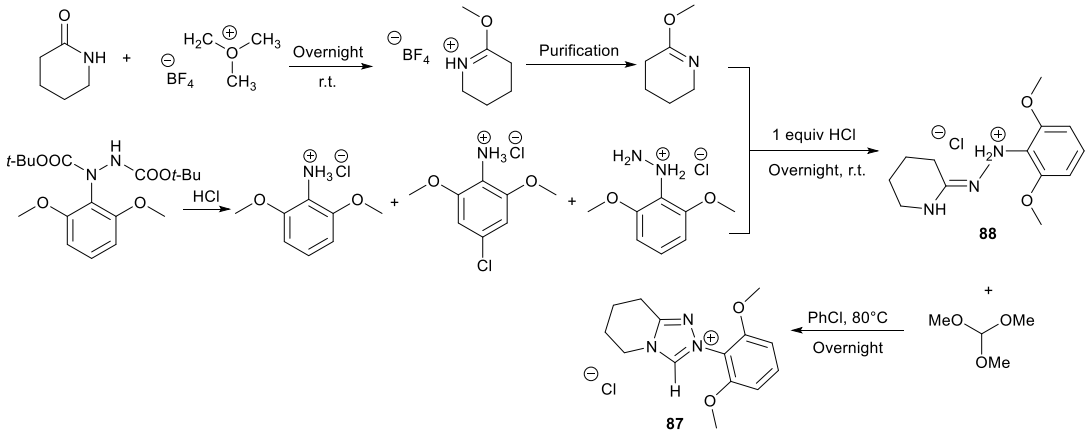

Scheme 2.17. Synthetic procedure towards 2-(2,6-dimethoxyphenyl)-5,6,7,8-tetrahydro-[1,2,4]triazolo[4,3-a]pyridin-2-ium tetrafluoroborate 87

Based on the procedure for the preparation of 2-(2,6-dimethoxyphenyl)-6,7-dihydro-5*H*-pyrrolo[2,1-c] [1,2,4] triazol-2-ium chloride **50** (section 2.7.3)[155], a synthesis of the title compound **87** was undertaken. Mass spectrometry suggested that only trace amounts of amidrazone **88** and final triazolium salt **87** were formed, and column chromatography of the product mixture was unsuccessful. The extremely low yield might be owed to the impact provided by the side ring. Previous reports of the synthesis of related salts in the literature show a decrease in yield with an increase in the size of the fused ring[152, 156].

Chapter 3. Kinetic Studies of the N-Heterocyclic Carbene-Catalysed Benzoin Condensation

3.1. Reaction Profiles by ^{1}H NMR Spectroscopy

In 2001, Leeper and White reported a kinetic analysis of the thiazolium-catalyzed benzoin condensation by ^{1}H NMR spectroscopy in methanol solution[170]. A simplified catalytic cycle is presented in Scheme 3.1, showing the conversion of benzaldehyde **27** to benzoin **89**. In this scheme, the conversion between thiazolium ion **90** to the thiazolyl carbene is part of step 1.

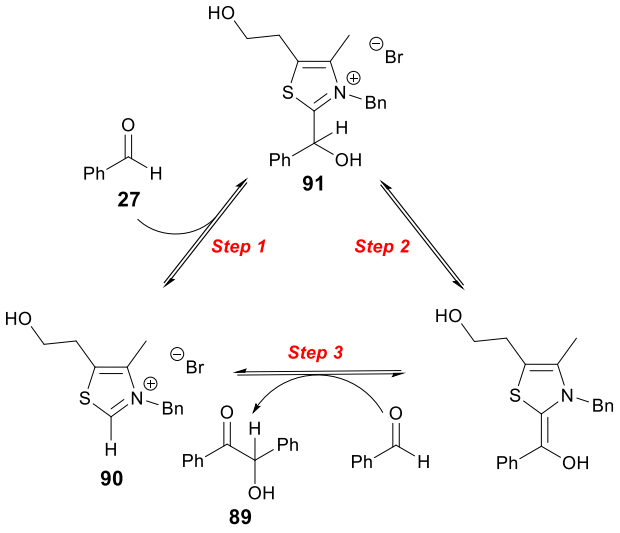

Scheme 3.1. Overall mechanism for the self-condensation benzaldehyde 27 catalyzed by thiazolium precatalyst 90 in methanol.

To allow for the potential identification of reaction intermediates, stoichiometric quantities of benzaldehyde and thiazolium catalyst **90** were added to a triethylamine buffered methanol-d_4 solution at 27 °C. Concentrations of benzaldehyde **27**, benzoin **89**, remaining catalyst, and adduct **91** were traced by ^{1}H NMR spectroscopy. Moreover, due to the utilization of methanol-d_4 as solvent, deuterium exchange occurs

concurrently, and the whole mechanism should be expanded as illustrated in Scheme 3.2. However, Leeper's work neglected the formation of the solvent adduct **92** from benzaldehyde, which generally occupies 1~10% of total aldehyde concentration[151, 170].

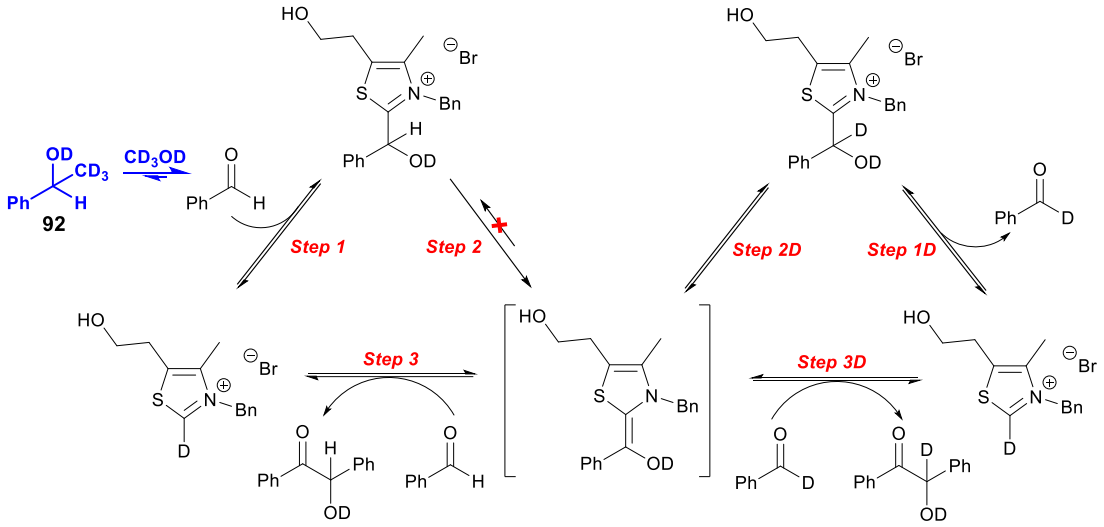

Scheme 3.2. Mechanistic model for the self-condensation of benzaldehyde 27 catalyzed by thiazolium precatalyst 90 in d_4-methanol solution

Based on Leeper's earlier mechanistic studies of the thiazolium-catalyzed process and previous joint work from the O'Donoghue and Smith groups with a range of triazolium salts[131, 132], the reaction profiles of triazolium salts **48**, **49**, and **51** towards the self-benzoin reactions of aldehydes **27** or **93** in a triethylamine-buffered (2:1 NEt_3:$HNEt_3Cl$) methanol-d_4 solution were investigated. The concentration of the catalyst employed was mainly limited by solubility, and 0.08 M triazolium precatalysts **48** and **49**, 0.04 M triazolium salt **51**, and stoichiometric concentrations of aldehyde **27** or **93** were utilized (Figure 3.1). Earlier joint work from our groups mainly focused on the entire catalytic cycle. Although this will form a component of this thesis, our main aim was to do a comparative kinetic study in order to explore the effect of substituents on the extent of formation of d^1 deuterated aldehyde. As mentioned earlier, kinetic reaction profiles for the benzoin and intramolecular Stetter reactions of a range of aldehydes had been explored by us previously. The synthesis

and mechanistic evaluation of triisopropyl catalyst **39** had not been investigated.

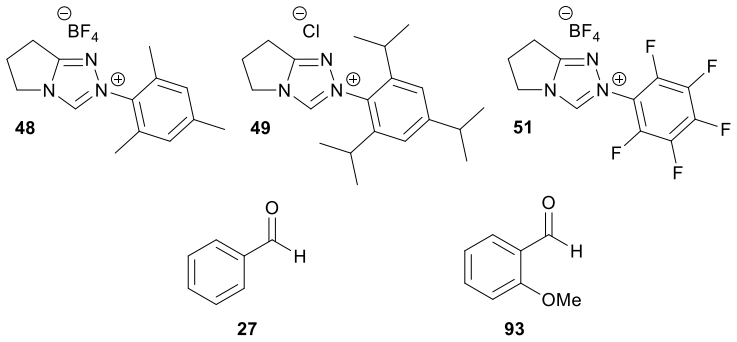

Figure 3.1. Triazolium salts and aldehyde substrates used in the kinetic evaluation of the benzoin condensation

One representative method, the self-condensation of benzaldehyde **27** catalyzed by *N*-triisopropyl triazolium salt **49**, will be introduced to demonstrate how the concentrations of components were determined during the course of reaction. Although NMR peak position varied with catalyst and aldehyde, this same procedure could be employed for each reaction studied.

3.2. Stoichiometric reaction of 2-[2,4,6-tri(2-propyl)phenyl]-6,7-dihydro-5*H*-pyrrolo[2,1-c][1,2,4]triazol-2-ium chloride 49 and benzaldehyde 27

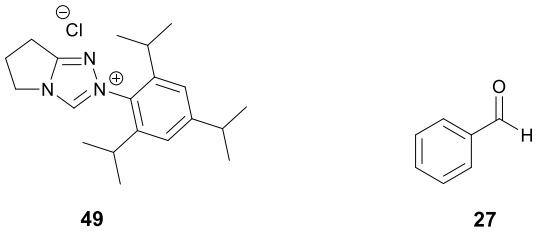

Solutions of triisopropyl triazolium salt **49** (0.08 M) and benzaldehyde **27** (0.08 M) in triethylamine buffered (0.18 M) methanol-d_4 was mixed in an NMR tube to initiate reaction. The reaction was followed in the NMR probe where the temperature was thermostatted at 25 °C. The solution components were analyzed by ^{1}H NMR spectroscopy at regular intervals of ~ 4 min, and three representative spectra taken at different time points during the procedure are shown in Figure 3.2b.

Six main components can be assigned from ^{1}H NMR spectra: benzaldehyde **27**, benzoin **89**, hemiacetal **27'**, benzoic acid **27"** , remaining triazolium salt **49D**, and the tetrahedral adduct **94** Figure 3.2a. Under our experimental conditions, the absence of any other intermediate apart from the adduct **94** indicated the fast decay of the Breslow intermediate relative to its formation. Small quantities of benzoic acid **27"** were also identified over the course of the reaction, presumably a result of the *in situ* oxidation of benzaldehyde by dissolved oxygen. All relevent peaks used for integration purposes are shown in Figure 3.2b.

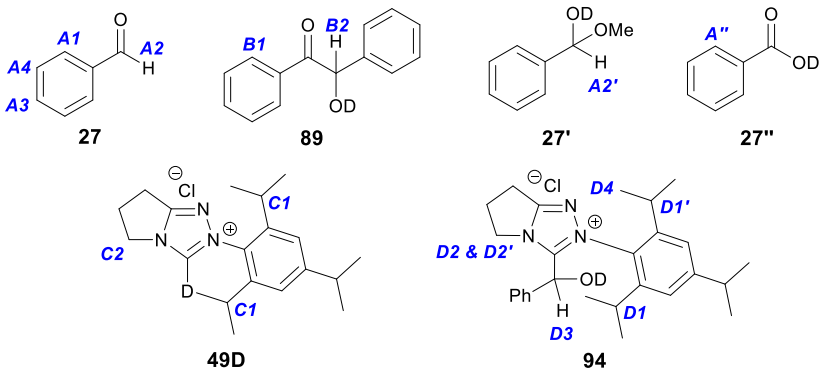

Figure 3.2a. Six components involved in the kinetic study of condensation of benzaldehyde 27 catalyzed by *N*-triisopropyl phenyl triazolium precatalyst 49.

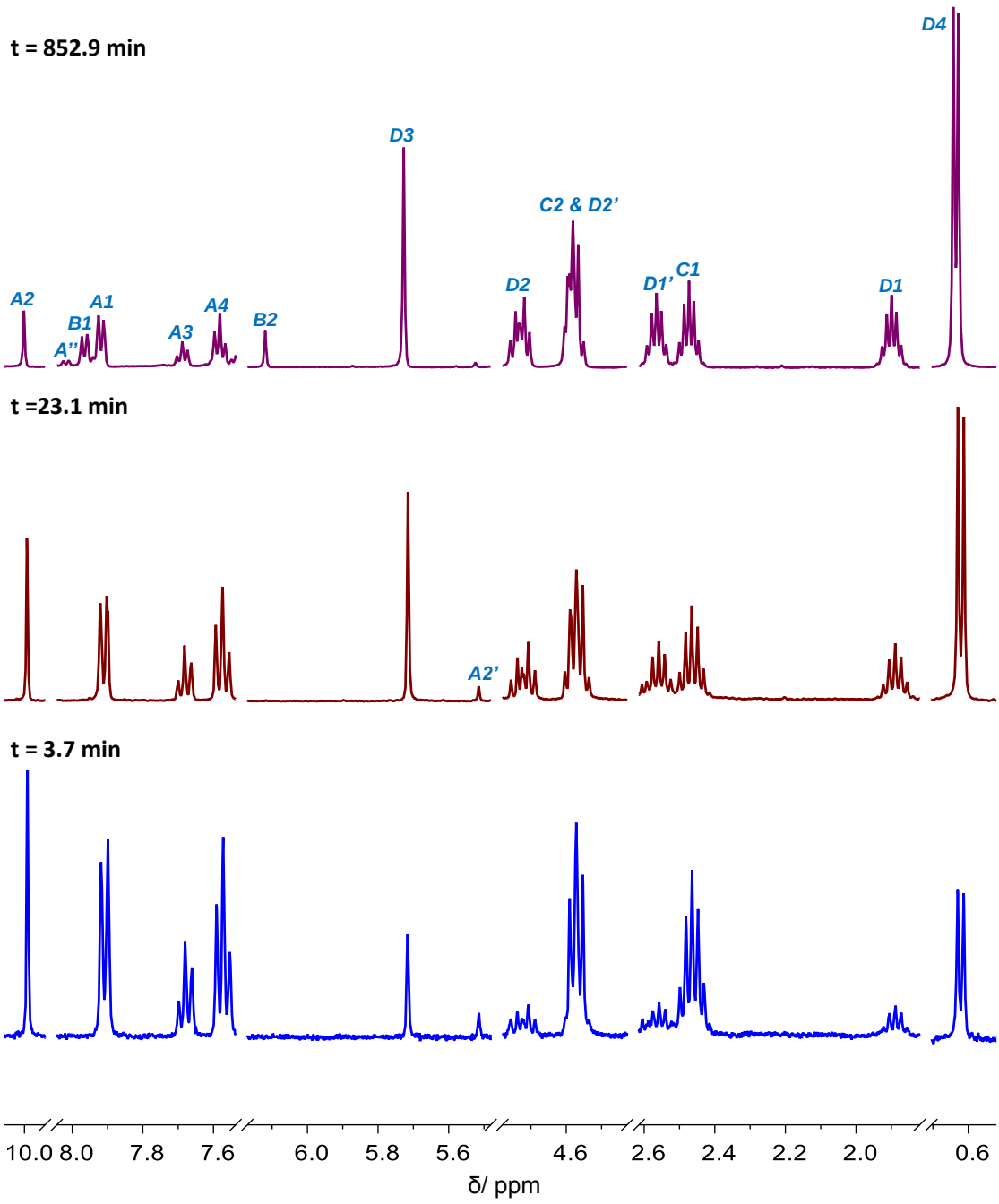

Figure 3.2b. Representative ^{1}H NMR spectra at 500 MHz showing progress of the benzoin condensation of benzaldehyde 27, catalysed by triisopropyl triazolium salt 49, in triethylamine-buffered methanol-d4 solution at 25 °C

In the buffered methanol-d_4 solution, the *NCN*-H of the precatalyst ion **49** was deuterated rapidly to give the triazolium ion **49D**. After the addition of benzaldehyde **27**, the integration of signals due to triazolium precatalyst and aldehyde decreased,

and the peaks corresponded to adduct **94** appeared immediately, and it was the only intermediate directly observed. For this thesis, no adduct has been directly isolated, and peak identification was based on a comparison with related compounds previously studied in our group[131, 132, 151].

The catalytic pathway of benzoin condensation in the presence of triazolium precatalysts **48**, **49**, and **51** in methanol-d_4 is presented in Scheme 3.3. Our previous studies of the catalytic cycle of *N*-phenyl and *N*-mesityl precatalyst show adduct formation should be reversible. The observation of formation of deuterated aldehyde suggests this to also be the case for triisopropyl catalyst. Although the formation of Breslow intermediate **95** was not observed, the appearance of deuterated adduct **94D** and the deuterated aldehyde **27D** also supports reaction *via* a Breslow-like intermediate.

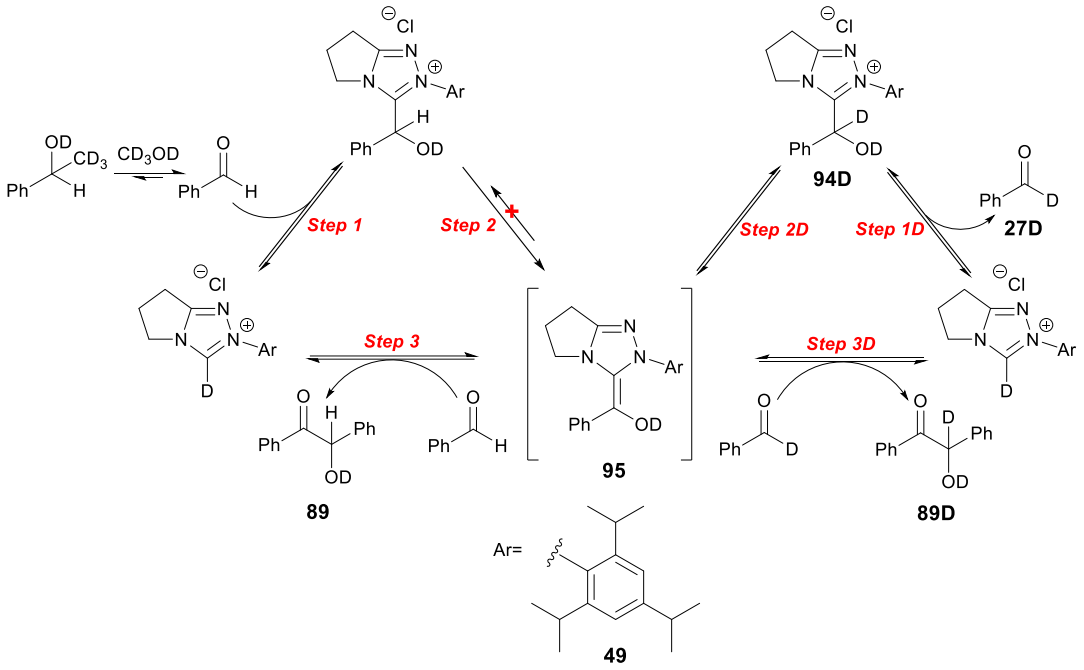

Scheme 3.3. Mechanistic model for the self-condensation of benzaldehyde 27 catalyzed by triazolium precatalyst 49 in d_4-methanol solution

For the purpose of integration, peaks were chosen where minimum overlap with other

species was involved. In most cases, a single peak could be utilized with baseline resolution to access the concentration of the relevant species.

From the NMR spectra, the four methyl groups on the *ortho*-diisopropyl substituents changed from equivalent to non-equivalent upon the formation of adduct **94** from triazolium precatalyst **49D**. The doublet at 0.62 ppm (***D4***), corresponding to one of the methyl groups was used to calculate the concentration of the total amount of adduct **94** (Equation 3.1). The remaining three doublets due to the three additional methyl groups significantly overlapped with buffer peaks thus could not be used for integration. The heptet signal at 2.46 ppm (***C1***), identified as two CH protons on the *ortho*-diisopropyl groups on the triazolium precatalyst's aromatic ring, was used to calculate the concentration of the remaining precatalyst **49D** (Equation 3.2).

The peak at 2.46 ppm (***C1***) transformed to two heptet signals at 2.56 ppm (***D1'***) and 1.89 ppm (***D1***) in the adduct. One of the heptet signals at 1.89 ppm (***D1***) can also be used to estimate the adduct concentration (Equation 3.3). The second heptet signal at 2.56 ppm (***D1'***), however, overlapped with solvent.

A third independent estimate of total adduct concentration could be obtained using alkyl protons on the fused ring. The triplet signal at 4.57 ppm (***C2***), corresponding to the pair of CH_2 protons on the five-membered fused ring (adjacent to the N atom), split into 2 doublet of triplet signals at 4.72 (***D2***) and 4.57 ppm (***D2'***). The triplet peak at 4.72 ppm (***D2***) can be utilized to calculate the adduct concentration (Equation 3.4). There is significant overlap between ***C2*** and ***D2'*** peaks. and the other CH_2 protons on the five membered fused ring were also overlapped with the triplet signal at 4.57 ppm (***C2***).

$$[\text{adduct (tot)}] = \frac{(A_{\text{D4}}/3)}{(A_{\text{D4}}/3 + A_{C1}/2)} \times 0.08 \qquad \textbf{Equation 3.1}$$

$$[\text{catalyst}] = \frac{A_{C1}/2}{(A_{D4}/3 + A_{C1}/2)} \times 0.08$$ **Equation 3.2**

$$[\text{adduct (tot)}]'' = \frac{(A_{D2})}{(A_{D2} + A_{C1}/2)} \times 0.08$$ **Equation 3.3**

$$[\text{adduct (tot)}]' = \frac{(A_{D1})}{(A_{D1} + A_{C1}/2)} \times 0.08$$ **Equation 3.4**

In some kinetic studies, like the reaction of triisopropyl triazolium precatalyst **49** and *ortho*-methoxybenzaldehyde **93**, the peak overlap between precatalyst and the corresponding adduct or solvent residues restricted the calculation of precatalyst concentration to analysis of a single peak as above. In these cases, the concentration of remaining triazolium ion has to be calculated from the difference between adduct signal at 4.72 ppm (***D2***) and the multiplet at 4.57 ppm (***C2*** and ***D2'***), corresponding to the mixture of CH_2 protons on the five-membered fused rings of both triazolium ion and adduct (Equation 3.5).

$$[\text{catalyst}]' = \frac{(A_{C2\ \&\ D2'} - A_{D2})/2}{(A_{D2} + (A_{C2\ \&\ D2'} - A_{D2})/2)} \times 0.08$$ **Equation 3.5**

The singlet at 5.72 ppm (***D3***) corresponds to the exchangeable tetrahedral proton on the adduct **94**. Utilizing this signal, the concentration of the unexchanged adduct **94** could be determined by Equation 3.6. The concentration of deuterated adduct **94D** was obtained from the difference between that of total and non-deuterated adduct species (Equation 3.7).

$$[\text{adduct (H)}] = \frac{(A_{D3})}{(A_{D4}/3 + A_{C1}/2)} \times 0.08$$ **Equation 3.6**

$$[\text{adduct (D)}] = [\text{adduct (tot)}] - [\text{adduct(H)}]$$ **Equation 3.7**

Benzaldehyde **27**, and *ortho*-methoxybenzaldehyde **93**, used in the six experiments

performed, exists in an equilibrium with corresponding methanol adducts **27'** and **93'**, respectively (Scheme 3.4).

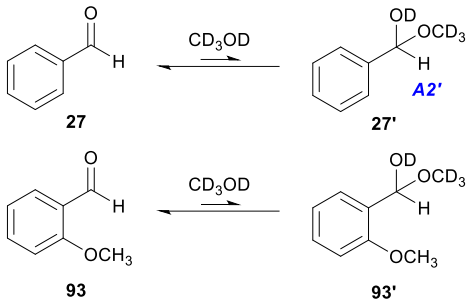

Scheme 3.4. Existing equilibrium between aldehyde 27, 93 and their solvent adducts 27', 93'

A singlet signal at 5.52 ppm (***A2'***) corresponding to the benzylic proton of hemiacetal **27'** was observed in the buffered methanolic solution. From the ratio of the aldehyde (***A2***) and the hemiacetal (***A2'***) proton, values for the equilibrium constant K_{add} and the fraction of the aldehyde present, f_{ald}, can be determined by Equation 3.8 and 3.9. These values are summarized in Table 3.1. To accurately reflect the total concentration of aldehyde present, we need to account for the concentration present as solvent adduct, using f_{ald}.

$$K_{add} = \frac{A_{A2\prime}}{A_{A1}} = \frac{[hemiacetal]}{[aldehyde]} \qquad \textbf{Equation 3.8}$$

$$f_{ald} = \frac{A_{A1}}{(A_{A2\prime}+A_{A1})} = \frac{[aldehyde]}{([aldehyde]+[hemiacetal])} \qquad \textbf{Equation 3.9}$$

Table 3.1. Equilibrium constants for formation of solvent adduct between aldehyde and methanol[151]

aldehyde	K_{add}	f_{ald}
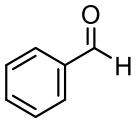	0.095	0.913
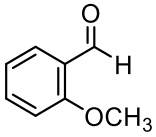	0.064	0.940

The proportional total amount of benzaldehyde **27** and benzoin **89** were calculated from the doublet signals at 7.91 (***A1***) and 7.95 ppm (***B1***), corresponding to the *ortho*-aryl CH protons (Equation 3.10 and 3.13). Triplet signals at 7.68 (***A3***) and 7.57 (***A4***) corresponding to the *para*- and *meta*-aryl CH protons of benzaldehyde can be used for an independent evaluation of concentration.

Integration of protonated benzaldehyde **27** was achieved using the singlet signal at 9.99 ppm (***A2***), recognized as the aldehydic hydrogen atom (Equation 3.11). The quantity of protonated benzoin **89** was obtained from the singlet peak at 6.12 ppm (***B2***), identified as the tetrahedral proton on benzoin (Equation 3.14). Furthermore, concentrations of deuterated benzaldehyde **27D** and benzoin product **89D** were determined from the concentration differences between total and protonated components (Equation 3.12 and 3.15).

$$[\text{aldehyde (tot)}] = \frac{1}{f_{\text{ald}}} \times \frac{(A_{\boldsymbol{A1}}/2)}{(A_{\text{D4}}/3 + A_{C1}/2)} \times 0.08 \qquad \textbf{Equation 3.10}$$

$$[\text{aldehyde (H)}] = \frac{1}{f_{\text{ald}}} \times \frac{A_{\text{A2}}}{(A_{\text{D4}}/3 + A_{C1}/2)} \times 0.08 \qquad \textbf{Equation 3.11}$$

$$[\text{aldehyde (D)}] = [\text{aldehyde (tot)}] - [\text{aldehyde(H)}] \qquad \textbf{Equation 3.12}$$

$$[\text{benzoin (tot)}] = \frac{(A_{B1}/2)}{(A_{D4}/3+A_{C1}/2)} \times 0.08 \qquad \textbf{Equation 3.13}$$

$$[\text{benzoin (H)}] = \frac{A_{B2}}{(A_{D4}/3+A_{C1}/2)} \times 0.08 \qquad \textbf{Equation 3.14}$$

$$[\text{benzoin (D)}] = [\text{benzoin (tot)}] - [\text{benzoin (H)}] \qquad \textbf{Equation 3.15}$$

3.3. Concentration profiles

Concentration profiles for the condensation of benzaldehyde **27** and *ortho*-methoxybenzaldehyde **93** are shown for the reactions catalyzed by *N*-triisopropylphenyl, *N*-mesityl, and *N*-pentafluorophenyl substituted triazolium precatalysts **48**, **49**, and **51** in Figures 3.3-3.7. The *N*-pentafluorophenyl triazolium salt **51** was highly reactive, thus adduct formation was finished within a few minutes, which complicated the acquisition of kinetic data from the profile.

Figure 3.3: Concentration profile for the self-condensation of benzaldehyde 27 (0.08 M), catalysed by *N*-mesityl triazolium precatalyst 48 (0.08 M), in 0.107 M NEt_3 and 0.053 M NEt_3·DCl in methanol-d_4

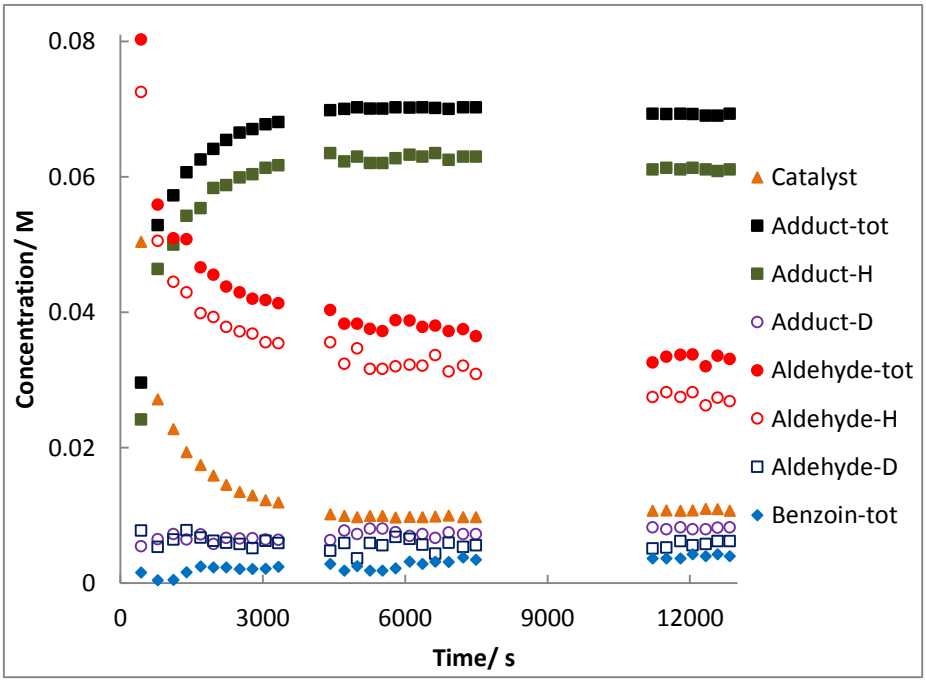

Figure 3.4: Concentration profile for the self-condensation of 2-methoxybenzaldehyde 93 (0.08 M), catalysed by *N*-mesityl triazolium precatalyst 48 (0.08 M), in 0.107 M NEt_3 and 0.053 M NEt_3·DCl in methanol-d_4

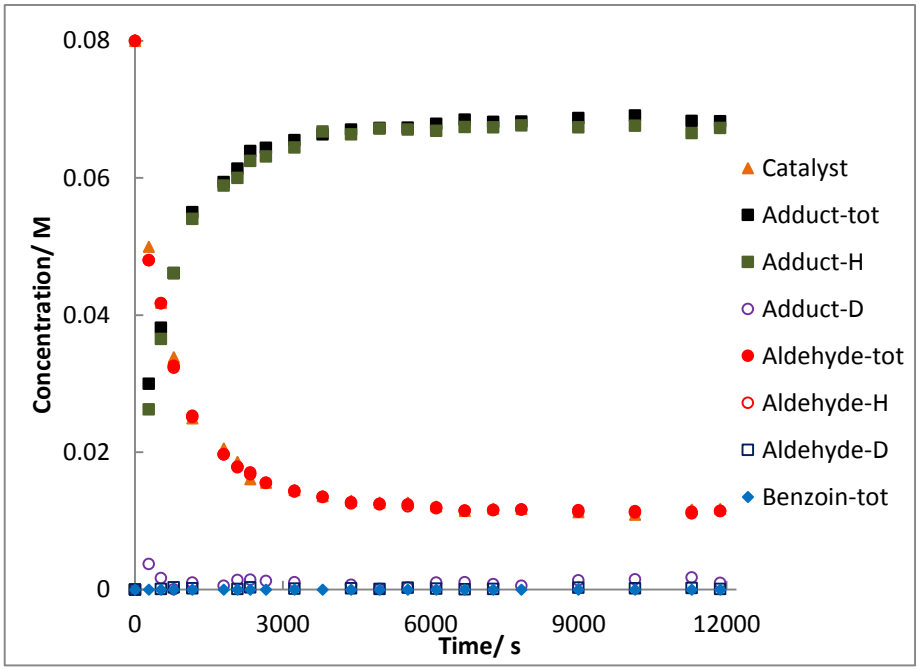

Figure 3.5: Concentration profile for the self-condensation of benzaldehyde 27 (0.08 M), catalysed by *N*-triisopropyl triazolium precatalyst 49 (0.08 M), in 0.107 M NEt_3 and 0.053 M NEt_3·DCl in methanol-d_4

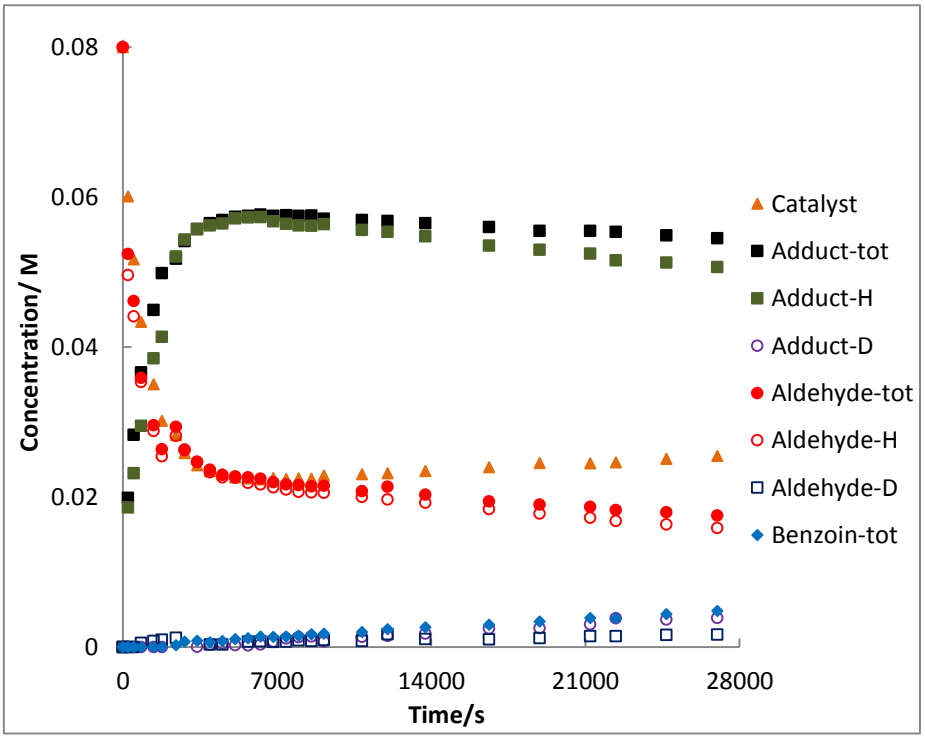

Figure 3.6: Concentration profile for the self-condensation of 2-methoxybenzaldehyde 93 (0.08 M), catalysed by *N*-triisopropyl triazolium precatalyst 49 (0.08 M), in 0.107 M NEt_3 and 0.053 M NEt_3·DCl in methanol-d_4

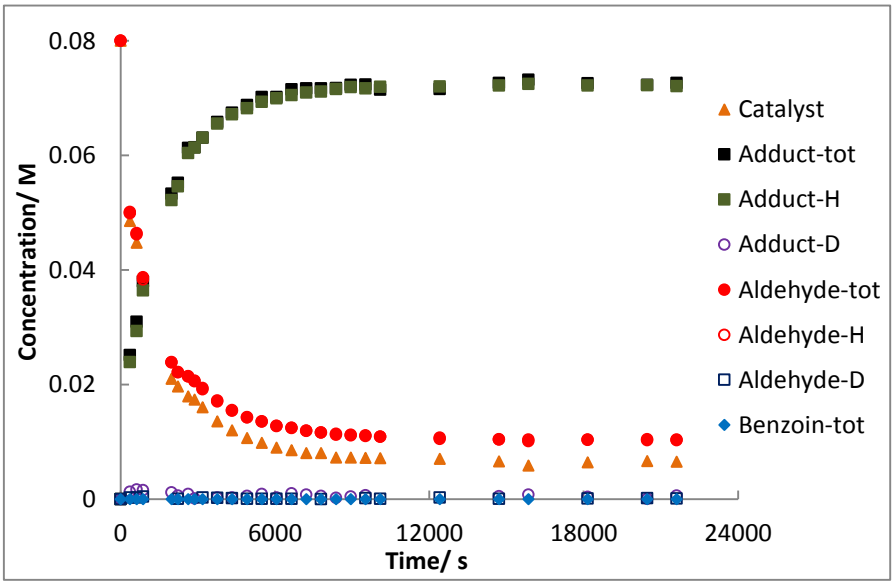

Figure 3.7: Concentration profile for the self-condensation of 2-methoxybenzaldehyde 93 (0.04 M), catalysed by *N*-pentafluorophenyl triazolium precatalyst 51 (0.04 M), in 0.107 M NEt_3 and 0.053 M NEt_3·DCl in methanol-d_4

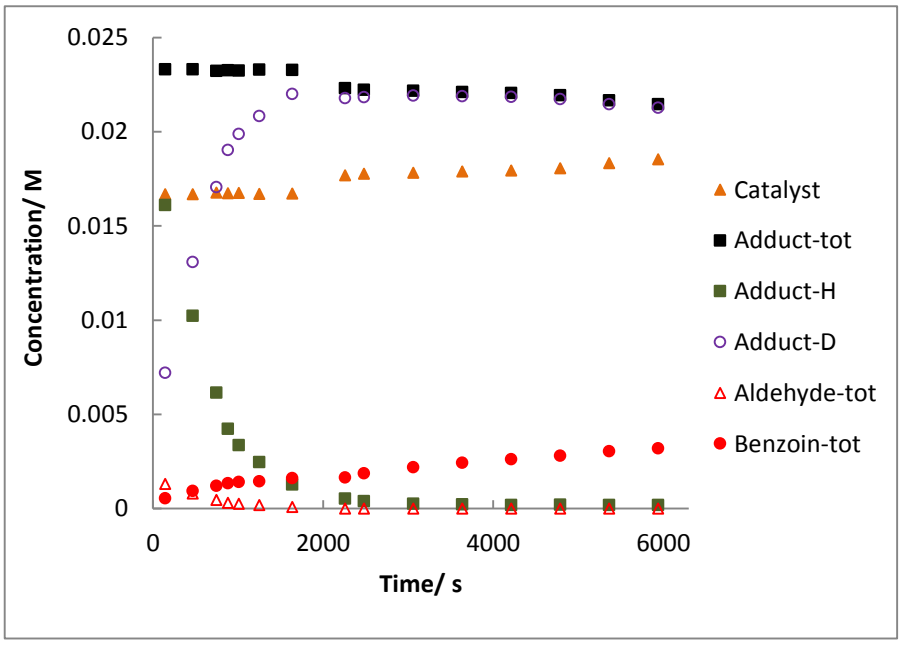

3.4. Determination of Rate Constants for Individual Steps

Using the reaction profiles, the kinetic data may be fitted to access values for steps along the reaction pathway.

3.4.1. Determination of k_1, k_{-1} and K_1

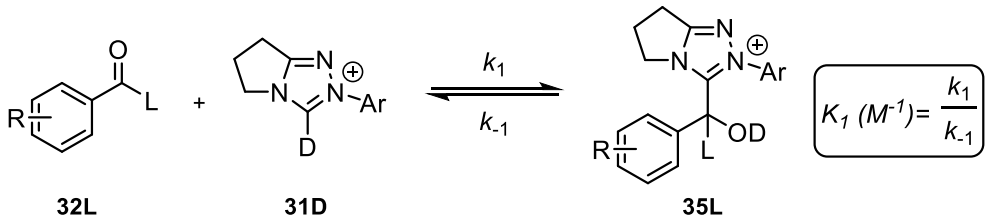

Scheme 3.5. Equilibrium for the formation of adduct 35L from the aldehyde 32L and NHC precatalyst 31D

At early stages of reaction before significant benzoin product formation (< 10%), the pseudo second order rate constant k_1 (M^{-1} s^{-1}) for adduct formation can be accessed by analysis of the equilibrium in Scheme 3.5. The rate expression of this reaction is provided in Equation 3.16, which could be transformed into Equation 3.17, where the concentration of aldehyde **32L** and catalyst **31D** are identical.

$$\frac{d[\mathrm{cat}]}{dt} = -k_1[\mathrm{cat}][\mathrm{ald}] + k_{-1}[\mathrm{add}] \qquad \textbf{Equation 3.16}$$

$$\frac{d[\mathrm{cat}]}{dt} = -k_1[\mathrm{cat}]^2 + k_1 \frac{[\mathrm{cat}]_e^2}{([\mathrm{cat}]_0 - [\mathrm{cat}]_e)}([\mathrm{cat}]_0 - [\mathrm{cat}]) \qquad \textbf{Equation 3.17}$$

The integration of Equation 3.17 is shown in Equation 3.18 to give the rate equation, where $[\mathrm{cat}]_0 = [\mathrm{ald}]_0 = b$, $y = ([\mathrm{cat}]_0 - [\mathrm{cat}]) = ([\mathrm{ald}]_0 - [\mathrm{ald}])$ and $y_e = ([\mathrm{cat}]_0 - [\mathrm{cat}]_e) = ([\mathrm{ald}]_0 - [\mathrm{ald}]_e)$. Thus, the k_1 value is expressed as the slope of a semilogarithmic plot of $(y_e(b^2 - yy_e)/(b^2(y_e - y))$ against time

$$\frac{y_e}{(b^2-y_e^2)} \ln \frac{y_e(b^2-yy_e)}{b^2(y_e-y)} = k_1 t$$ **Equation 3.18**

Plots for the *N*-mesityl **48** and *N*-triisopropyl triazolium **49** catalyzed reactions with aldehyde substrates are shown in Figure 3.8. These plots should be linear if a pseudo second order equilibration exists. The *N*-pentafluorophenyl triazolium catalyst **51** was so reactive that adduct formation achieved equilibrium within 3 minutes, thus rate constants for adduct formation were not determined.

Figure 3.8. Semilogarithmic plots of [$y_e(b^2 - yy_e)/(b^2(y_e - y))$] against time for the reactions of substituted aromatic aldehydes 27 and 93 with triazolium precatalyst 48 and 49

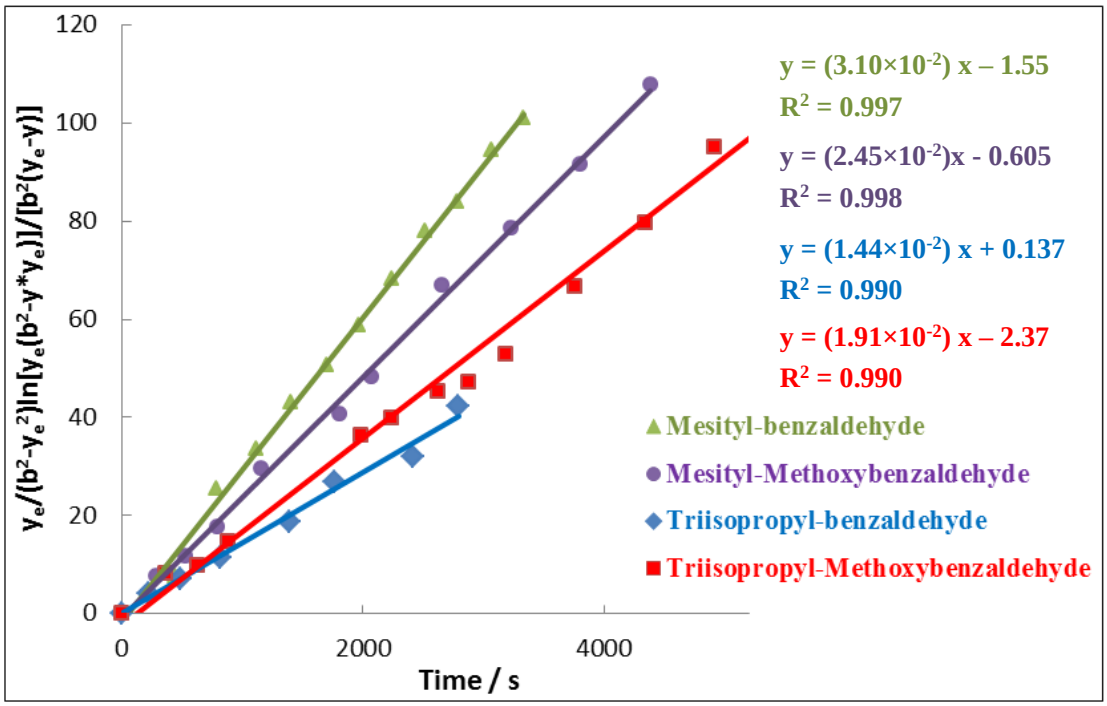

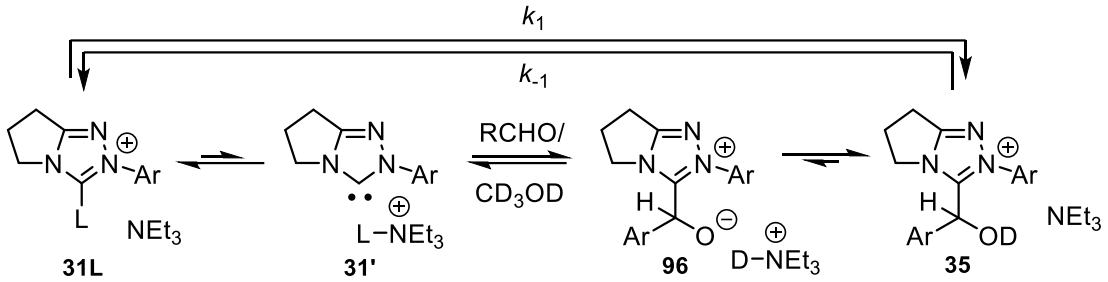

Scheme 3.6. Detailed mechanism of formation of adduct 35

Overall, excellent kinetic fits are observed to a kinetic equation (equation 3.18) describing a pseudo second order approach to equilibrium. This supports our assumption that triethylamine base is catalytically regenerated upon formation of hydroxyaryl adduct, as otherwise, an overall third order reaction would be expected.

The estimated K_1 (M^{-1}) values were obtained from the concentration profile. The concentrations of total adduct, total catalyst and total aldehyde at equilibrium points were applied in Equation 3.19. Knowing values for K_1 and k_1 allowed the determination of the pseudo first order rate constant, k_{-1} (s^{-1}), for the reverse decomposition of adduct using the relation in Equation 3.20. Values of k_1, k_{-1}, and K_1 are summarized in Table 3.2.

$$K_1 = \frac{[\text{add (tot)}]_e}{[\text{cat}]_e \times [\text{ald (tot)}]_e} = \frac{[\text{add (tot)}]_e}{[\text{cat}]_e^{\,2}} \qquad \textbf{Equation 3.19}$$

$$k_{-1} = k_1 / K_1 \qquad \textbf{Equation 3.20}$$

Table 3.2. Summary of k_1, k_{-1}, and K_1 for the self-condensation of one equivalent of aldehyde 27 and 93, in the presence of stoichiometric triazolium precatalyst 48 (0.08 M), 49 (0.08 M), and 51 (0.04 M), in 0.107 M NEt_3 and 0.053 M NEt_3·DCl in methanol-d_4 at 25 °C

catalyst	aldehyde	K_1, M^{-1} [a]	k_1, M^{-1} s^{-1} [b]	k_{-1}, s^{-1} [c]
	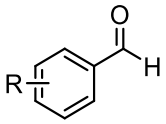			
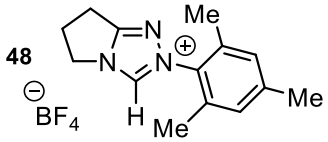 **48**	R= H	**138**	3.10×10^{-2}	2.25×10^{-4}
		(160)	(2.76×10^{-2})	(1.64×10^{-4})
	R= 2-OMe	**524**	2.45×10^{-2}	4.67×10^{-5}
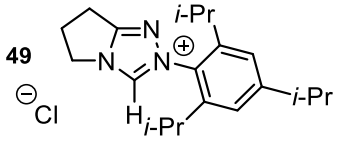 **49**	R= H	**115**	1.44×10^{-2}	1.25×10^{-4}
	R= 2-OMe	**1738**	1.91×10^{-2}	1.10×10^{-5}
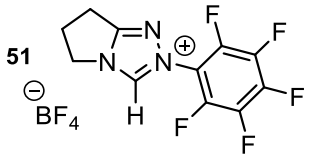 **51**	R= 2-OMe	**> 5000**	-	-

(a) Estimated from Equation 3.19. (b) Obtained from the slope of a semilogarithmic plot of $(y_e(b^2 - yy_e)/(b^2(y_e - y))$ against time using Equation 3.18. (c) Obtained from Equation 3.20. Values in brackets were obtained from Richard Massey's PhD thesis.

Our data in Table 3.2 may be compared with previous data amassed by the O'Donoghue and Smith groups (Table 3.3) under three different sets of reaction conditions. Entries **1a-f** refer to analogous conditions in triethylamine-buffered methanol-d_4 to those employed by us in the present project. Data for entries **2-3** were acquired in dichloromethane-d_2. Overall, although absolute *K* values differ depending on the solvent and conditions, the same trends are observed.

Table 3.3. Summarized K_{exp} (M^{-1}) values from literature with different conditions[131, 132, 151]

Entry	catalyst	aldehyde	K_{exp}, M^{-1} [c]
	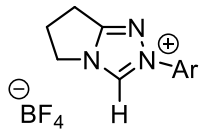	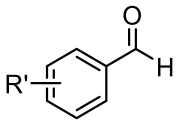	
1a		R'= H	**11.4**
1b	Ar= Ph	R'= 2-OMe	**118**
1c		R'= 2-Me	**14.7**
2a	Ar = Ph	R'= H	**3**
2b		R'= 2-OMe	**56**
2c	Ar = Mesityl	R'= H	**31**
2d		R'= 2-OMe	**143**
3a	Ar= Ph	R'= 2- (*E*)-$OCH_2CH=CHCO_2Et$	**27**
3b	Ar = Mesityl		**140**

Starting conditions: Entry 1, aldehyde (0.04 M), NHC precatalyst (0.04 M) in CD_3OD and Et_3N:Et_3N·HCl (2:1, 0.18 M) buffer at 25 °C. Entry 2, aldehyde (0.01 M), NHC precatalyst (0.002 M) in CD_2Cl_2 and Et_3N (0.002 M) at 25 °C. Entry 3, aldehyde (0.04 M), NHC precatalyst (0.008 M) in CD_2Cl_2 and Et_3N (0.008 M) at 25 °C.

In general, as described in more detail in the introduction, *ortho*-alkyl or *ortho*-heteroatom substituents on either the catalyst or aldehyde were found to increase the equilibrium constant for adduct formation. The observed increases in K_{exp} were substantially higher for 2-heteroatom than for 2-alkyl substituents. We have postulated that *ortho*-substituents on catalyst force the *N*-aryl group out of plane with the central triazole thereby allowing easier accommodation of the hydroxyaryl moiety, thus increasing K_{exp}. *Ortho*-substituents on aldehyde, which potentially twist the carbonyl out of conjugation, also possibly allow better accommodation of the hydroxyaryl moiety. In this case, product stabilization could also potentially come from the formation of an intramolecular hydrogen bond with the *ortho*-methoxy substituent (Figure 3.9).

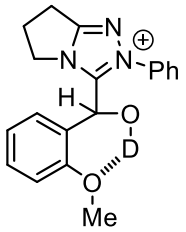

Figure 3.9: Proposed intramolecular hydrogen bond

For adduct formation from benzaldehyde (R= H), our new data shows that there is no further increase of *K* by changing trimethyl to triisopropyl aryl-substituents of catalyst. In fact, the *K* value decreases 32.6% which may be because of the slightly higher electron-donating ability of isopropyl group. By contrast, the increased *K* value (3.3-fold) for 2-methoxybenzaldehyde (R= 2-OMe) emphasizes the better accommodation of the hydroxyaryl moiety, provided by the bulkier *ortho*-isopropyl on catalyst in conjunction with the twist from *ortho*-methoxyl aryl-substituent on aldehyde. The greater twist from co-planarity potentially resulting from the bulkier *ortho*-isopropyl groups may also allow for easier formation of an intramolecular hydrogen bond with the 2-OMe substituent of aldehyde (Figure 3.9).

Previous results with the *N*-mesityl catalyst **48** showed *K* increases 4.6 fold in dichloromethane-d_2 when comparing benzaldehyde **27** and 2-methoxybenzaldehyde **93** (Entries **2c** and **2d**, Table 3.3). In our new experiment in methanol-d_4 (Table 3.2), a similar 3.8 fold increase is observed for the *N*-mesityl catalyst, and 15.1 fold for the *N*-triisopropyl precatalyst **49**. This may indicate the larger twist, provided by the 2-aryl-substituents, for the bulkier *ortho*-isopropyl group than the *ortho*-methyl aryl-substituents on the catalyst in combination with a 2-OMe substituent on aldehyde.

Table 3.4. Summary of k_1, k_{-1}, and K_1 for the self-condensation of benzaldehyde 27 in the presence of stoichiometric triazolium precatalyst 47 or 48 (0.08 M or 0.04 M) in 0.107 M NEt_3 and 0.053 M NEt_3·DCl in methanol-d_4 at 15 or 25 °C[131, 132, 151]

catalyst	aldehyde	K_1, M^{-1}	k_1, M^{-1} s^{-1}	k_{-1}, s^{-1}
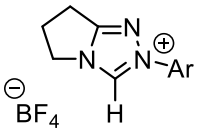	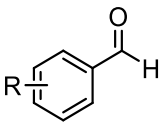			
Ar= Ph[a]	R'= H	**11.4**	1.33×10^{-2}	1.21×10^{-3}
	R'= 2-OMe	**118**	3.44×10^{-2}	2.92×10^{-4}
Ar= Ph[b]	R'= 2-$OCH_2CH{=}CHCO_2Et$	**319**	1.52×10^{-2}	4.76×10^{-5}
Ar= Mesityl[b]		**3082**	3.85×10^{-2}	1.25×10^{-5}

a) 0.08 M of precatalyst at 25 °C; b) 0.04 M of precatalyst at 15 °C

Our previous analysis of k_1 and k_{-1} values have shown that small increases in k_1 and slightly larger decreases in k_{-1} in the presence of 2-OMe substituents on aldehyde contribute to observed increases in K_1[131, 132, 151]. For instance, for the *N*-phenyl precatalyst (Table 3.4, R'= H versus 2-OMe), the k_1 increases by 2.6 fold. In the case of our new data for *N*-mesityl catalyst, in contrast with previous results, there is a small 21 % decrease in k_1 (Table 3.2, R= H versus 2-OMe). However, as there is still a larger decrease in k_{-1} (4.8 fold), the net observed effect is still a 3.8 fold increase in K_1. In the case of isopropyl catalyst (Table 3.2, R= H versus 2-OMe), k_1 increases (1.3 fold) and k_{-1} decreases (11.4 fold) as previously, resulting in a larger increase in K_1 (15 fold). Overall, from our new results, the mesityl and isopropyl catalysts show bigger effects on k_{-1} than k_1 with 2-methoxy substituents on aldehyde.

In particular, the large 11.4 fold decrease in the rate of decomposition of adduct (k_{-1}) formed from reaction of triisopropyl precatalyst **27** and 2-methoxybenzaldehyde **93** indicates particular stability of this adduct. The further steric hindrance provided by the isopropyl groups may hinder deprotonation at OH to initiate decomposition.

3.4.2. Determination of k_2

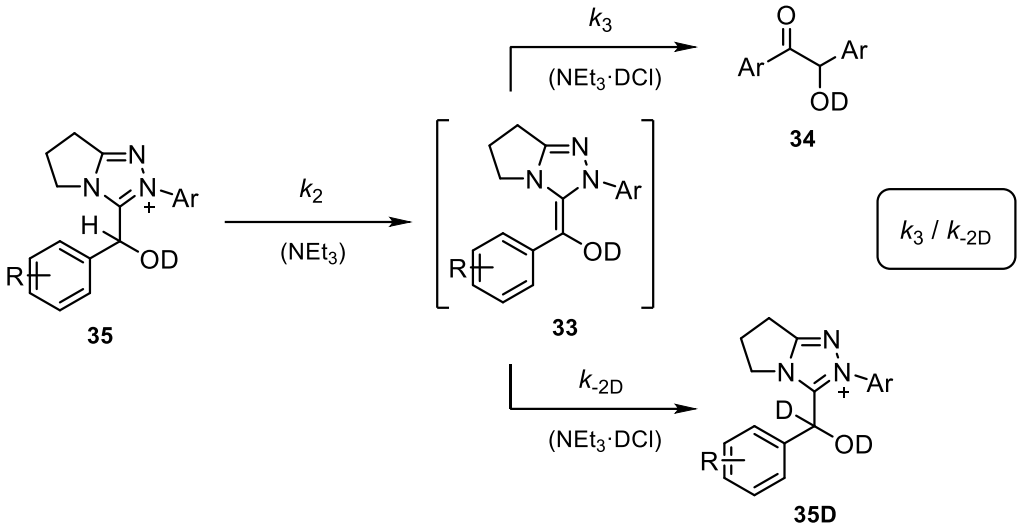

Scheme 3.7. Mechanism of formation of Breslow intermediate 33 followed by the onward reaction to benzoin 34 and backward deuteration towards adduct 35D

Owing to the relatively short life-time of the Breslow intermediate **33**, direct kinetic investigations of its formation and decay are difficult[170]. However, under our conditions, the deuteration of Breslow intermediate to form the deuterated adduct **35D** is essentially irreversible (Scheme 3.7). This allows the crucial calculation of the pseudo first order rate constant, k_2 (s^{-1}), of the formation of Breslow intermediate **33** from the consumption of protonated adduct **35** after the equilibrium concentrations have been achieved. The concentration of triethylamine was in reasonable excess over adduct concentration thus the process will be close to pseudo first order in adduct concentration. This analysis will at least allow for a good approximation of relative k_2 values. The expression of the adduct consumption rate is shown in Equation 3.21.

The integrated form is given in Equation 3.22, and the k_2 value can be obtained as the slope of the semilogarithmic plots of the protonated adduct concentration against time. The plots of *N*-mesityl and *N*-triisopropyl phenyl triazolium salts **48** and **49** with aldehydes are shown in Figure 3.10, and the plots of *N*-pentafluorophenyl triazolium

ion **51** is presented in Figure 3.11 separately due to its high reactivity. The k_2 values are summarized in Table 3.5,

$$-\frac{d[\text{add (H)}]}{dt} = k_2[\text{add(H)}] \qquad \textbf{Equation 3.21}$$

$$[\text{add (H)}] = [\text{add (H)}]_0 e^{-k_2 t} \qquad \textbf{Equation 3.22}$$

Figure 3.10. Semilogarithmic plots of [adduct (H)] against time for the reactions of aldehydes 27 and 93 with *N*-mesityl and *N*-triisopropyl phenyl triazolium precatalyst 48 and 49

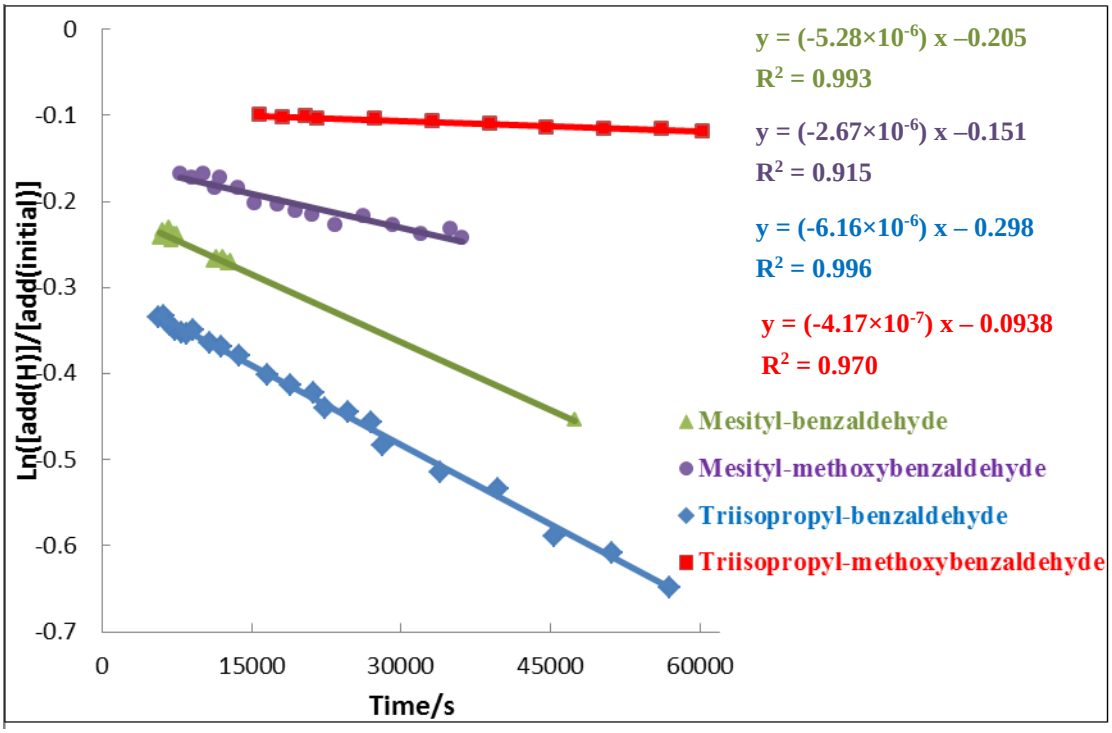

Figure 3.11. Semilogarithmic plots of [adduct (H)] against time for the reactions of 2-methoxybenzaldehyde 93 with *N*-pentafluoro phenyl triazolium precatalyst 51

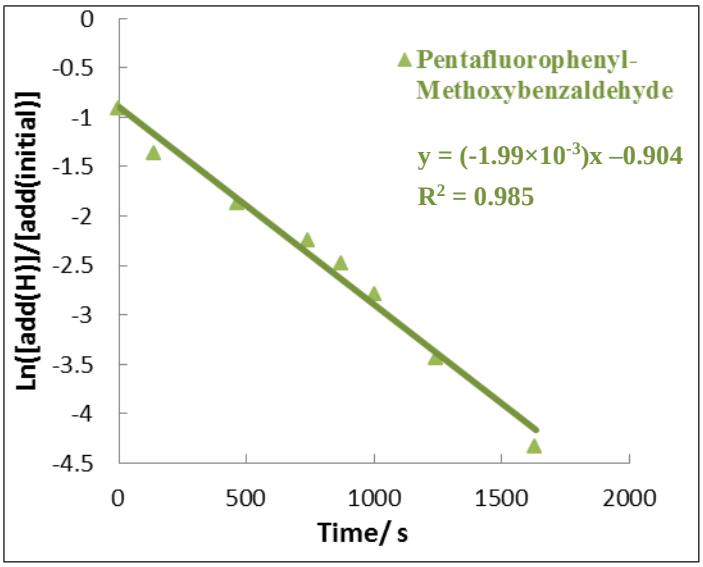

Table 3.5. Summary of k_2 for the self-condensation of one equivalent of aldehyde 27 and 93, catalysed by triazolium precatalyst 48 (0.08 M), 49 (0.08 M), and 51 (0.04 M), in 0.107 M NEt_3 and 0.053 M NEt_3·DCl in methanol-d_4 at 25 °C

catalyst	aldehyde	k_2, s^{-1}
	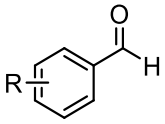	
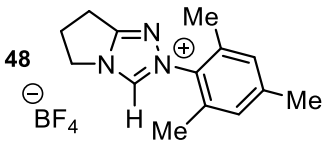 **48**	R= H	5.28×10^{-6} (1.03×10^{-5})
	R= 2-OMe	2.67×10^{-6}
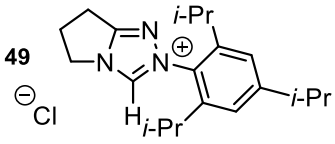 **49**	R= H	6.17×10^{-6}
	R= 2-OMe	4.17×10^{-7}
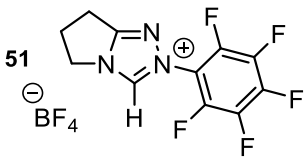 **51**	R= 2-OMe	1.99×10^{-3}

The k_2 values were calculated from the slope of a semilogarithmic plot of [adduct(H)] against time.

From the results, the more electron-deficient adducts provide larger rate constants for deprotonation. For example, the k_2 value for reaction between *ortho*-methoxybenzaldehyde **93** and *N*-pentafluorophenyl precatalyst **51** is 745- and 4772-fold higher than for the analogues of the *N*-mesityl and *N*-triisopropyl precatalyst **48** and **49**, respectively. Similarly, Richard Massey observed a 3.5-fold larger k_2 value between the reaction of *para*-fluorobenzaldehyde and *para*-methoxybenzaldehyde catalyzed by *N*-phenyl precatalyst showing electron-withdrawing substituents on aldehyde also increase k_2. Overall, a normal electronic substituent effect largely influences k_2.

The methyl and isopropyl groups have similar Hammett σ-values, although the isopropyl is a slightly more electron-donating[171]. Thus similar k_2 values would be expected as is observed for both catalysts with benzaldehyde. The large 6.4 fold decrease in k_2 for 2-methoxybenzaldehyde could be a result of steric hindrance of deprotonation at the benzylic carbon for the triisopropyl catalyst.

3.4.3. Evaluation of d^1 deuteration

Figures 3.12 and 3.13 show the changes in the concentrations of deuterated adduct, d^1 deuterated aldehyde and benzoin product over our reaction timescales for the reaction of *N*-mesityl and *N*-triisopropyl phenyl catalysts with benzaldehyde. These are the three possible products from onwards reaction of the H-hydroxyaryl adduct *via* the Breslow intermediate as in Scheme 3.7. In the case of 2-methoxybenzaldehyde, with *N*-mesityl and triisopropyl phenyl catalysts, no further reaction of the adducts are observed under our conditions. For the significantly more active *N*-pentafluorophenyl catalyst, further reaction is observed and the products are shown in Figure 3.14.

Figure 3.12. Plots of concentrations of benzoin product, deuterated adduct, and d^1 deuterated aldehyde against time for the self-condensation of benzaldehyde 27 catalyzed by *N*-mesityl triazolium salt 48

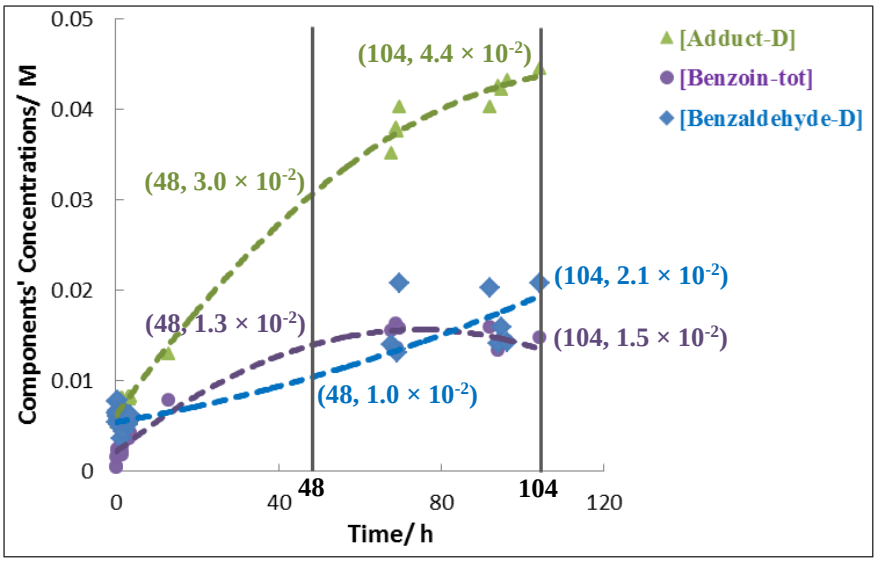

Figure 3.13. Plots of concentrations of benzoin product, deuterated adduct, and d^1 deuterated aldehyde against time for the self-condensation of benzaldehyde 27 catalyzed by *N*-triisorpopyl phenyl triazolium salt 49

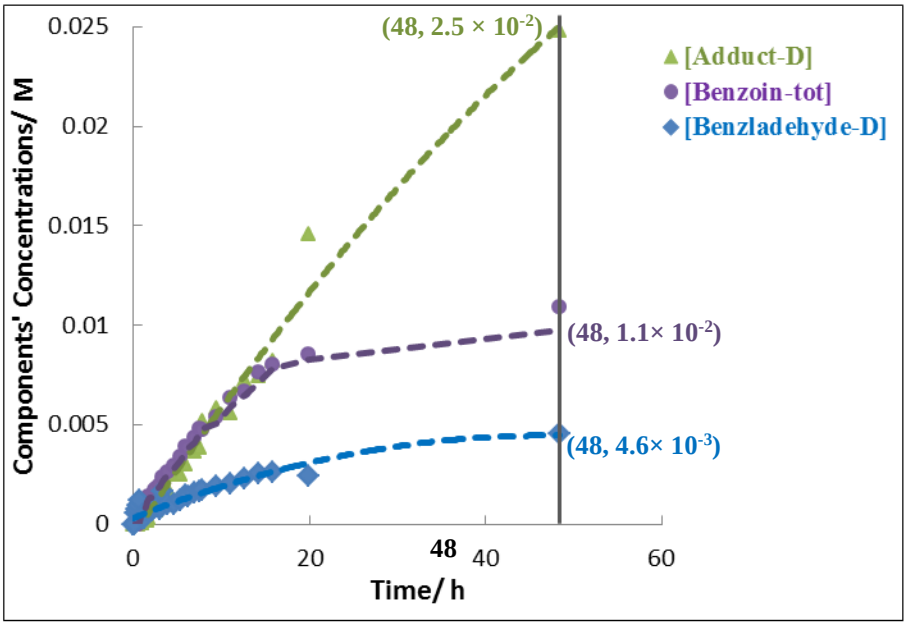

Figure 3.14. Plots of concentrations of benzoin product, deuterated adduct, and d^1 deuterated aldehyde against time for the self-condensation of 2-methoxybenzaldehyde 93 catalyzed by *N*-pentafluorophenyl triazolium salt 51

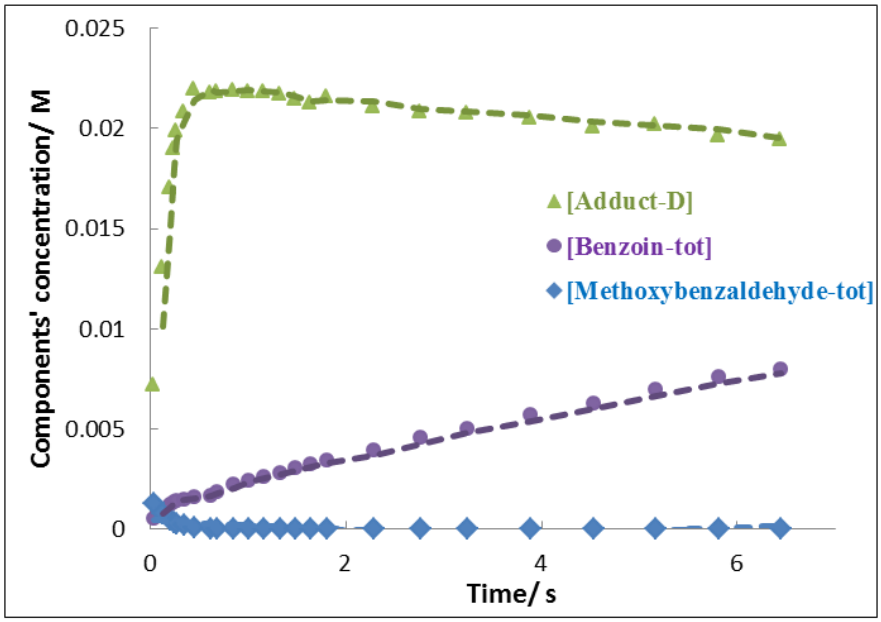

After 48 hours, the concentrations of deuterated adduct, d^1 deuterated aldehyde and benzoin product in the reaction catalyzed by *N*-mesityl triazolyl catalyst are 0.03: 0.01: 0.013 M. For the corresponding *N*-triisopropyl reaction, the analogous ratio is 0.025: 0.0046: 0.011 M. The lower conversion in the presence of triisopropyl catalyst to adduct is a result of the lower k_1 for this catalyst with benzaldehyde compared with the *N*-mesityl catalyst.

After accounting for the smaller conversion with triisopropyl catalyst, similar levels of deuterium incorporation into adduct/aldehyde are observed after 48 hours of reaction, although still slightly lower for *N*-triisopropyl. This is consistent with the similar K_1, k_1 and k_{-1} values. These data show the importance of reaction time in the analysis of extents of deuteration. For the *N*-mesityl catalyst after 104 hours, the ratio changes to 0.044: 0.021: 0.015 M, showing that the percentage deuteration is still increasing with time whereas there is a smaller change in the concentration of benzoin product.

Chapter 4. Experimental

4.1. General Instrumentation

NMR: NMR samples were prepared in deuterium oxide-d_2, chloroform-d_1, methanol-d_4, dichloromethane-d_2, and dimethyl sulfoxide-d_6. The chemical shifts for residual solvent peak in ^{1}H and ^{13}C NMR spectra are reported in Table 4.1.

Table 4.1. Signals due to NMR solvents

Solvent	δ_H, ppm	δ_C, ppm
deuterated chloroform	7.26	77.2
deuterium oxide	4.79	-
deuterated dichloromethane	5.32	53.8
deuterated methanol	2.50	39.5
deuterated dimethyl sulfoxide	3.31	49.0

Data are presented as follows: chemical shift (ppm), integration, multiplicity (s = singlet, d = doublet, t = triplet, q = quartet, p = quintet, h= heptet, m = multiplet, br = broad), coupling constants (Hz), and assignment. Varian Mercury-400, Bruker Avance-400, Varian Inova-500, Varian VNMRS-600 and Varian VNMRS-700 instruments were used to record the NMR spectra at 400, 500, 600 and 700 MHz.

EA: Elemental analyses were obtained from the Microanalytical Unit (Department of Chemistry, Durham University), and performed on an Exeter CE-440 Elemental Analyser.

MS: A waters *TQD* mass spectrometer was used to perform the low resolution mass spectrometry, and Thermo-Finnigan *LTQ FT* mass spectrometer was used to perform

the high resolution mass spectrometry.

Chromatography: Thin layer chromatography was performed using silica-backed Machery-Nagel Polygram SILG/UV_{254} plates. Column chromatography was performed using silica gel.

4.2. Materials:

NMR Solvents: Deuterium oxide-d_2 (99.9 atom % D), methanol-d_4 (99.8 atom % D), dimethyl sulfoxide-d_6 (99.9 atom % D) and dichloromethane-d_2 (99.8 atom % D) were purchased from Cambridge Isotope Laboratories. Chloroform-d_1 (99.8 atom % D) was purchased from Apollo Scientific, and Euriso-top.

Reagents: Benzaldehyde and triethylamine were purchased from Sigma-Aldrich and distilled before use. Triethylamine hydrochloride from Sigma-Aldrich was vacuum dried prior to use. Unless stated, all other chemicals were reagent grade and used without further purification. Reactions involving air or moisture sensitive reagents were performed under an argon atmosphere using oven-dried glassware. Solvents were dried prior to use using an Innovative Technology Inc. solvent purification system.

4.3. Synthetic Procedures

4.3.1. 2-Phenyl-6,7-dihydro-*5H*-pyrrolo[2,1-c][1,2,4]triazol-2-ium tetrafluoroborate 47

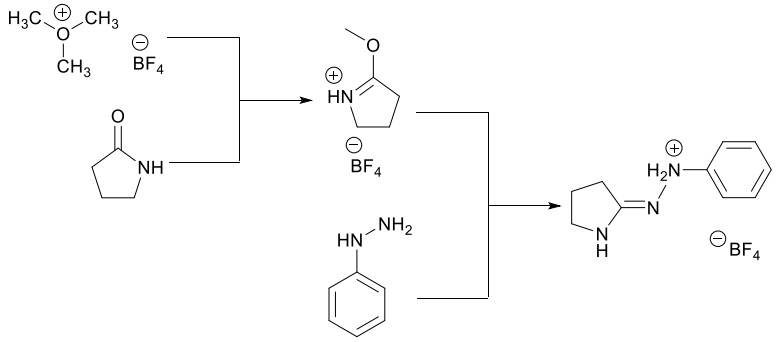

Based on a procedure by Rovis and co-workers[161], trimethyloxonium tetrafluoroborate (1.51 g, 10.2 mmol) was added to a 2-pyrrolidinone solution (0.79 g, 9.29 mmol) in dry dichloromethane (42 mL), and stirred at room temperature for 24 hours, under an argon environment. After the addition of phenylhydrazine (1.00 mL, 10.2 mmol), the reaction mixture was stirred for 48 hours at room temperature under an inert atmosphere, then concentrated under reduced pressure to yield the amidrazone as a brown solid which was directly used without further purification.

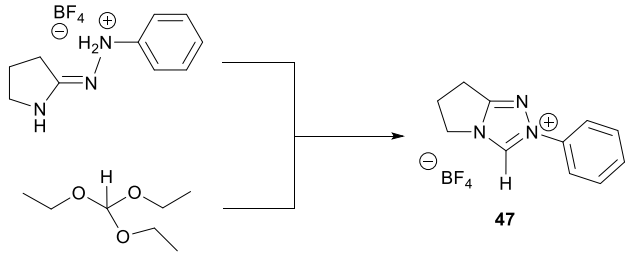

The residue was dissolved by using methanol (5 mL) and triethyl orthoformate (8.4 mL, 49.5 mmol) and refluxed for 24 hours. Solvent was removed under reduced pressure and ethyl acetate was used to precipitate and wash the solid to yield the title compound as a brown solid (0.88 g, 52%), with spectroscopic details in accordance with the literature. **^{1}H NMR** (500 MHz, $CDCl_3$): δ_H 2.90 (2H, m, CH_2), 3.27 (2H, dd, *J*=7.21, 8.25 Hz, CH_2), 4.67 (2H, m, CH_2), 7.52-7.64 (3H, m, ArH), 7.83 (2H, m, ArH), 10.12 (1H, s, NCH(N)); **^{13}C NMR** (176 MHz, D_2O): δ_C 21.3 (CH_2), 26.5 (CH_2),

47.3 (CH_2), 121.3 (2 × ArCH), 130.1 (2 × ArCH), 130.9 (ArCH), 135.3 (ArCN), 163.8 (NCN); ***m/z*** (ES+): 186 ($[M–BF_4]^+$, 100%)

4.3.2. 2-Mesityl-6,7-dihydro-5*H*-pyrrolo[2,1-c][1,2,4]triazol-2-ium tetrafluoroborate 48

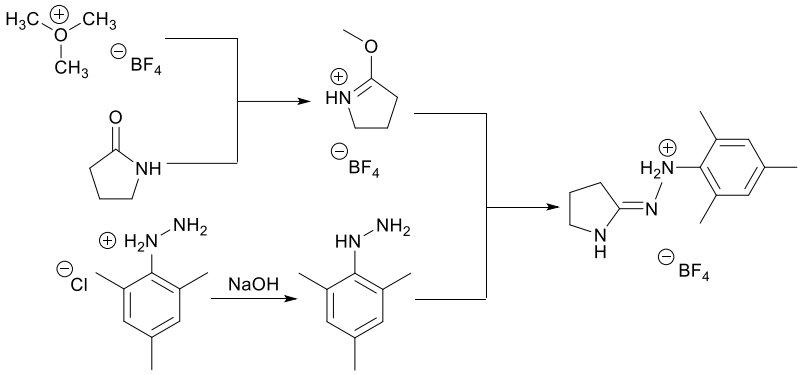

Based on a procedure by Smith and co-workers[172], trimethyloxonium tetrafluoroborate (0.87 g, 6.00 mmol) was added to a 2-pyrrolidinone (0.50 g, 5.85 mmol) solution in anhydrous dichloromethane (30 mL), and stirred for 24 hours at room temperature under an argon environment. Mesityl hydrazine hydrochloride (1.50 g, 8.00 mmol) was dissolved in aqueous sodium hydroxide (1 M, 8 mL, 8 mmol), and extracted into dichloromethane. This dichloromethane solution was immediately added to the reaction mixture, and stirred for another 48 hours at room temperature under argon. The solvent was removed under reduced pressure to give the amidrazone as a dark red solid which was directly used without further purification.

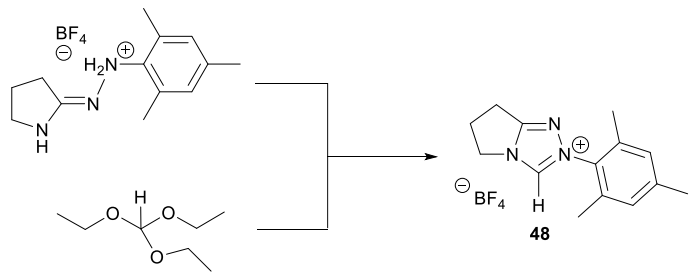

The residue was dissolved in chlorobenzene (10 mL) and triethyl orthoformate (5 mL),

and refluxed for 72 hours. The solvent was removed under reduced pressure, and trituration using hexane and ethyl acetate yield the title compound as a brown solid (1.76 g, 92%), with spectroscopic details in accordance with the literature. **^{1}H NMR** (400 MHz, $CDCl_3$): δ_H 2.08 (6H, s, 2 × CH_3), 2.38 (3H, s, CH_3), 2.91 (2H, m, CH_2), 3.26 (2H, dd, *J*=7.23, 8.30 Hz, CH_2), 4.67 (2H, dd, *J*=6.71, 8.15 Hz, CH_2), 6.99 (2H, s, 2 × ArCH), 9.51 (1H, s, NCH(N)); **^{13}C NMR** (176 MHz, $CDCl_3$): δ_C 17.5 (2 × CH_3), 21.5 (CH_3), 22.1 (CH_2), 26.8 (CH_2), 48.1 (CH_2), 129.9 (2 × ArCH), 132.0 (ArC), 135.3 (2 × ArC), 141.6 (ArC), 142.2 (ArCN), 162.9 (NCN) ***m/z*** (ES+): 228 ([M–BF_4]$^+$, 100%). **EA** Calc. for $C_{14}H_{18}N_3BF_4$: %C 53.36, %H 5.76, %N 13.33; Found: %C 52.86, %H 5.76, %N 13.06.

4.3.3. 2-Pentafluorophenyl-6,7-dihydro-*5H*-pyrrolo[2,1-c][1,2,4]triazol-2-ium tetrafluoroborate 51

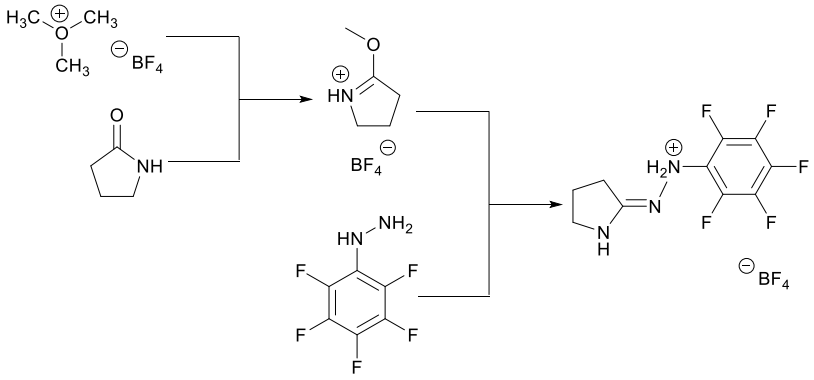

Based on a procedure by Rovis and co-workers[161], trimethyloxonium tetrafluoroborate (1.61 g, 11.0 mmol) was added into an anhydrous dichloromethane (50 mL) solution of 2-pyrrolidinone (0.94 g, 11.0 mmol) and stirred for 24 hours at room temperature under an argon environment. Pentafluorophenyl hydrazine (2.16 g, 11.0 mmol) was added into the solution, and then stirred for a further 48 hours at room temperature under argon. The solvent was removed under vacuum yielding the amidrazone as an orange solid which was used without further purification. R_f (dichloromethane: methanol 95:5) = 0.15, yellow spot.

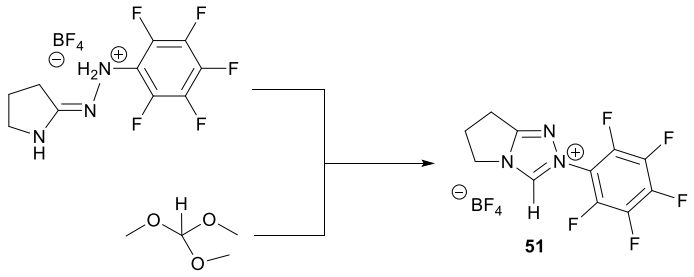

The amidrazone was dissolved in trimethyl orthoformate (20 mL) and refluxed for 24 hours. The solvent was removed under vacuum to yield a brown oil. Further precipitation and trituration with ethyl acetate followed by diethyl ether yielded the title compound as a white solid (2.66 g, 67%), with spectroscopic details in accordance with the literature. R_f (dichloromethane: methanol 95:5) = 0.15, colorless spot; **^{1}H NMR** (400 MHz, CD_3OD): δ_H 2.92 (2H, p, *J*=7.65 Hz, CH_2), 3.32 (2H, CH_2, covered by solvent residue peak), 4.59 (2H, t, *J*=7.41 Hz, CH_2); **^{13}C NMR** (176 MHz, CD_3OD): δ_C 24.3 (CH_2), 29.2 (CH_2), 58.2 (CH_2), 113.6 (ArC), 139.7 (ArCN), 144.4 (2 × ArCF), 145.3 (ArCF), 146.4 (2 × ArCF), 167.5 (NCN); **^{19}F NMR** (400 MHz, $CDCl_3$): δ_F –146.53 (2F, d, *J*=19.4 Hz, ArF), 147.51 (1F, t, *J*=21.5 Hz, ArF), –150.58 (br s, BF_4), –150.63 (q, BF_4), –159.64 (2F, t, *J*=19.0 Hz, ArF); ***m/z*** (ES+): 276 ([M–BF_4]$^+$, 100%)

4.3.4. 2-Perfluorophenyl-5,6,7,8-tetrahydro-[1,2,4]triazolo[4,3-a]pyridin-2-ium tetrafluoroborate 52

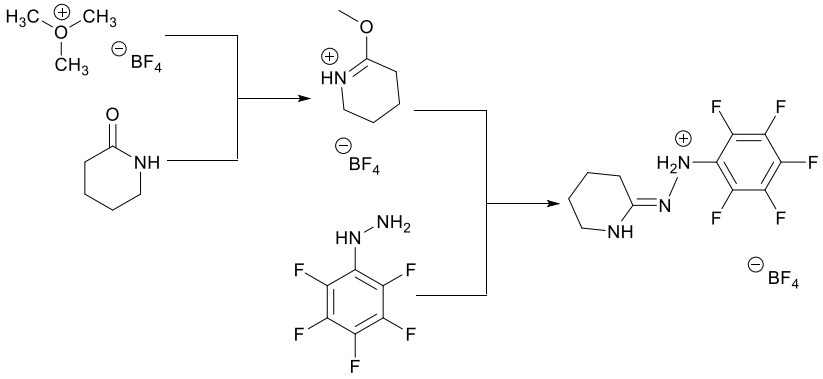

Using procedures adapted from Rovis and Gravel[156, 161], trimethyloxonium tetrafluoroborate (1.61 g, 11.0 mmol) was added into an anhydrous dichloromethane

(50 mL) solution of 2-piperidone (1.1 g, 11.0 mmol), and stirred overnight at room temperature under argon. Pentafluorophenyl hydrazine (2.16 g, 11.0 mmol) was added into the solution, and stirred for a further 48 hours at room temperature under argon to obtain a red solution. The solvent was removed under reduced pressure, yielding the amidrazone as an orange solid, which was used without further purification.

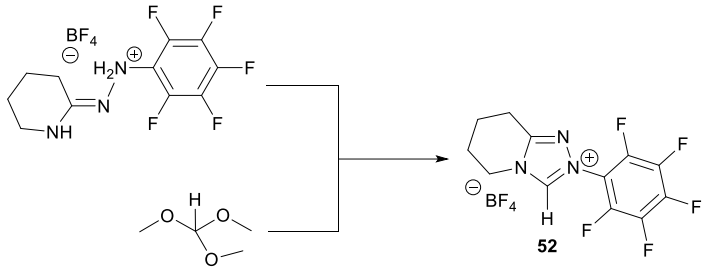

Trimethyl orthoformate (20 mL) was used to dissolve the orange residue, and the mixture was refluxed 24 hours. Solvent was removed under reduced pressure to obtain the crude product as viscous brown oil. Precipitation and trituration using ethyl acetate and diethyl ether yielded the title compound as a white solid (1.86 g, 56%), with spectroscopic details in accordance with the literature. **^{1}H NMR** (400 MHz, $(CD_3)_2SO$): δ_H 1.99 (2H, tdd, *J*= 2.8, 5.2, 10.1 Hz, CH_2), 2.06 (2H, m, CH_2), 3.11 (2H, t, *J*= 6.4 Hz, CH_2), 4.39 (2H, t, *J*=6.0 Hz, CH_2), 10.61 (1H, s, NCH(N)); **^{13}C NMR** (176 MHz, $CDCl_3$): 18.5, 20.8, 21.2, 46.8, 111.4, 136.9, 139.4, 144.5, 143.8, 146.5, 155.0; **^{19}F NMR** (400 MHz, $CDCl_3$): δ_F –146.09 (2F, m, ArF), 148.47 (1F, tt, *J*=3.33, 23.14 Hz, ArF), –160.14 (2F, m, ArF); **HRMS** (ES+): $[M–BF_4]^+$ $C_{12}H_9N_3F_5$ requires 290.0711, found 290.0708.

4.3.5. 2-Perfluorophenyl-6,7,8,9-tetrahydro-*5H*-[1,2,4]triazolo[4,3-a]azepi n-2-ium tetrafluoroborate 53

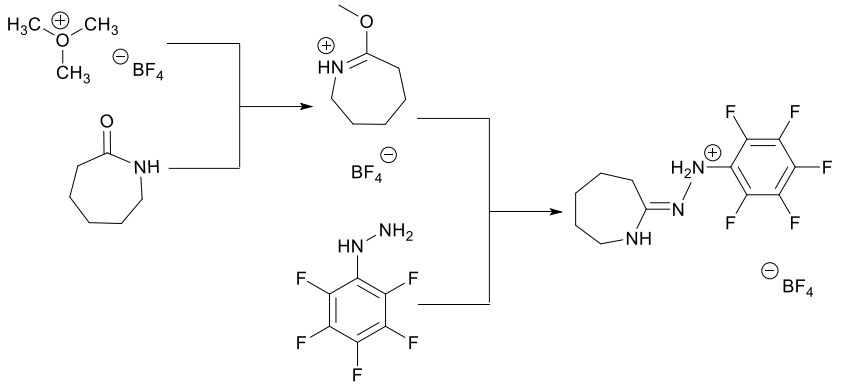

Using procedures adapted from Rovis and Gravel[156, 161], trimethyloxonium tetrafluoroborate (1.61 g, 11.0 mmol) was added to an anhydrous dichloromethane (50 mL) solution of *ε*-caprolactam (1.25 g, 11.0 mmol), and stirred overnight at room temperature under an argon environment. Pentafluorophenyl hydrazine (2.16 g, 11.0 mmol) was added and the solution turned orange immediately. After 24 hours stirring, some amidrazone product precipitated as orange crystals. Removal of all solvent yielded an orange residue, which was used without further purification.

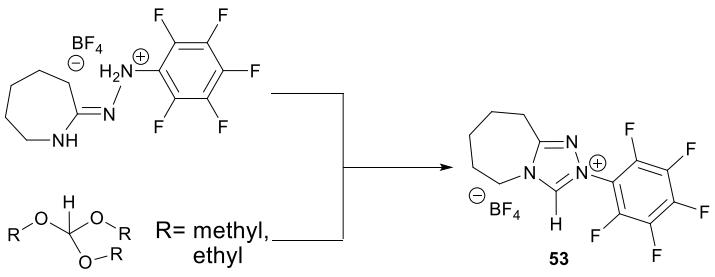

To compare the effects of different reagents, trimethyl orthoformate (20 mL), and triethyl orthoformate (20 mL) were both independently used to dissolve the orange residue. Both of the solutions were refluxed for 48 hours. The remaining solvent was removed under reduced pressure and the crude products were obtained as viscous brown oils. The oils were further purified by multi-phase recrystallization from dichloromethane: diethyl ether and chloroform: diethyl ether systems to give beige solids. Recrystallization from toluene yielded the product as a white fluffy solid. All

the solvent phases from the recrystallization step were collected and slow evaporation followed by freezing allowed the precipitation of more product as a colorless needle-like crystals (1.16 g, 27%). **^{1}H NMR** (400 MHz, $(CD_3)_2SO$): δ_H 1.78 (2H, m, CH_2), 1.93 (4H, m, 2 × CH_2), 3.18 (2H, m, CH_2), 4.51 (2H, m, CH_2), 10.59 (1H, s, NCH(N)); **^{13}C NMR** (400 MHz, $CDCl_3$): 24.1, 25.6, 26.7, 29.3, 45.0, 111.3, 136.9, 139.5, 141.4, 143.9, 147.6, 159.9; **^{19}F NMR** (400 MHz, $CDCl_3$): δ_F –146.00 (2F, m, ArF), -148.62 (1F, tt, *J*=3.24, 23.14, ArF), –160.14 (2F, m, ArF); ***m/z*** (ES+): 304 ([M–BF_4]$^+$, 100%)

4.3.6. 2-(2,6-Dimethoxyphenyl)-6,7-dihydro-*5H*-pyrrolo[2,1-c][1,2,4]triazol -2-ium chloride 50

4.3.6.1. Di-*tert*-butyl 1-(2,6-dimethoxyphenyl)hydrazine-1,2-dicarboxylate 69

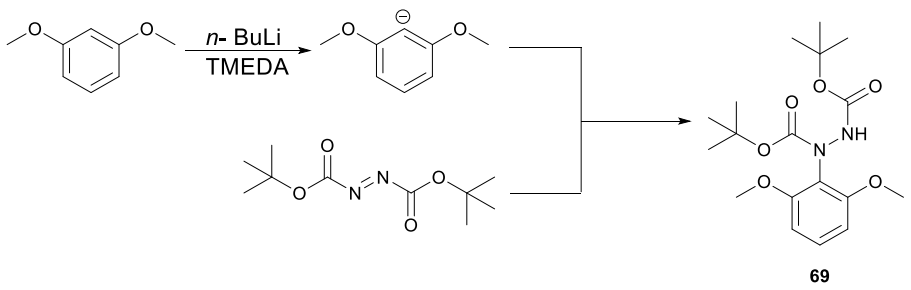

69

Using a procedure reported by Glorius and co-workers[154, 155], four attempts to prepare the title compound were performed. The procedure below reports the best outcome, however, the different equivalents used in the three other attempts are summarized in Table 4.2.

Freshly opened *n*-butyl lithium (2.5 M in hexane, 6 mL, 15 mmol, 1.5 equiv) was added dropwise to a solution of 1,3-dimethoxybenzene (1.31 mL, 10 mmol, 1 equiv) and tetramethylethylenediamine (TMEDA, 2.25 mL, 15 mmol, 1.5 equiv) in

anhydrous tetrahydrofuran (80 mL) at 0 ºC. After 45-60 minutes stirring (the stirring time was determined by using the method described in section 2.7.2), the reaction mixture was cooled to -78 ºC, and the solution of di-*tert*-butyl diazo-1,2-dicarboxylate (DBAD, 2.30 g, 10 mmol, 1 equiv) in anhydrous tetrahydrofuran (20 mL) was added slowly *via* cannula over 15 minutes. After 30 minutes of stirring, the reaction mixture was quenched at -78 ºC with addition of acetic acid (0.87 mL, 15 mmol, 1.5 equiv), subsequently warmed to room temperature, diluted with ethyl acetate (200 mL), and poured into distilled water (300 mL). The water phase was extracted with ethyl acetate (3×50 mL), and the combined organic phases were washed with brine, dried over sodium sulphate, filtered and concentrated under reduced pressure to give the crude product as a yellow oil. Flash column chromatography (hexane: ethyl acetate= 3:1) was used for further purification, and solvent was removed under vacuum yielding the title compound as a faint yellow solid with distinctive smell (2.86 g, 78%). The product exists as a ~ 2:1 mixture of carbamate rotamers, with spectroscopic details in accordance with the literature. R_f (hexane: ethyl acetate 75:25) = 0.27; **^{1}H NMR** (400 MHz, $(CD_3)_2SO$): δ_H Major rotamer: 1.30 (9H, s, $C(CH_3)_3$), 1.37 (9H, s, $C(CH_3)_3$), 3.76 (6H, s, $(CH_3)_2$), 6.63 (2H, d, *J*=8.4 Hz, ArH), 7.19 (1H, t, *J*=8.4 Hz, ArH), 8.83 (1H, br s, NH); Minor rotamer: 1.41 (9H, s, $C(CH_3)_3$), 1.43 (9H, s, $C(CH_3)_3$), 3.73 (6H, s, $(CH_3)_2$), 6.64 (2H, d, *J*=8.4 Hz, ArH), 7.21 (1H, t, *J*=8.4 Hz, ArH), 8.48 (1H, br s, NH); **^{13}C NMR** (176 MHz, $(CD_3)_2SO$): δ_C Major rotamer: 28.2, 28.5, 56.0, 79.2, 80.2, 104.7, 119.8, 128.7, 154.2, 156.6. Minor rotamer: 28.3, 28.5, 56.3, 79.4, 80.2, 105.2, 119.8, 129.0, 153.7, 155.7. **HRMS** (ES+): $[M+H]^+$ $C_{18}H_{29}N_2O_6$ requires: 369.2026, found: 369.2001; **E.A**: Calc. for $C_{18}H_{29}N_2O_6$: %C 58.68, %H 7.66, %N 7.6; Found: %C 58.51, %H 7.67, %N 7.64.

Table 4.2. Effect of reaction conditions on yield for the synthesis of di-*tert*-butyl 1-(2,6-dimethoxyphenyl)hydrazine-1,2-dicarboxylate 69.

Attempt	Age of BuLi solution[a]	BuLi equiv[b]	TMEDA[b] equiv	Yield (%)
1	4 months	1	1	29
2	4 months	1.5	1.5	48
3	Freshly opened	1.5	1.5	78
4	2 months	1.5	1.5	59

a) *n*-Butyl lithium solution in hexane was sealed and preserved in fridge (-2 ºC), however, decomposition still can be seen as the clear solution changed cloudy. b) Quantities of reagents are compared with DBAD

4.3.6.2. 2,6-Dimethoxyphenyl hydrazine hydrochloride 74

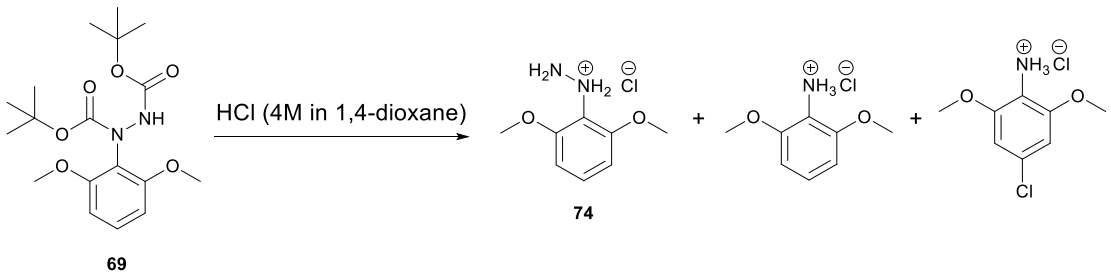

Di-*tert*-butyl 1-phenyl hydrazine-1,2-dicarboxylate **69** (1.84 g, 5 mmol) was dissolved in anhydrous methanol (12.5 mL) and hydrochloric acid (4 M in 1,4-dioxane, 12.5 mL, 50 mmol) was added slowly to the solution. The mixture was stirred for 4 hours at room temperature and the color turned orange. All volatiles were then removed under reduced pressure to give the title compound as an orange solid containing ~ 15% 2,6-dimethoxyaniline, which can be directly used without further purification. R_f (dichloromethane: methanol 95:5) = 0.20 **^{1}H NMR** (400MHz, CD_3OD): δ_H hydrazine hydrochloride salt: 3.94 (6H, s, $(CH_3)_2$), 6.76 (2H, d, *J*= 8.4 Hz, ArH), 7.18 (1H, t, *J*= 8.4 Hz, ArH); **^{13}C NMR** (176 MHz, CD_3OD): δ_C 55.2, 104.2, 125.9, 151.9; **m/z** (ES+) hydrazine: 169 ($[M\text{-}Cl]^+$, 100 %).

4.3.6.3. 2-Methoxy-4,5-dihydro-3*H*-pyrrole 72

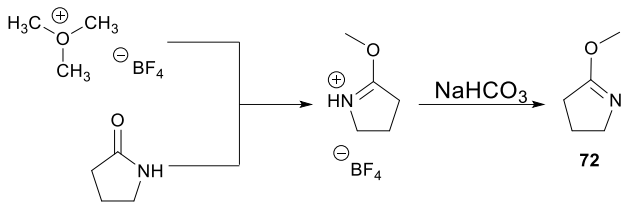

According to a literature procedure[155], 2-pyrrolidone (0.4 mL, 5 mmol) was dissolved in anhydrous dichloromethane (25 mL) and trimethyloxonium tetrafluoroborate (0.82 g, 5.5 mmol). The mixture was stirred overnight under argon at room temperature utill all the insoluble trimethyloxonium tetrafluoroborate solid was consumed. Saturated sodium bicarbonate solution (25 mL) was added slowly over 20 minutes. The organic phase was separated and the aqueous phase was extracted with dichloromethane (3 × 50 mL). The combined organic layers were dried over sodium sulphate and filtered. Most of the dichloromethane was removed on a rotary evaporator, with the pressure >250 mbar as the imino product **72** is volatile, to give the title compound as faint yellow oil with a distinctive odor, which can be directly used without further purification. **^{1}H NMR** (400 MHz, $(CD_3)_2SO$): δ_H 1.90 – 2.00 (2H, m, CH_2), 2.36 – 2.42 (2H, m, CH_2), 3.50 – 3.55 (2H, m, CH_2), 3.70 (3H, s, CH_3)

4.3.6.4. Amidrazone 73

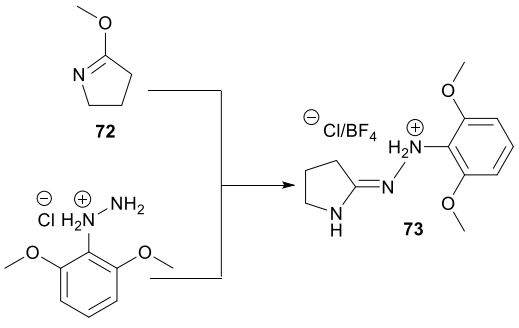

Imino ether **72** was dissolved in methanol (20 mL) and added to the hydrazine hydrochloride which caused the evolution of a white gas. A hydrochloric acid solution (4 M in 1,4-dioxane, 12.5 mL, 5 mmol) was added slowly to the solution, resulting in the further evolution of large amount of white gas. The mixture was stirred at room

temperature overnight under argon, and the solution turned dark red. All volatiles were removed under reduced pressure to give the amidrazone **73** as a brown oil, which was further dried under high vacuum, initially yielding a foamy solid, and subsequently a sticky oil when exposed to the atmosphere, which was used directly without purification. R_f (dichloromethane: methanol 90:10) = 0.27.

To change the counter ion and check the influence of acid type, in a new synthesis entry, tetrafluoroboric acid-diethyl ether complex (1 mL, ~10 mmol) was used instead of the 1,4-dioxane hydrochloric acid solution. Otherwise the procedure is identical to that above.

4.3.6.5. 2-(2,6-Dimethoxyphenyl)-6,7-dihydro-*5H*-pyrrolo[2,1-c][1,2,4]triazol-2-ium chloride 50

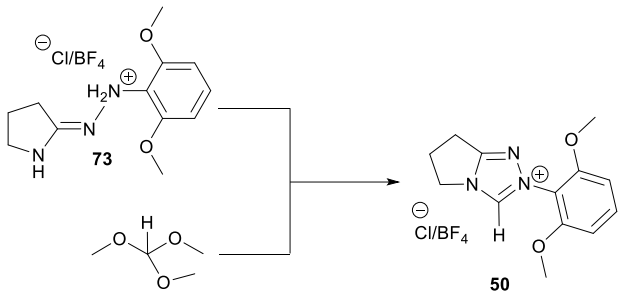

Amidrazone **73** was dissolved in anhydrous chlorobenzene (5 mL) and trimethyl orthoformate (6.6 mL, 40 mmol) was added to the solution. A reflux condenser with a calcium chloride drying tube was fitted and the mixture was heated to 80 ºC overnight. Then the mixture was cooled down to room temperature and stirred for one week under an argon environment. All the solvent was removed under reduced pressure and the crude product was obtained as a brown oil. Multi-phase recrystallization from dichloromethane: diethyl ether followed by chloroform: diethyl ether removed most of the impurities while some aniline salt and hydrazine salt can still be detected by NMR and mass spectroscopy. This crude product appeared initially as a brown solid, and quickly turned into sticky oil when exposed to the atmosphere. Flash column

chromatography (dichloromethane: methanol 90:10) yield the title triazolium salt as a brown oil (0.23g, 16%), with spectroscopic details in accordance with the literature: R_f (dichloromethane: methanol 90:10) = 0.19; **^{1}H NMR** (400 MHz, $CDCl_3$): δ_H 2.89 (2H, app q, *J*= 7.7 Hz, CH_2), 3.25 (2H, dd, *J*= 7,2, 8.2 Hz, CH_2), 3.84 (6H, s, $(CH_3)_2$), 4.93 (2H, t, *J*= 7.4 Hz, CH_2), 6.70 (2H, d, *J*= 8.6 Hz, ArH), 7.51 (1H, t, *J*= 8.6 Hz, ArH), 11.27 (1H, s, NCH(N)); **^{13}C NMR** (400 MHz, $CDCl_3$): δ_c 22.2, 27.1, 48.7, 56.6, 104.4, 113.4, 133.6, 144.2, 155.7, 161.5; m/z (ES+) 246 ($[M-Cl]^+$, 100 %);

4.3.7. 2-(2,6-Dimethoxyphenyl)-5,6,7,8-tetrahydro-[1,2,4]triazolo[4,3-a]pyridin-2-ium tetrafluoroborate 87

4.3.7.1. 2-Methoxy-3,4,5,6-tetrahydro-pyridine 97

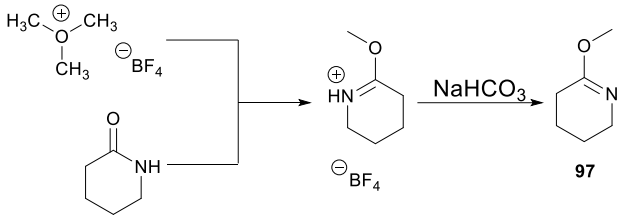

Based on the literature procedure[152, 156] and synthesis procedure of 2-methoxy-4,5-dihydro-3H-pyrrole in section 2.7.3, 2-piperidone (0.52 g, 5 mmol) was dissolved in anhydrous dichloromethane (25 mL), and trimethyloxonium tetrafluoroborate (0.82 g, 5.5 mmol) was added. The mixture was stirred under an inert atmosphere overnight. Saturated sodium bicarbonate (25 mL) was added slowly over 20 minutes. The organic layer was separated and the aqueous layer was extracted by dichlorormethane (3 × 25 mL). The combined organic layers were dried with sodium sulfate and filtered. Most of the solvent was evaporated with the pressure >200 mbar to give the title compound as a yellow oil with distinctive smell, which can be used directly without further purification. **^{1}H NMR** (400 MHz, $CDCl_3$): δ_H 1.62 (2H, m, CH_2), 1.76 (2H, m, CH_2), 2.22 (2H, m, CH_2), 3.53 (2H, m, CH_2), 3.70

(3H, s, OCH_3).

4.3.7.2. Amidrazone 88

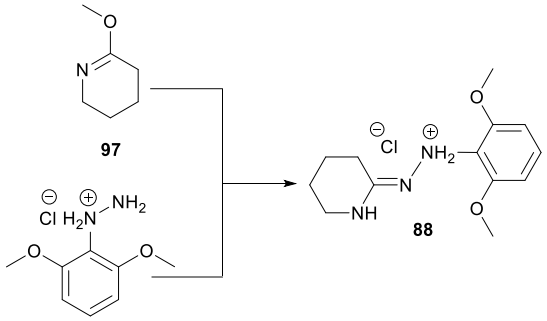

2-Methoxy-3,4,5,6-tetrahydro-pyridine **97** was dissolved in methanol (20 mL) and added to the hydrazine hydrochloride (**74**, with the same synthetic procedure in section 2.7.3), which caused the evolution of a white gas. A hydrochloric acid solution (4 M in 1,4-dioxane, 12.5 mL, 5 mmol) was slowly added to the solution which lead to the further evolution of a large amount of white gas. The mixture was stirred at room temperature overnight under an inert atmosphere, and the solution turned dark brown. All volatiles were removed under reduced pressure to give the amidrazone **88** as a brown oil, which upon further drying by high vacuum, lead to a foam solid, but soon turned into sticky oil when exposed to the atmosphere. The crude amidrazone was used directly without purification. R_f (dichloromethane: methanol 90:10) = 0.20; **m/z** (ES+) 250 ($[M–Cl]^+$, 100%).

4.3.7.3. 2-(2,6-Dimethoxyphenyl)-5,6,7,8-tetrahydro-[1,2,4]triazolo[4,3-a]pyridin-2-ium tetrafluoroborate 87

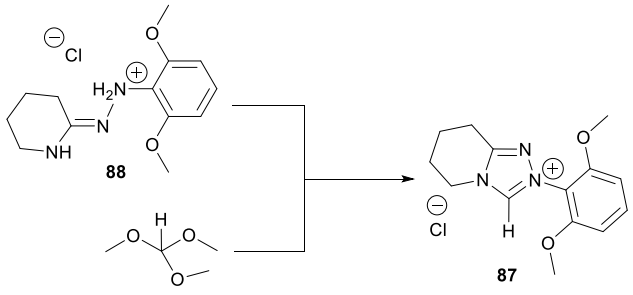

Amidrazone **88** was dissolved in anhydrous chlorobenzene (5 mL) and trimethyl orthoformate (6.6 mL, 40 mmol) was added to the solution. A reflux condenser with a calcium chloride drying tube was fitted and the mixture was heated to 80 ºC overnight. All the solvent was removed under reduced pressure and the crude product was obtained as a brown oil. Flash column chromatography (dichloromethane: methanol 90:10) was applied to separate the title compound but failed. R_f (dichloromethane: methanol 90:10) = 0.12; **m/z** (ES+) 260 ($[M–Cl]^+$, 100%).

4.3.7.4. Quantification of deprotonation of *n*-butyl lithium

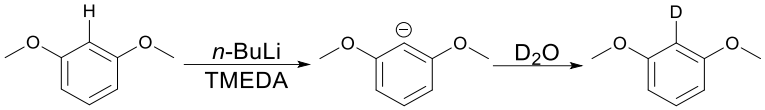

n-Butyl lithium (2.5 M, in hexane, opened for 4 months, 6 mL, <15 mmol) was added dropwise to an anhydrous tetrahydrofuran solution (50 mL) of 1,3-dimethoxybenzene (1.31 mL, 10 mmol) and tetramethylethylenediamine (TMEDA, 2.24 mL, 15 mmol) at 0 ºC under argon. After every five to ten minutes, a small portion of the reaction mixture was taken out and quenched by deuterium oxide immediately. Since the amount of the organic component was very small, the extraction process by using deuterated chloroform was not necessary. NMR was used to monitor the reaction process by comparing the integration of different aromatic peaks.

4.3.8. Synthesis of di- and tri-isopropyl phenyl hydrazine

Three synthetic procedures were attempted for the preparation of the title compounds. The first procedure was based on the traditional phenyl hydrazine synthesis starting with di-*ortho*-isopropyl aniline. The other two involved carbanion generation followed by the addition to the di-*tert*-butyl diazo-1,2-dicarboxylate (DBAD) to introduce the Boc protected hydrazine group, which can be easily deprotected in

acidic conditions. In the latter case, tri-isopropylbenzene and 2-bromo-1,3,5-triisopropylbenzene were employed as starting materials due to commercial availabilities. Furthermore, previous studies in our group have demonstrated that substituents in the *para*-position have a limited effect on catalytic performance.

4.3.8.1. Traditional phenyl hydrazine synthesis *via* di-*ortho*-isopropyl aniline

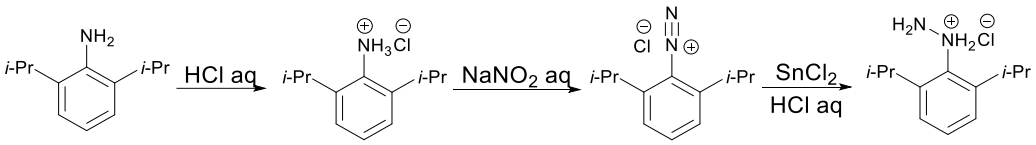

Based on the previous literature[162-165], concentrated hydrochloric acid solution (36 %, 4 mL) was added to 2,5-diisopropyl aniline (0.9 g, 6 mmol) at room temperature over two hours with thorough stirring, resulting in the formation of a white fluffy precipitate. The mixture was cooled down to -5 ~ 0 ºC, and a solution of sodium nitrite (0.42 g, 6 mmol) in distilled water (2 mL) was added dropwise within one hour. The white precipitate changed colour to initially bright yellow and later dark red with further addition of sodium nitrite solution. The mixture was stirred for a further fifteen minutes, and a solution of tin chloride (2.72 g, 14 mmol) in concentrated hydrochloric acid (36%, 3 mL) was added gradually over two hours. The reaction mixture aggregated into a faint red ball, and was stirred for one hour to 2 months, forming trace amounts of the title compound, which can only be detected by mass spectrometry. ***m/z*** (ES+): 193 ($[M+H]^+$, 68.56%.

4.3.8.2. *n*-Butyl Lithium based Di-*tert*-butyl 1-(2,4,6-triisopropylphenyl)hydrazine-1,2-dicarboxylate Synthesis

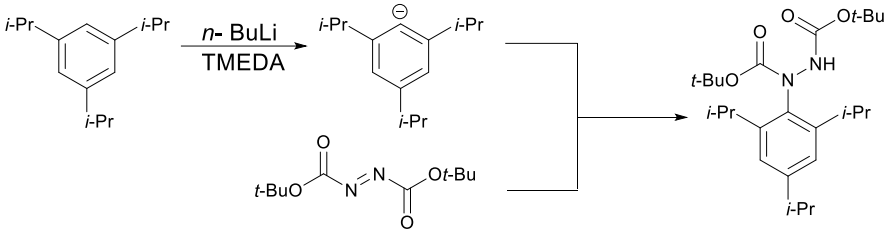

Based on the synthetic procedure of di-*tert*-butyl 1-(2,6-dimethoxyphenyl)hydrazine-1,2-dicarboxylate[154, 155, 166] in section 2.7.1, a similar synthetic procedure was attempted. *n*-Butyl lithium (4.8 mL, 2.5 M in hexane, 12 mmol) was added into an anhydrous tetrahydrofuran (60 mL) solution of 1,3,5-triisopropyl benzene (2.42 mL, 10 mmol) and tetramethylethylenediamine (TMEDA, 2 mL, 14 mmol) at 0 ºC dropwise under argon. After one hour stirring, the reaction mixture was cooled down to -78 ºC. An anhydrous tetrahydrofuran (20 mL) solution of di-*tert*-butyl diazo-1,2-dicarboxylate (DBAD, 2.30 g, 10 mmol) was added into the mixture dropwise via cannula. After thirty minutes to 2 days of stirring (different conditions are summarized in Table 4.3), acetic acid (0.87 mL, 10 mmol) was used to quench the reaction. Ethyl acetate (200 mL) was used to dilute the mixture, and distilled water (300 mL) was added to dissolve the white precipitate. The water phase was extracted with ethyl acetate (3 × 50 mL), and the combined organic phases were washed with brine, dried over sodium sulphate, filtered and concentrated under reduced pressure to give a yellow oil. However, all the attempts were unsuccessful as evidence of any product was not detected by mass spectrometry.

Table 4.3. Three attempted preparations of di-*tert*-butyl 1-(2,4,6-triisopropylphenyl) hydrazine-1,2-dicarboxylate with various reaction times and temperature during the addition of tin(II) chloride solution.

Attempt	Reaction time and temperature conditions[a]	Yield
1	30 minutes stirring at -78 ºC	Trace amount
2	30 minutes stirring at -78 ºC, followed with stirring overnight at 0 ºC	Trace amount
3	30 minutes stirring at -78 ºC, followed with 2 days room temperature stirring	Trace amount

a) The increase of reaction temperature and time was aimed to overcome the energy threshold provided by steric bulky substituents.

4.3.8.3. Grignard reagent based Synthesis of Di-*tert*-butyl 1-(2,4,6-triisopropylphenyl)hydrazine-1,2-dicarboxylate 80

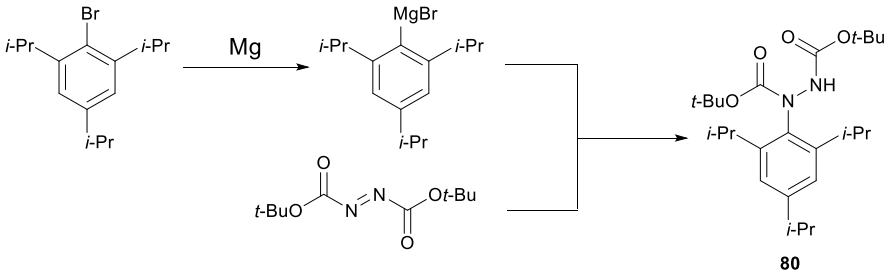

80

Based on literature procedures[159, 167, 168], several attempts to prepare the title compound were made. The recommended conditions is described in the text and equivalents used for other attempts are concluded within table 4.4.

Under low humidity conditions, mortar-polished, high-vacuum dried magnesium turnings (0.58 g, 24 mmol, 1.2 equiv) were heated to 90 ºC for one hour under argon, and cooled down to room temperature. A few drops of 2-bromo-1,3,5-triisopropylbenzene and anhydrous tetrahydrofuran were added to the magnesium turnings. After the reaction mixture turned dark colour and became exothermal, indicating the initiation of the Grignard reaction, the remaining

2-bromo-1,3,5-triisopropylbenzene (6 mL, 24 mmol, 1.2 equiv) and anhydrous tetrahydrofuran (9 mL) were added dropwise. Alternatively, 2-bromo-1,3,5-triisopropylbenzene and anhydrous tetrahydrofuran can be added within one fraction, while the water bath was utilized to control the reaction temperature at 55 ºC. The reaction was stirred for 90 minutes, then cooled to room temperature, and the Grignard reagent was added to an anhydrous tetrahydrofuran (20 mL) solution of di-*tert*-butyl diazo-1,2-dicarboxylate (DBAD, 4.60 g, 20 mmol, 1 equiv) *via* cannula at -78 ºC. After 30 minutes of stirring, acetic acid (1.8 mL, 24 mmol, 1.2 equiv) was added to quench the reaction. The reaction mixture was diluted with water, and extracted with diethyl ether, then washed with brine, dried over sodium sulfate and filtered. Vacuum concentration gave the crude title compound as a yellow sticky oil, which has a distinctive smell and can be used directly without further purification. R_f (diethyl ether: ethyl acetate 90:10) = 0.39; ***m/z*** (ES+): 457 ($[M+Na]^+$, 78.21%; **HRMS** (ES+): $[M+H]^+$ $C_{25}H_{43}N_2O_4$ requires 435.3223, found 435.3213.

Table 4.4. Yield various against the quantities of reagents for synthesis of di-*tert*-butyl 1-(2,4,6-triisopropylphenyl)hydrazine-1,2-dicarboxylate 80

Attempt	Mg[a,b] equiv	Bromobenzene[b] equiv	Yield[c] (%)
1	1	1	44
2	1.5	2	62
3	1.5	1.5	64
4	1.2	1.2	56

a) Mg turnings were mortar-polished, high-vacuum dried before using. b) Quantities of reagents are compared with DBAD. c) The yield of 2,4,6-triisopropylphenyl hydrazine hydrochloride **83** was used since **80** was deprotonated directly without purification.

4.3.8.4. 2,4,6-Triisopropylphenyl hydrazine hydrochloride 83

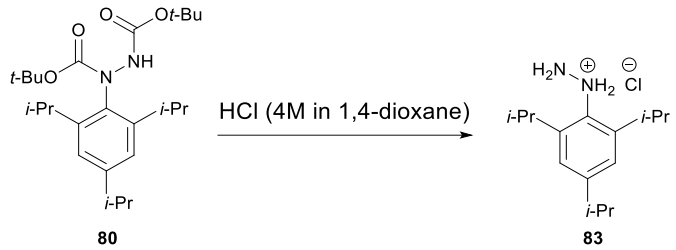

80 **83**

Di-*tert*-butyl 1-(2,4,6-triisopropylphenyl)hydrazine-1,2-dicarboxylate **80** (1.84 g, 5 mmol) was dissolved in anhydrous methanol (12.5 mL) and hydrochloric acid (4 M in 1,4-dioxane, 12.5 mL, 50 mmol) was added slowly to the solution. The mixture was stirred for 4 hours at room temperature and the color turned orange, and a white precipitate formed. The resulting mixture was kept in the freezer (-18 ºC) overnight, and the precipitate was removed by filtration and washed with hexane. All volatiles were then removed under reduced pressure to give a brown solid mixture. Hexane was used to dissolve all the non-polar impurities, and the remaining light brown solid was washed with cold diethyl ether to yield the title compound as a white powder. **^{1}H NMR** (400 MHz, DMSO): δ_H 1.19-1.29 (18H, m, CH_3), 2.88 (1H, h, *J*= 6.99 Hz, CH), 2.41 (2H, h, *J*= 6.95 Hz, CH), 7.01 (2H, s, ArH). **HRMS** (ES+): $[M\text{-}Cl]^+$ $C_{15}H_{27}N_3$ requires: 235.2174, found: 235.2187.

4.3.9. Synthesis of 2-(2,6-Dimethoxyphenyl)-6,7-dihydro-*5H*-pyrrolo[2,1-c] [1,2,4] triazol-2-ium chloride 49

4.3.9.1. Amidrazone 84

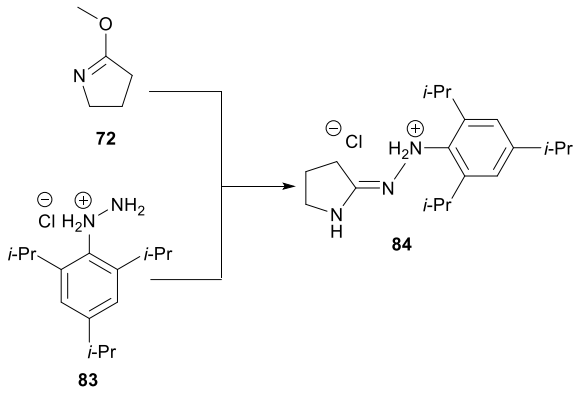

Imino ether 72 (Section 4.3.6.3) was dissolved in methanol (20 mL) and added to the hydrazine hydrochloride **83**, which caused the evolution of a white gas. A catalytic amount of hydrochloric acid solution (few drops, <1 mol%) was added. The mixture was stirred at 60 °C overnight, and the solution turned light yellow. All volatiles were removed under reduced pressure to give the amidrazone **84** as a pale yellow solid, which can be directly used without further purification. **HRMS** (ES+): $[M\text{-}Cl]^+$ $C_{19}H_{32}N_3$ requires: 302.2596, found: 302.2594.

4.3.9.2. 2-(2,6-Dimethoxyphenyl)-6,7-dihydro-*5H*-pyrrolo[2,1-c][1,2,4]triaz ol-2-ium chloride 49

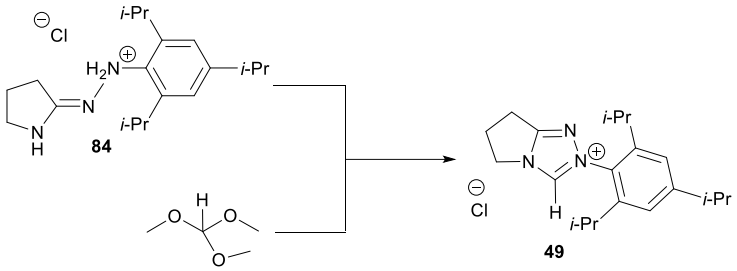

Amidrazone **84** was dissolved in anhydrous chlorobenzene (5 mL) and trimethyl orthoformate (6.6 mL, 40 mmol) was added to the solution. A reflux condenser with a calcium chloride drying tube was fitted and the mixture was heated to reflux for 2 hours, generating some solid. The solvent was removed under reduced pressure and the crude product was obtained as a yellow oil. Ethyl acetate washing of the oil yielded the title compound as a pale yellow powder (0.45g, 29%); **^{1}H NMR** (400 MHz, DMSO): δ_H 1.07 (6H, d, *J*= 6.8 Hz, CH_3), 1.14 (6H, d, *J*= 6.8 Hz, CH_3), 1.23 (6H, d, *J*= 6.9 Hz, CH_3), 2.37 (2H, h, *J*= 6.7 Hz, CH), 2.74 (2H, p, *J*= 7.7 Hz, CH_2), 2.98 (1H, h, *J*= 6.9 Hz, CH), 3.18 (2H, t, *J*=7.7 Hz, CH_2), 4.44 (2H, t, *J*= 7.4 Hz, CH_2), 10.37 (1H, s, NCH(N)); **^{13}C NMR** (176 MHz, $CDCl_3$): δ_c 21.9, 24.1, 24.2, 24.5, 28.2, 34.2, 48.0, 122.9, 129.8, 142.1, 145.6, 152.7, 163.9; **m/z** (ES+) 312 ($[M\text{-}Cl]^+$, 100 %); **HRMS** (ES+): $[M\text{-}Cl]^+$ $C_{20}H_{30}N_3$ requires: 312.2440, found: 312.2444.

4.4. Kinetic studies of the NHC-catalyzed benzoin condensation

Solutions of triethylamine buffer in methanol-d_4 were prepared using dried triethylamine hydrochloride and distilled triethylamine. ^{1}H NMR spectra were recorded on an Oxford Varian Inova 500 spectrometer thermostated at 25 °C, with a relaxation delay (d1) of 5 s, sweep width of 10000.0 Hz, acquisition time (at) of 2 s and 45° pulse angle (pw). Spectra were run with 32 transients (nt, total running time ~4 min). Measurement times were taken from the mid-point of the acquisition.

Chapter 5. Conclusions and Future work

Overall, seven *N*-aryl substituted bicyclic triazolium salts **47-53** were successfully prepared during this project as shown in Figure 5.1. Six of these salts were previously reported in the literature, however, the syntheses were further optimized during this project. The synthesis of triisopropyl triazolium salt **49** had not been previously reported. Furthermore, crystal structures were obtained for triazolium salts **48** and **53**.

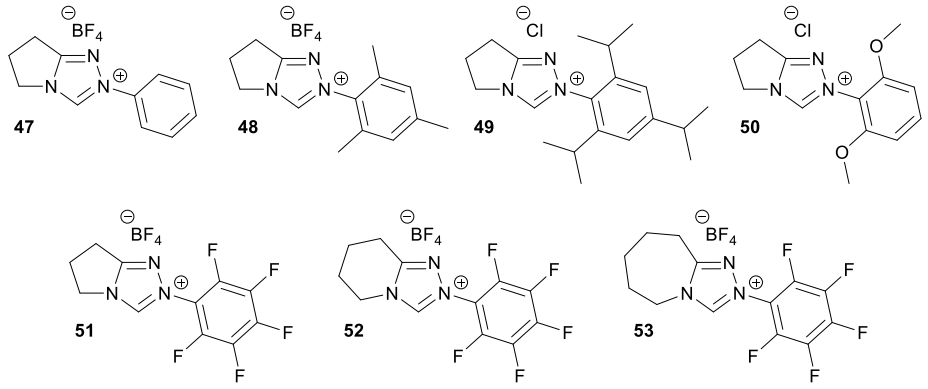

Figure 5.1 Structure of seven *N*-aryl substituted bicyclic triazolium salts 47-53

The second aim of the project was to kinetically evaluate the triazolium salts in the triethylamine-buffered benzoin reaction in MeOD. Although a broad range of aldehydes could be considered, for the shorter timeframe of this project the focus was on benzaldehyde and 2-methoxybenzaldehyde. The reaction of the *N*-mesityl **48** and *N*-phenyl **47** catalysts with benzaldehyde had been previously studied in our group under these conditions, however, reaction with 2-methoxybenzaldehyde was only studied previously in DCM for the *N*-mesityl catalyst. The reaction of triisopropylphenyl catalyst **49** and cyclohexyl- and cycloheptyl-fused catalysts **52** and **53** had not been previously kinetically evaluated. Although cyclohexyl and heptyl catalysts were successfully prepared, isolated and purified, there was insufficient time to fully evaluate these catalysts kinetically. This will be pursued during my PhD programme.

Overall, six kinetic studies evaluating the catalytical properties of triazolium salts **48**, **49**, and **51** for the self-condensation of benzaldehyde or *ortho*-methoxybenzaldehyde were analyzed respectively. The appearance and consumption of reactants, intermediates, products and by-products are monitored *in situ* by ^{1}H NMR spectroscopy, at 25 °C, in triethylamine-buffered methanol-d_4 solution. The 3-hydroxyaryl adduct substrate was the only observed intermediate, meanwhile, the formation of Breslow intermediate could be proved by the deuteration of hydroxyaryl adduct.

Equilibrium constants for hydroxyaryl adduct formation were determined (K_1, M^{-1}) from the reaction of triazolium catalyst with aldehyde. All previous measurements had shown that *ortho*-substituents on the *N*-aryl group of catalyst *increase* K_1 although *ortho*-methyl was the only alkyl example. Our results surprisingly show that the change from *N*-mesityl to *N*-triisopropyl results in a small 1.2-fold *decrease* in K_1 for the reaction of benzaldehyde in MeOD although both values are still ~10-fold higher than for the unsubstituted N-phenyl catalyst. By contrast, for the reaction of 2-methoxybenzaldehyde, K_1 increases in the order *N*-phenyl (118) < *N*-mesityl (524) < *N*-triisopropyl (1738). Thus the effect of the additional steric bulk of the *ortho*-isopropyl substituent versus an *ortho*-methyl has limited effect for the reaction of benzaldehyde, however, the combination of *ortho*-substituents on *both* catalyst and aldehyde does show a synergistic effect in increasing K_1. The observed increases in K_1 are mainly a result of lower rate constants for decomposition of adduct back to aldehyde (k_{-1}). Smaller changes are observed in the rate constant for formation of adduct (k_1). This increased stability of the adducts may be partly a result of steric hindrance of deprotonation of the OH group of adduct, which is the first step in the decomposition back to free catalyst and aldehyde.

The extent of deuterium incorporation into reactant aldehyde was evaluated in triethylamine-buffered deuteriomethanol. Under these reaction conditions, the further reaction of Breslow intermediate towards benzoin product, deuterated adduct and

deuterated aldehyde was only observed for the reaction of benzaldehyde with *N*-mesityl and triisopropyl catalysts. Similar levels of deuterium incorporation into adduct/aldehyde were observed after 48 hours of reaction, although slightly lower for *N*-triisopropyl, which is consistent with the similar K_1, k_1 and k_{-1} values. These data show the importance of reaction time in the analysis of extents of deuteration.

For the reaction of 2-methoxybenzaldehyde with *N*-mesityl and triisopropyl catalysts bigger differences in deuteration would be expected as larger variations in K_1, k_1 and k_{-1} are observed, however, the more sluggish onwards reaction of the adducts in these cases in triethylamine-buffered methanol prevented a quantitative assessment. Future work will evaluate levels of deuteration using stronger bases, *e.g.* DBU, methoxide and *tert*-butoxide,in deuteriomethanol, other deuterated alcohol solvents and D_2O. Future work will also explore the influence of temperature, and a broader range of aldehydes in this context, including linear and branched aliphatic aldehydes.

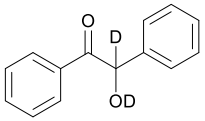

89D

Figure 5.2. Deuterated benzoin product observed in kinetic study

The reactivity of the *N*-pentafluorophenyl triazolium catalyst meant that even the benzoin reaction of 2-methoxybenzaldehyde is observed. Surprisingly, no free aldehyde is observed after 800 second (~ 10 mins). Initially, aldehyde is consumed quantitatively to H-adduct. Subsequently, rapid deuterium exchange occurs on the adduct. An increase in benzoin formation is observed showing that all d^1 deuterated aldehyde upon decomposition of the Breslow intermediate is consumed immediately in the benzoin reaction. Consistent with this, the benzylic proton of benzoin product **89D** is not observed in ^1H NMR spectra indicating complete deuteration.

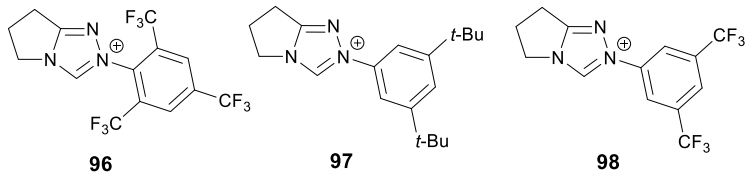

Figure 5.3. Candidates of triazolium precatalyst for future syntheses

Future work will also consider further variation of catalyst architecture incorporating both steric bulk and electron withdrawing substituents in the *N*-aryl substituent *e.g.* the fluoromesityl substituent (2,4,6-tris-trifluoromethylphenyl) **96**. It may be valuable to prepare *meta*-aryl substituted NHCs with bulky alkyl and/or electron-withdrawing substituents, such as 3,5-bis-*tert*-butylphenyl, and 3,5-bis-trifluoromethylphenyl. The effect of fused ring size[152, 156, 173] on overall reaction profiles will be evaluated using the catalysts **97** and **98** successfully prepared in this project. The synthetic literature shows that small changes in the size of the fused ring can lead to quite dramatic changes in the chemoselectivities of benzoin and Stetter reactions, and the origins of these observations are not understood. In these cases, it is also possible that large variations in extents of deuteration may be observed.

Recent work in the literature has seen the immobilization of imidazolyl NHCs on solid supports[174]. In the longer term scope of the project, the potential immobilization of triazolyl carbenes may be essential to effect the catalytic formation of deuterated aldehydes once the effect of catalyst architecture on deuteration is more understood. The use of flow chemistry conditions may also be explored to evaluate whether improvements in deuteration levels may be obtained.

In a parallel project in our laboratory, the benzoin and Stetter reactions of bis-aminocyclopropenylidenes (BACS), a new class of carbenes, are being investigated. Surprisingly, recent literature shows these catalysts do not give benzoin products and favour more Stetter-like reactions, the opposite chemoselectivity to triazolyl carbenes[175, 176]. Recent unpublished work from our group shows that the

hydroxyaryl adducts formed from these catalysts are particularly stable and do show parallel deuterium incorporation. The evaluation of these catalysts for the d^1 deuteration of aldehydes will also be performed. Overall, all of these studies of partitioning of Breslow-like intermediates towards deuteration versus other reactions provides a bigger picture quantitative understanding of chemoselectivity in these carbene-catalysed processes.

A novel outcome of this project was the identification of dimethoxyacetal NHC adduct **65** and characterization *via* X-ray crystallography. Future work of my PhD will attempt to develop a further, more-detailed synthetic evaluation of the adduct's formation including mechanistic studies, and build up the possible application of the adduct as a precursor towards NHC-formaldehyde **66** and a new type of Breslow intermediate **67** (Scheme 5.1).

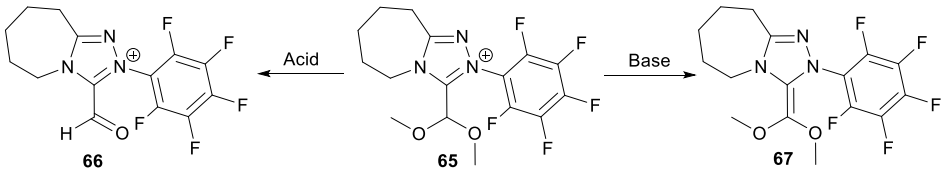

Scheme 5.1. Potential application of the 2-perfluorophenyl-6,7,8,9-tetrahydro-*5H*-[1,2,4] triazolo[4,3-a]azepin-2-ium tetrafluoroborate dimethoxy acetal adduct 65

Chapter 6. Reference:

1. O. Mosin and I. Ignatov, *Journal of Health, Medicine and Nursing*, 2014, **8**, 107-146.
2. O. Mosin and I. Ignatov, *Journal of Health, Medicine and Nursing*, 2014, **6**, 73-110.
3. O. Mosin and I. Ignatov, *Journal of Health, Medicine and Nursing*, 2014, **7**, 101-140.
4. H. J. Neuburg, J. Atherley and L. Walker, *Girdler-Sulfide Process Physical Properties*, Atomic Energy of Canada Limited, Chalk River Nuclear Laboratories, 1977.
5. C. G. Swain and R. F. Bader, *Tetrahedron*, 1960, **10**, 182-199.
6. P. Paulsen and W. Cooke, *Anal. Chem.*, 1963, **35**, 1560-1560.
7. E. Odeblad, B. N. Bhar and G. Lindström, *Arch. Biochem. Biophys.*, 1956, **63**, 221-225.
8. T. Bastow, R. Hodge and A. Hill, *J. Membr. Sci.*, 1997, **131**, 207-215.
9. Z. Tian, D. R. Reed and S. R. Kass, *Int. J. Mass Spectrom.*, 2015, **377**, 130-138.
10. J. Atzrodt, V. Derdau, T. Fey and J. Zimmermann, *Angew. Chem., Int. Ed.*, 2007, **46**, 7744-7765.
11. W. JamesáCatallo, *Chem. Soc. Rev.*, 1997, **26**, 401-406.
12. A. Di Giuseppe, R. Castarlenas and L. A. Oro, *C. R. Chim.*, 2015, **18**, 713-741.
13. T. Maegawa, Y. Fujiwara, Y. Inagaki, H. Esaki, Y. Monguchi and H. Sajiki, *Angew.Chem*, 2008, **120**, 5474-5477.
14. T. Maegawa, Y. Fujiwara, Y. Inagaki, Y. Monguchi and H. Sajiki, *Adv. Synth. Catal.*, 2008, **350**, 2215-2218.
15. P. Avenier, X. Solans-Monfort, L. Veyre, F. Renili, J.-M. Basset, O. Eisenstein, M. Taoufik and E. A. Quadrelli, *Top. Catal.*, 2009, **52**, 1482-1491.
16. T. Maegawa, N. Ito, K. Oono, Y. Monguchi and H. Sajiki, *Synthesis*, 2009, **2009**, 2674-2678.
17. J. Atzrodt and V. Derdau, *J. Labelled Compd. Radiopharm.*, 2010, **53**, 674-685.
18. Y. Sawama, T. Yamada, Y. Yabe, K. Morita, K. Shibata, M. Shigetsura, Y. Monguchi and H. Sajiki, *Adv. Synth. Catal.*, 2013, **355**, 1529-1534.
19. J. L. Garnett and R. Hodges, *J. Am. Chem. Soc.*, 1967, **89**, 4546-4547.
20. J. Garnett and R. Hodges, *Chem. Commun. (London)*, 1967, 1001b-1003.
21. M. R. Blake, J. L. Garnett, I. K. Gregor, W. Hannan, K. Hoa and M. A. Long, *J. Chem. Soc., Chem. Commun.*, 1975, 930-932.
22. N. Gol'dshleger, V. Es'kova, A. Shilov and A. Shteinman, *Zh. Fiz. Khim.*, 1972, **46**, 1353-1354.
23. D. A. Buckingham, L. G. Marzilli and A. M. Sargeson, *J. Am. Chem. Soc.*, 1967, **89**, 5133-5138.
24. J. Elvidge, J. Jones, C. O'Brien and E. Evans, *J. Chem. Soc. D*, 1971, 394-395.
25. J. I. Legg and J. Steele, *Inorg. Chem.*, 1971, **10**, 2177-2182.
26. M. Aresta and F. Ciminale, *J. Chem. Soc., Dalton Trans.*, 1981, 1520-1523.
27. D. A. Buckingham, I. Stewart and P. A. Sutton, *J. Am. Chem. Soc.*, 1990, **112**, 845-854.
28. A. J. Clarkson, A. G. Blackman and C. R. Clark, *J. Chem. Soc., Dalton Trans.*, 2001, 758-765.
29. N. Foroughifar, A. Mobinikhaledi, M. Amrollahi and M. Zendehdel, *Appl. Magn. Reson.*, 2004, **26**, 483-488.
30. N. Foroughifar, A. Mobinikhaledi, N. Foroughifar and S. Hoseini, *Asian J. Chem.*, 2007, **19**, 5181.
31. B. A. Arndtsen, R. G. Bergman, T. A. Mobley and T. H. Peterson, *Acc. Chem. Res.*, 1995, **28**, 154-162.
32. L. Rubio‐Pérez, R. Azpíroz, A. Di Giuseppe, V. Polo, R. Castarlenas, J. J. Pérez‐Torrente and L. A. Oro, *Chem.-Eur. J.*, 2013, **19**, 15304-15314.

33. A. Di Giuseppe, R. Castarlenas, J. J. Pérez‐Torrente, F. J. Lahoz and L. A. Oro, *Chem.-Eur. J.*, 2014, **20**, 8391-8403.
34. P. A. Hunt, *Dalton Trans.*, 2007, 1743-1754.
35. R. N. Perutz and S. Sabo‐Etienne, *Angew. Chem., Int. Ed.*, 2007, **46**, 2578-2592.
36. A. L. Reznichenko and K. C. Hultzsch, in *Molecular Catalysis of Rare-Earth Elements*, Springer, 2010, pp. 1-48.
37. A. Di Giuseppe, R. Castarlenas, J. J. Pérez‐Torrente, F. J. Lahoz, V. Polo and L. A. Oro, *Angew. Chem., Int. Ed.*, 2011, **50**, 3938-3942.
38. S. H. Lee, S. I. Gorelsky and G. I. Nikonov, *Organometallics*, 2013, **32**, 6599-6604.
39. W. Baratta, G. Bossi, E. Putignano and P. Rigo, *Chem.-Eur. J.*, 2011, **17**, 3474-3481.
40. A. Harthun, R. Giernoth, C. J. Elsevier and J. Bargon, *Chem. Commun.*, 1996, 2483-2484.
41. G. Lázaro, M. Iglesias, F. J. Fernández‐Alvarez, S. Miguel, J. Pablo, J. J. Pérez‐Torrente and L. A. Oro, *ChemCatChem*, 2013, **5**, 1133-1141.
42. H. Junge, N. Marquet, A. Kammer, S. Denurra, M. Bauer, S. Wohlrab, F. Gärtner, M. M. Pohl, A. Spannenberg and S. Gladiali, *Chem.-Eur. J.*, 2012, **18**, 12749-12758.
43. J. M. Buchanan, J. M. Stryker and R. G. Bergman, *J. Am. Chem. Soc.*, 1986, **108**, 1537-1550.
44. B. A. Arndtsen and R. G. Bergman, *SCIENCE-NEW YORK THEN WASHINGTON-*, 1995, 1970-1972.
45. G. Anderson, S. Saum, R. Cross and S. Morris, *Organometallics*, 1983, **2**, 780-782.
46. B. Moreno, S. Sabo-Etienne, B. Chaudret, A. Rodriguez, F. Jalon and S. Trofimenko, *J. Am. Chem. Soc.*, 1995, **117**, 7441-7451.
47. J. P. Collman, H. Fish, P. S. Wagenknecht, D. A. Tyvoll, L.-L. Chng, T. A. Eberspacher, J. I. Brauman, J. W. Bacon and L. H. Pignolet, *Inorg. Chem.*, 1996, **35**, 6746-6754.
48. C. Perthuisot, M. Fan and W. D. Jones, *Organometallics*, 1992, **11**, 3622-3629.
49. A. Borovik, S. Bott and A. Barron, *Angew.Chem.*, 2000, **112**, 4283-4284.
50. J. H. Lee, K. S. Yoo, C. P. Park, J. M. Olsen, S. Sakaguchi, G. Prakash, T. Mathew and K. W. Jung, *Adv. Synth. Catal.*, 2009, **351**, 563-568.
51. P. Ade, N. Aghanim, C. Armitage-Caplan, M. Arnaud, M. Ashdown, F. Atrio-Barandela, J. Aumont, C. Baccigalupi, A. J. Banday and R. Barreiro, *Astron. Astrophys.*, 2014, **571**, A16.
52. G. Aad, B. Abbott, J. Abdallah, S. A. Khalek, O. Abdinov, R. Aben, B. Abi, M. Abolins, O. AbouZeid and H. Abramowicz, *J. High Energy Phys.*, 2015, **2015**, 1-89.
53. R. Giles, G. Ahn and K. W. Jung, *Tetrahedron Lett.*, 2015, **56**, 6231-6235.
54. G. V. Smith and F. Notheisz, *Heterogeneous catalysis in organic chemistry*, Academic Press, 1999.
55. S. Gladiali, G. Mestroni, M. Beller and C. Bolm, *Wiley–VCH, Weinheum*, 2004, **2**, 145.
56. J. Atkinson, M. Luke and R. Stuart, *Can. J. Chem.*, 1967, **45**, 1511-1518.
57. J. Philipson and R. L. Burwell Jr, *J. Am. Chem. Soc.*, 1970, **92**, 6125-6133.
58. W. Brown and J. Garnett, *J. Am. Chem. Soc.*, 1958, **80**, 5272-5274.
59. G. Calf and J. Garnett, *J. Phys. Chem.*, 1964, **68**, 3887-3889.
60. L. Ackermann, R. Vicente and A. R. Kapdi, *Angew. Chem., Int. Ed.*, 2009, **48**, 9792-9826.
61. H. V. Thulasiram, R. M. Phan, S. B. Rivera and C. D. Poulter, *J. Org. Chem.*, 2006, **71**, 1739-1741.
62. E. J. Moriconi, J. P. St. George and W. Forbes, *Can. J. Chem.*, 1966, **44**, 759-769.
63. E. Kiran, P. G. Debenedetti and C. J. Peters, *Supercritical fluids: fundamentals and applications*,

Springer Science & Business Media, 2012.
64. L. H. Weldon and C. L. Wilson, *J. Chem. Soc.*, 1946, 244-245.
65. P. E. Savage, *Chem. Rev.*, 1999, **99**, 603-622.
66. E. Lyckman, C. Eckert and J. Prausnitz, *Chem. Eng. Sci.*, 1965, **20**, 703-706.
67. J. M. Prausnitz, *Computer calculations for multicomponent vapor-liquid and liquid-liquid equilibria*, Prentice Hall, 1980.
68. T. Junk and W. J. Catallo, *Tetrahedron Lett.*, 1996, **37**, 3445-3448.
69. N. H. Werstiuk and C. Ju, *Can. J. Chem.*, 1989, **67**, 812-815.
70. N. H. Werstiuk and C. Ju, *Can. J. Chem.*, 1989, **67**, 5-10.
71. E. Shabanova, K. Schaumburg and F. S. Kamounah, *J. Chem. Res., Synop.*, 1999, 364-365.
72. J. M. Barthez, A. V. Filikov, L. B. Frederiksen, M.-L. Huguet, J. R. Jones and S.-Y. Lu, *Can. J. Chem.*, 1998, **76**, 726-728.
73. H. Shizuka and S. Tobita, *J. Am. Chem. Soc.*, 1982, **104**, 6919-6927.
74. J. G. Larson and W. K. Hall, *J. Phys. Chem.*, 1965, **69**, 3080-3089.
75. H. Gerberich and W. K. Hall, *J. Catal.*, 1966, **5**, 99-110.
76. J. W. Hightower and W. K. Hall, *Trans. Faraday Soc.*, 1970, **66**, 477-489.
77. J. W. Hightower and P. Saunders, *J. Phys. Chem.*, 1970, **74**, 4323-4329.
78. K. L. Tuck and P. J. Hayball, *J. Labelled Compd. Radiopharm.*, 2001, **44**, 1005-1011.
79. J. Brewer, J. Jones, K. Lawrie, D. Saunders and A. Simmonds, *J. Labelled Compd. Radiopharm.*, 1994, **34**, 391-400.
80. K. Wähälä and S. Rasku, *Tetrahedron Lett.*, 1997, **38**, 7287-7290.
81. S. Rasku and K. Wähälä, *Tetrahedron*, 2000, **56**, 913-916.
82. E. Leppälä and K. Wähälä, *J. Labelled Compd. Radiopharm.*, 2004, **47**, 25-30.
83. K. Liu, J. Williams, H. Lee, M. M. Fitzgerald, G. M. Jensen, D. B. Goodin and A. E. McDermott, *J. Am. Chem. Soc.*, 1998, **120**, 10199-10202.
84. S. V. Evchenko, F. S. Kamounah and K. Schaumburg, *J. Labelled Compd. Radiopharm.*, 2005, **48**, 209-218.
85. T. Furuta, A. Suzuki, M. Matsuzawa, H. Shibasaki and Y. Kasuya, *Steroids*, 2003, **68**, 693-703.
86. C. Berthelette and J. Scheigetz, *J. Labelled Compd. Radiopharm.*, 2004, **47**, 891-894.
87. J. Scheigetz, C. Berthelette, C. Li and R. J. Zamboni, *J. Labelled Compd. Radiopharm.*, 2004, **47**, 881-889.
88. J. Yao and R. F. Evilia, *J. Am. Chem. Soc.*, 1994, **116**, 11229-11233.
89. M. Yamamoto, K. Oshima and S. Matsubara, *Org. Lett.*, 2004, **6**, 5015-5017.
90. Y. Elemes and U. Ragnarsson, *J. Chem. Soc., Perkin Trans. 1*, 1996, 537-540.
91. U. Schöllkopf, U. Groth and C. Deng, *Angew. Chem., Int. Ed.*, 1981, **20**, 798-799.
92. B. Lygo and L. D. Humphreys, *Tetrahedron Lett.*, 2002, **43**, 6677-6679.
93. P. Beak and R. A. Brown, *J. Org. Chem.*, 1982, **47**, 34-46.
94. A. Ahmed, J. Clayden and M. Rowley, *Tetrahedron Lett.*, 1998, **39**, 6103-6106.
95. J. Clayden, J. H. Pink, N. Westlund and F. X. Wilson, *Tetrahedron Lett.*, 1998, **39**, 8377-8380.
96. J. Eames, G. S. Coumbarides, M. J. Suggate and N. Weerasooriya, *Eur. J. Org. Chem.*, 2003, **2003**, 634-641.
97. R. Grainger, A. Nikmal, J. Cornella and I. Larrosa, *Org. Biomol. Chem.*, 2012, **10**, 3172-3174.
98. E. M. Higgins, J. A. Sherwood, A. G. Lindsay, J. Armstrong, R. S. Massey, R. W. Alder and A. C. O'Donoghue, *Chem. Commun.*, 2011, **47**, 1559-1561.

99. Y. Zhao, X. Lim, Y. Pan, L. Zong, W. Feng, C.-H. Tan and K.-W. Huang, *Chem. Commun.*, 2012, **48**, 5479-5481.
100. J. Bigeleisen, *Science*, 1965, **147**, 463-471.
101. P. G. Clark, M. Lein and R. A. Keyzers, *Org. Biomol. Chem.*, 2012, **10**, 1725-1729.
102. R. A. Keyzers, C. A. Gray, M. H. Schleyer, C. E. Whibley, D. T. Hendricks and M. T. Davies-Coleman, *Tetrahedron*, 2006, **62**, 2200-2206.
103. H. Sorek, A. Rudi, Y. Benayahu, N. Ben-Califa, D. Neumann and Y. Kashman, *J. Nat. Prod.*, 2007, **70**, 1104-1109.
104. P. G. Clark, 2011.
105. A. Thompson and N. Cromwell, *J. Am. Chem. Soc.*, 1939, **61**, 1374-1376.
106. R. A. Olofson and D. Zimmerman, *J. Am. Chem. Soc.*, 1967, **89**, 5057-5059.
107. T. Axenrod, L. Loew and P. Pregosin, *J. Org. Chem.*, 1968, **33**, 1274-1274.
108. J. Cymerman Craig and L. R. Kray, *J. Org. Chem.*, 1968, **33**, 871-872.
109. A. Lapworth, *J. Chem. Soc., Trans.*, 1903, **83**, 995-1005.
110. A. Burgstahler, J. Walker, Donald, J. Kuebrich and R. Schowen, *J. Org. Chem.*, 1972, **37**, 3754-3754.
111. P. L. Polavarapu, L. P. Fontana and H. F. Smith, *J. Am. Chem. Soc.*, 1986, **108**, 94-99.
112. A. G. Griesbeck, S. Bondock and P. Cygon, *J. Am. Chem. Soc.*, 2003, **125**, 9016-9017.
113. B.-T. Gröbel and D. SEEBACH, *Synthesis*, 1977, **1977**, 357-402.
114. D. Enders and T. Balensiefer, *Acc. Chem. Res.*, 2004, **37**, 534-541.
115. J. S. Johnson, *Angew. Chem., Int. Ed.*, 2004, **43**, 1326-1328.
116. B. Goldfuss and M. Schumacher, *J. Mol. Struct.*, 2006, **12**, 591-595.
117. P. S. Tobin, S. K. Basu, R. S. Grosserode and D. M. Wheeler, *J. Org. Chem.*, 1980, **45**, 1250-1253.
118. E. J. Corey and D. Crouse, *J. Org. Chem.*, 1968, **33**, 298-300.
119. R. Singh, R. M. Kissling, M.-A. Letellier and S. P. Nolan, *J. Org. Chem.*, 2004, **69**, 209-212.
120. J. C. Green, R. G. Scurr, P. L. Arnold and F. G. N. Cloke, *Chem. Commun.*, 1997, 1963-1964.
121. M. Regitz, *Angew. Chem., Int. Ed.*, 1996, **35**, 725-728.
122. T. Ugai and S. Tanaka, *J. Am. Chem. Soc.*, 1958, **80**, 3719.
123. S. T. T. Ugai, S. Dokawa, J. Pharm, 1943, **63**, 269.
124. R. T. S. Mizuhara, H. Arata, *Proc. Japan Academy*, 1951, **27**, 302.
125. R. Breslow, *J. Am. Chem. Soc.*, 1958, **80**, 3719-3726.
126. J. E. Thomson, K. Rix and A. D. Smith, *Org. Lett.*, 2006, **8**, 3785-3788.
127. G. A. Grasa, R. M. Kissling and S. P. Nolan, *Org. Lett.*, 2002, **4**, 3583-3586.
128. A. Chan and K. A. Scheidt, *Org. Lett.*, 2005, **7**, 905-908.
129. D. Enders, J. Han and A. Henseler, *Chem. Commun.*, 2008, 3989-3991.
130. R. S. Massey, C. J. Collett, A. G. Lindsay, A. D. Smith and A. C. O'Donoghue, *J. Am. Chem. Soc.*, 2012, **134**, 20421-20432.
131. C. J. Collett, R. S. Massey, O. R. Maguire, A. S. Batsanov, A. C. O'Donoghue and A. D. Smith, *Chem. Sci.*, 2013, **4**, 1514-1522.
132. C. J. Collett, R. S. Massey, J. E. Taylor, O. R. Maguire, A. C. O'Donoghue and A. D. Smith, *Angew.Chem*, 2015, **127**, 6991-6996.
133. G. J. LaBonia, The University of Mississippi, 2014.
134. E. Buchner and T. Curtius, *Berichte der deutschen chemischen Gesellschaft*, 1885, **18**,

2377-2379.
135. A. Igau, H. Grutzmacher, A. Baceiredo and G. Bertrand, *J. Am. Chem. Soc.*, 1988, **110**, 6463-6466.
136. A. J. Arduengo III, R. L. Harlow and M. Kline, *J. Am. Chem. Soc.*, 1991, **113**, 361-363.
137. D. Bourissou, O. Guerret, F. P. Gabbai and G. Bertrand, *Chem. Rev.*, 2000, **100**, 39-92.
138. L. Benhamou, E. Chardon, G. Lavigne, S. Bellemin-Laponnaz and V. César, *Chem. Rev.*, 2011, **111**, 2705-2733.
139. D. Martin, M. Melaimi, M. Soleilhavoup and G. Bertrand, *Organometallics*, 2011, **30**, 5304-5313.
140. P. S. Skell, *Tetrahedron*, 1985, **41**, 1427-1428.
141. M. N. Hopkinson, C. Richter, M. Schedler and F. Glorius, *Nature*, 2014, **510**, 485-496.
142. M. K. Denk, A. Hezarkhani and F. L. Zheng, *Eur. J. Inorg. Chem.*, 2007, **2007**, 3527-3534.
143. D. Seebach and D. Enders, *Angew. Chem., Int. Ed.*, 1975, **14**, 15-32.
144. N. Kuhn and T. Kratz, *Synthesis*, 1993, **1993**, 561-562.
145. D. Enders, K. Breuer, G. Raabe, J. Runsink, J. H. Teles, J. P. Melder, K. Ebel and S. Brode, *Angew. Chem., Int. Ed.*, 1995, **34**, 1021-1023.
146. A. J. Arduengo III, J. R. Goerlich and W. J. Marshall, *J. Am. Chem. Soc.*, 1995, **117**, 11027-11028.
147. M. K. Denk, A. Thadani, K. Hatano and A. J. Lough, *Angew. Chem., Int. Ed.*, 1997, **36**, 2607-2609.
148. R. W. Alder, P. R. Allen, M. Murray and A. G. Orpen, *Angew. Chem., Int. Ed.*, 1996, **35**, 1121-1123.
149. A. J. Arduengo, R. L. Harlow, W. J. Marshall and T. Prakasha, *Heteroat. Chem.*, 1996, **7**, 421-426.
150. S. E. O'Toole, C. A. Rose, S. Gundala, K. Zeitler and S. J. Connon, *J. Org. Chem.*, 2010, **76**, 347-357.
151. R. MASSEY, Durham University, 2013.
152. P.-C. Chiang, M. Rommel and J. W. Bode, *J. Am. Chem. Soc.*, 2009, **131**, 8714-8718.
153. P.-C. Chiang, Y. Kim and J. W. Bode, *Chem. Commun.*, 2009, 4566-4568.
154. F. Liu, X. Bugaut, M. Schedler, R. Fröhlich and F. Glorius, *Angew. Chem., Int. Ed.*, 2011, **50**, 12626-12630.
155. M. Schedler, R. Fröhlich, C. G. Daniliuc and F. Glorius, *Eur. J. Org. Chem.*, 2012, **2012**, 4164-4171.
156. S. M. Langdon, M. M. Wilde, K. Thai and M. Gravel, *J. Am. Chem. Soc.*, 2014, **136**, 7539-7542.
157. U. Tilstam and H. Weinmann, *Org. Process Res. Dev.*, 2002, **6**, 906-910.
158. K. Jones, R. F. Newton and C. J. Yarnold, *Tetrahedron*, 1996, **52**, 4133-4140.
159. V. R. Yatham, W. Harnying, D. Kootz, J. r.-M. Neudörfl, N. E. Schlörer and A. Berkessel, *J. Am. Chem. Soc.*, 2016, **138**, 2670-2677.
160. J. P. Demers and D. H. Klaubert, *Tetrahedron Lett.*, 1987, **28**, 4933-4934.
161. M. S. Kerr, J. Read de Alaniz and T. Rovis, *J. Org. Chem.*, 2005, **70**, 5725-5728.
162. X.-N. Wang, P.-L. Shao, H. Lv and S. Ye, *Org. Lett.*, 2009, **11**, 4029-4031.
163. J. Rudolph, P. Wickens, C.-Y. Chuang, L. Chen, S. Magnuson, A. Olague and N. Qi, *Journal*, 2009.
164. L. A. Gharat, N. Muthukaman, N. Khairatkar-Joshi and V. G. Kattige, *Journal*, 2015.

165. B. Cardinal-David, D. E. Raup and K. A. Scheidt, *J. Am. Chem. Soc.*, 2010, **132**, 5345-5347.
166. N. E. Wurz, C. G. Daniliuc and F. Glorius, *Chemistry–A European Journal*, 2012, **18**, 16297-16301.
167. X. Wu, B. P. Fors and S. L. Buchwald, *Angew. Chem., Int. Ed.*, 2011, **50**, 9943-9947.
168. T. W. Chapp, D. S. Glueck, J. A. Golen, C. E. Moore and A. L. Rheingold, *Organometallics*, 2009, **29**, 378-388.
169. J. Wu, C. Zhao and J. Wang, *J. Am. Chem. Soc*, 2016, **138**, 4706-4709.
170. M. J. White and F. J. Leeper, *J. Org. Chem.*, 2001, **66**, 5124-5131.
171. J. E. Leffler and E. Grunwald, *Rates and equilibria of organic reactions: as treated by statistical, thermodynamic and extrathermodynamic methods*, Courier Corporation, 2013.
172. K. B. Ling and A. D. Smith, *Chem. Commun.*, 2011, **47**, 373-375.
173. S. Kuwano, S. Harada, R. Oriez and K.-i. Yamada, *Chem. Commun.*, 2012, **48**, 145-147.
174. S. N. Riduan, J. Y. Ying and Y. Zhang, *J. Catal.*, 2015.
175. B. T. Ramanjaneyulu, S. Mahesh and R. V. Anand, *Org. Lett.*, 2015, **17**, 3952-3955.
176. M. M. Wilde and M. Gravel, *Org. Lett.*, 2014, **16**, 5308-5311.